Assessment of myocardial viability using magnetic resonance imaging

Jablonowski, Robert

2015

Link to publication

Citation for published version (APA):
Jablonowski, R. (2015). *Assessment of myocardial viability using magnetic resonance imaging.* [Doctoral Thesis (compilation), Clinical Physiology (Lund)]. Department of Clinical Physiology, Lund University.

Total number of authors:
1

Assessment of myocardial viability using magnetic resonance imaging

ROBERT JABLONOWSKI
DEPARTMENT OF CLINICAL PHYSIOLOGY | LUND UNIVERSITY | 2015

Assessment of myocardial viability using magnetic resonance imaging

Front cover photo:
A short-axis late gadolinium enhancement magnetic resonance (MR) image demonstrating fibrosis (white areas) in the hypertrophied septal wall in a young patient with hypertrophic cardiomyopathy. See study IV for details.

LUND UNIVERSITY
Faculty of Medicine

Assessment of myocardial viability using magnetic resonance imaging

Robert Jablonowski M.D.

DOCTORAL DISSERTATION
by due permission of the Faculty of Medicine, Lund University, Sweden.

To be defended at Föreläsningssal 3, Skåne University Hospital, Lund

on Wednesday 13 May 2015 at 13:00

Faculty opponent

Professor David Bluemke M.D.,
National Institutes of Health, Bethesda, MD, USA

Organization	Document name
LUND UNIVERSITY Department of Clinical Physiology Skåne University Hospital Lund SE-221 85 Lund, Sweden	DOCTORAL DISSERTATION
	Date of issue 2015-04-08
Author(s) Robert Jablonowski	Sponsoring organization: Swedish research council, Swedish Heart and Lung foundation, Medical faculty at Lund University and Region of Scania

Title and subtitle: Assessment of myocardial viability using magnetic resonance imaging

Myocardial infarction (MI) following an acute coronary occlusion is a leading cause of morbidity and mortality. During revascularization microemboli may complicate treatment and affect cardiac function. The long-term effects of microembolization are not fully elucidated. Following an MI it is important to accurately determine the size of the infarction, as it can be used for guidance in terms of prognosis. However, in the setting of an acute MI, the infarct size may be overestimated due to the inclusion of a reversible injured area around the infarction, the peri-infarct zone. In chronic MI and in non-ischemic cardiomyopathies, heterogeneous fibrotic areas have been proposed as substrate for arrhythmias which may cause sudden cardiac death (SCD). Quantification of these areas may provide better risk stratification than current guidelines. In young people the most common cause for SCD is hypertrophic cardiomyopathy (HCM) possibly due to fibrosis that cause fatal arrhythmias. However, the origin of fibrosis in HCM is still unclear. Magnetic resonance imaging (MRI) can be used to assess function, perfusion and viability using late gadolinium enhancement (LGE). Therefore, this thesis investigates how MRI can be used for diagnosis, prognosis and for understanding the pathophysiological mechanisms behind ischemic and non-ischemic cardiomyopathy. Study I showed that coronary microembolization causes long-term, regional left ventricular dysfunction and that even small microemboli, which may escape the distal coronary protective devices, influence cardiac function. Study II demonstrated that infarct quantification with a 2D-PSIR and a 3D-IR sequence show good agreement in patients which allows for the sequences to be used interchangeably. Both LGE-sequences optimized for *in vivo* use yield an overestimation of infarct size *ex vivo*. Study III is an experimental study which showed that contrast-enhanced MRI overestimates infarct size compared to histopathology in the acute phase but not at seven days. This is associated with a significantly higher extracellular volume in the peri-infarction zone acutely compared to seven days later, possibly due to edema. Study IV showed that young patients with HCM had decreased perfusion in areas with hypertrophy and even lower perfusion in fibrotic myocardium. The stress-induced hypoperfused regions exceed regions with LGE indicating that hypoperfusion precede fibrosis and may be a more sensitive marker of diseased myocardium. Study V demonstrated that a heterogeneous LGE borderzone predicts appropriate ICD-therapy to a larger extent than ejection fraction, total, and core LGE size.

Key words: Magnetic resonance imaging, myocardial infarction, hypertrophic cardiomyopathy, fibrosis, viability

Classification system and/or index terms (if any)

Supplementary bibliographical information	Language: English
ISSN and key title: 1652-8220	ISBN:978-91-7619-127-9

Recipient's notes	Number of pages 181	Price
	Security classification	

I, the undersigned, being the copyright owner of the abstract of the above-mentioned dissertation, hereby grant to all reference sources permission to publish and disseminate the abstract of the above-mentioned dissertation.

Signature _[signature]_   Date _2015-04-08_

Assessment of myocardial viability using magnetic resonance imaging

Robert Jablonowski M.D.

Cover:

A short-axis late gadolinium enhancement magnetic resonance (MR) image demonstrating hyperenhancement (white areas) in the hypertrophied septal wall in a young patient with hypertrophic cardiomyopathy. See study IV for details.

Be happy for this moment. This moment is your life.

– OMAR KHAYYAM

Contents

List of publications

This thesis is based on the following studies, which in the text will be referred to by their Roman numeral. My contribution to the studies was to take part in the design (study II-V), collect data from both experimental work (study II and III) and patients (study IV), analyze data and interpret the results (study I-V) and to write manuscripts (study II-V).

I.   Carlsson M, **Jablonowski R**, Martin AJ, Ursell PC, Saeed M. Coronary microembolization causes long-term detrimental effects on regional left ventricular function. *Scand Cardiovasc J. 2011;1-10*

II. **Jablonowski R**, Nordlund D, Kanski M, Ubachs J, Koul S, Heiberg E, Engblom H, Erlinge D, Arheden H, Carlsson M. Infarct quantification using 3D inversion recovery and 2D phase sensitive inversion recovery; validation in patients and ex vivo. *BMC Cardiovasc Disord. 2013;13:110*

III. **Jablonowski R**, Engblom H, Kanski M, Nordlund D, Koul MS, van der Pals J, Englund E, Heiberg E, Erlinge D, Carlsson M, Arheden H. Infarct size day one is overestimated on contrast-enhanced CMR compared to day seven: Relation between T2-weighted and late gadolinium enhancement CMR, TTC, and biopsies to measure extracellular volume. *Submitted*

IV. **Jablonowski R**, Fernlund E, Aletras AH, Engblom H, Heiberg E, Liuba P, Arheden H, Carlsson M. Regional stress-induced ischemia in non-fibrotic hypertrophied myocardium in young HCM patients. *Submitted*

V.   **Jablonowski R**, Chaudhry U, van der Pals J, Engblom H, Arheden H, Heiberg E, Wu KC, Borgquist R, Carlsson M. Cardiac magnetic resonance for prediction of appropriate ICD-therapy in ischemic and non-ischemic cardiomyopathy patients using late gadolinium enhancement heterogeneity: comparison of three analysis methods. *Submitted*

Summary

Myocardial infarction (MI) following an acute coronary occlusion is a leading cause of morbidity and mortality. During revascularization, *microemboli* may complicate treatment and affect cardiac function. The long-term effects of microembolization are not fully elucidated.

Following an MI it is important to accurately determine the size of the infarction, as it can be used for guidance in terms of prognosis. However, in the acute setting after an MI the infarct size may be overestimated due to the inclusion of a possible reversibly injured area around the infarction, the *peri-infarction zone*.

In chronic MI and in non-ischemic cardiomyopathies, heterogeneous fibrotic areas have been proposed as substrate for arrhythmias which may cause sudden cardiac death (SCD). Quantification of these areas may provide better risk stratification than current guidelines.

In young people and athletes the most common cause for SCD is *hypertrophic cardiomyopathy* (HCM), possibly due to areas of fibrosis causing fatal arrhythmias. However, the pathophysiological mechanism behind the development of fibrosis in HCM is still unclear. Magnetic resonance imaging (MRI) can be used to assess function, perfusion and viability using late gadolinium enhancement (LGE). Therefore, this thesis investigates how MRI can be used for diagnosis, prognosis and for understanding the pathophysiological mechanisms behind ischemic and non-ischemic cardiomyopathy.

Study I showed that coronary microembolization causes long-term, regional left ventricular dysfunction and that even small microemboli, which may escape the distal protective devices, influence cardiac function.

Study II demonstrated that infarct quantification with a 2D-PSIR and a 3D-IR sequence shows good agreement in patients, which allows for the sequences to be used interchangeably. Both these LGE-sequences optimized for *in vivo*-use yield an overestimation of infarct size *ex vivo*.

Study III is an experimental study which showed that contrast-enhanced MRI overestimates myocardial infarct size compared to histopathology in the acute phase but not at seven days. This is associated with a significantly higher extracellular volume in the peri-infarction zone acutely compared to seven days later, possibly due to edema.

Study IV showed that young patients with HCM had decreased perfusion in areas with hypertrophy and even lower perfusion in LGE positive, fibrotic myocardium. The stress-induced hypoperfused regions exceed regions with fibrosis indicating that

hypoperfusion precede fibrosis and may be a more sensitive marker of diseased myocardium.

Finally, **Study V** demonstrated that a heterogeneous LGE borderzone, quantified by two different algorithms, predicts appropriate ICD-therapy to a larger extent than ejection fraction, total, and core LGE size.

Populärvetenskaplig sammanfattning

När det blir stopp i ett av hjärtats kranskärl blockeras blodflödet till hjärtat, vilket kan orsaka blodbrist i en del av hjärtmuskeln. Detta kan i sin tur leda till hjärtinfarkt, vilket tar död på hjärtmuskelceller och skadar hjärtat. Vid den efterföljande behandlingen av hjärtinfarkt kan små proppar i kranskärlen, så kallade *mikroembolier*, ytterligare förvärra skadan på hjärtat och påverka hjärtfunktionen negativt.

Efter en infarkt är det av stor betydelse att bestämma infarktens storlek på ett korrekt sätt, eftersom det är vägledande för frågor rörande patientens livskvalitet och livslängd. Ett område runt själva infarkten, den så kallade *peri-infarkt zonen*, kan dock göra det svårt att bestämma hjärtinfarktens storlek i det akuta skedet efter infarkten. Peri-infarkt zonen kan nämligen leda till att infarktens storlek och således skadan på hjärtat överskattas.

Hjärtinfarkt drabbar oftast äldre människor men även unga människor kan drabbas av hjärtsjukdomar. Den vanligast hjärtsjukdomen bland barn och unga vuxna är onormal tillväxt av hjärtmuskeln, så kallad *hypertrof kardiomyopati* (HCM). HCM kan innebära att hjärtat inte pumpar ut blod effektivt nog eller att det bildas ärr i hjärtmuskeln, vilket i sin tur kan leda till plötslig hjärtdöd. Orsaken till sådan ärrvävnad i hjärtat är ännu inte helt klarlagd. Att förstå uppkomsten av ärrvävnad i hjärtmuskeln är dock viktigt för att eventuell förebyggande behandling ska kunna ges i tid. Kontrastförstärkt magnetresonanstomografi (MR) kan användas för att avbilda hjärtat i detalj och gör det därmed möjligt att undersöka ärrvävnad i hjärtat.

En hjärtinfarkt läker så småningom ut och skadan ombildas då till ett ärr, vilket kan orsaka oregelbunden hjärtrytm, så kallade *arytmier*, hos patienten. Arytmier är livshotande då det kan leda till plötslig hjärtdöd. Det finns dock förebyggande behandling att ge patienter som riskerar att drabbas av arytmier, i form av en implanterbar defibrillator (ICD). Kriterierna för vilka patienter som ska få en ICD är dock inte optimala och många patienter får en ICD inopererad utan att ha nytta av den. Med en bättre förståelse för vem som faktiskt skulle ha nytta av en ICD skulle onödigt lidande och komplikationer kunna undvikas i större utsträckning än idag.

Syftet med denna avhandling var att se hur MR kan användas för diagnostik, studera sjukdomsförlopp och för att förutsäga sjukdomsutfall hos patienter med ärrvävnad i hjärtat. För att närmare studera sjukdomsförloppen användes även experimentella djurstudier i avhandlingen.

I **delarbete I** visades i en djurmodell att små mikroembolier i kranskärlen ger upphov till små infarkter i hjärtat och orsakar nedsatt hjärtfunktion som delvis återhämtas över tid.

I **delarbete II** visades att storleksbestämning av hjärtinfarkt med två olika MR-tekniker, 2D- och 3D-MR, visar samstämmiga resultat hos patienter men att dessa tekniker överskattar hjärtinfarkten storlek i en djurmodell när hjärtat har tagits ut.

I **delarbete III** visades att MR överskattar infarktens storlek vid akut hjärtinfarkt men inte vid sju dagar jämfört med referensmetod i en djurmodell. Detta kan förklaras av att peri-infarkt zonen förvinner vid sju dagar och det kan bero på regress av ödem.

I **delarbete IV** visades att patienter med HCM har sänkt blodtillförsel i områden med förtjockad hjärtmuskelvägg och att blodtillförseln är ytterligare sänkt i områden med ärrvävnad. Studien visade även att områden i hjärtmuskeln med blodbrist ökar när patienterna belastas. Hjärtmuskelns område med blodbrist visade sig även vara större än områden med ärrvärvad, vilket talar för att ärrvävnad uppkommer som följd av blodbrist till hjärtmuskeln.

I **delarbete V** visades att storleken på gränszonen mellan områden med ärrvävnad och levande hjärtmuskel kan förutsäga vilka patienter som kommer ha nytta av behandling med ICD bättre än idag etablerade kriterier.

Sammanfattningsvis ger denna avhandling ökad insikt kring 1) hjärtinfarkt, 2) hur små blodproppar i kranskärlen påverkar hjärtfunktionen, 3) orsaken till ärrvävnad vid HCM, samt 4) hur MR kan bidra med information om sjukdomsutfall hos patienter med ärrvävnad i hjärtat.

Abbreviations

AAR	area at risk
ATP	adenosine triphosphate
B_0	main magnetic field
CABG	coronary artery by-pass grafting
CFR	coronary flow reserve
CK-MB	creatine kinase isoenzyme MB
CMR	cardiovascular magnetic resonance imaging
CrP	creatinine phosphate
CT	computed tomography
cTnI	cardiac troponin I
cTnT	cardiac troponin T
DCM	dilated cardiomyopathy
DOTA	tetraazacyclododecane-tetraacetic acid
DTPA	diethylenetriaminepentaacetic acid
ECG	electrocardiography
ECM	extracellular matrix
ECV	extracellular volume
EDV	end-diastolic volume
ESV	end-systolic volume
FPP	first-pass-perfusion
FWHM	full-width at half-maximum
Gd	gadolinium
GRE	gradient-recalled echo
^{1}H	hydrogen
HCM	hypertrophic cardiomyopathy
ICD	implantable cardioverter defibrillator
ICM	ischemic cardiomyopathy
IHD	ischemic heart disease
IS	infarct size
MaR	myocardium at risk
MMP	matrix metalloproteases
MRI	magnetic resonance imaging
mPTP	mitochondrial permeability transition pore
MVO	microvascular obstruction
NICM	non-ischemic cardiomyopathy

IR	inversion recovery
LBBB	left bundle branch block
LAD	left anterior descending artery
LV	left ventricle
LVM	left ventricular mass
LVOT	left ventricular outflow tract
M	net magnetization vector
MI	myocardial infarction
PC	phase-contrast
PCI	percutaneous coronary intervention
PET	positron emission tomography
PSIR	phase-sensitive inversion recovery
RF	radio frequency
ROS	reactive oxygen species
SAM	systolic anterior motion
SCD	sudden cardiac death
SPECT	single photon emission computed tomography
SSFP	steady state free precession
SV	stroke volume
TGF-β	transforming growth factor beta
T	tesla
^{99m}Tc	technetium
TI	inversion time
TTC	triphenyltetrazolium chloride
VF	ventricular fibrillation
VT	ventricular tachycardia

1. Introduction

Viable myocardium refers to cells in the heart that are intact and alive. Complete loss of myocardial viability refers to cells that have been irreversibly damaged, something that can occur in patients with ischemic heart disease (IHD). Every year in the United States approximately 735 000 people suffer from a myocardial infarction (MI).[1] MI is the primary cause of heart failure and ischemic cardiomyopathy (ICM). As MI mainly target the adult population, adverse outcomes following cardiac disease also occur in adolescents. Hypertrophic cardiomyopathy (HCM), a non-ischemic cardiomyopathy (NICM), represents the most common cause of sudden cardiac death in adolescents and in athletes.[2,3] Detailed studies of myocardial viability using cardiovascular magnetic resonance imaging (CMR) has the potential to increase knowledge of the underlying pathophysiological mechanisms, improve diagnosis and clinical management of ICM and NICM patients. Therefore, studies of myocardial viability using CMR is the focus of this thesis.

1.1 Myocardial viability

1.1.1 Viable myocardium

The ventricular myocardial tissue consists of layers of *myocytes*, the contracting cells, surrounded by a network of extracellular matrix (ECM) proteins.[4] The myocytes only constitute one third of the cell population in the myocardium but occupy approximately 75 % of the space.[4] Viable myocytes are composed of bundles of myofibrils which in turn consist of small contractile units, *sarcomeres*. The rest of the structural space in the intersitium comprises of the cardiac microvasculature, nerves and ECM. The extracellular matrix is made up of collagen and gel-like mixture of glycosaminoglycans, glycoproteins, proteoglycans, cytokines, growth factors and proteases.[4,5] Apart from vascular cells in the interstitium, there are also inflammatory cells and fibroblasts.[4,6] Fibroblasts are central to collagen and ECM homeostasis as they secrete pro-collagen chains that are assembled into fibrils of collagen and cross-linked to prevent degradation.[7,8] However, there is a constant collagen turnover with deposition from fibroblasts which is in equilibrium with degradation by proteases. This balance between synthesis and degradation is paramount for normal myocardial

function. The ECM both serves as a scaffold for the cellular components but also serves to transmit contractile force and elasticity, mainly via fibrillar collagen type I and type III respectively. In the myocytes, adenosin triphosphate (ATP) and creatinine phosphate (CrP) are the main sources of energy, with around 75 % going towards contraction and 25 % to uphold ion pumps and protein synthesis.[9] Moreover, myocytes may be viable but with contractile dysfunction. Thus, viable myocardium refers to all viable myocytes that are either normally functioning or dysfunctional with the potential to recover.

1.1.2 Loss of myocardial viability

If myocardial viability is lost through necrosis or apoptosis, this will ultimately lead to fibrotic remodeling. This type of fibrosis is called *replacement fibrosis*,[10] Figure 1.1. The process of replacement fibrosis can be divided into three phases: 1) inflammatory phase; 2) proliferative phase; and 3) maturation phase.[11]

    1) Myocyte necrosis or apoptosis initiates the inflammatory phase. The loss of cell membrane integrity activates growth factors and cytokines, leading to infiltration of leukocytes.[12] Proteases are subsequently activated, such as matrix metalloproteases (MMP), and leads to degradation of the cardiac matrix. Fragmentation of fibrillar collagen and glycosaminoglycans, mainly hyaluronan, activates fibroblasts and promotes an inflammatory response.[13] Type I collagen fragments appears in the blood already 15 - 30 minutes after a coronary occlusion.[14] As the cardiac matrix is degraded a provisional, dynamic, ECM is formed consisting of plasma-derived fibrin and fibronectin from the hyperpermeable blood vessels. This dynamic ECM facilitates infiltration, migration and proliferation of inflammatory cells, endothelial cells and fibroblasts. This phase is present from insult to approximately four days after insult.[15]

    2) The next phase is the proliferative phase, where pathways are activated to inhibit inflammation. The plasma-derived matrix is lysed by the plasminogen system and replaced by a second order provisional cellular matrix of fibronectin and hyaluronan produced by fibroblasts and macrophages.[13] Angiogenesis is mediated via macrophages to provide a microvascular network for the reparative cells. In this phase the differentiation of fibroblasts to myofibroblasts is essential for collagen deposition in the repair process.[16] The differentiation and activation of fibroblasts is mainly modulated by mechanical tension, TGF-β and fibronectin.[17,18] The renin angiotensin aldosterone system can also activate fibroblasts via angiotensin II.[5] Matricellular proteins is a group of proteins that are not expressed in normal myocardial tissue but are important in regulating the pro-fibrotic effects in the proliferative phase.[19] At the end of this phase, anti-fibrotic signals are activated to prevent uncontrolled fibrosis. This phase usually occurs 4 - 14 days after insult.

    3) In the final stage, which lasts up to two months after insult, the collagen scar matures. The collagen produced by the myofibroblasts is assembled into fibrils and cross-linked forming a dense collagen scar.[20] The myofibroblasts and vascular cells

become quiescent and undergo apoptosis which yields a scar with low metabolic activity. The collagen scar enhances the tensile strength of the injured area but also contributes to increased passive stiffness.[20] Thus, the scar represents an area of confluent fibrosis following myocyte death.
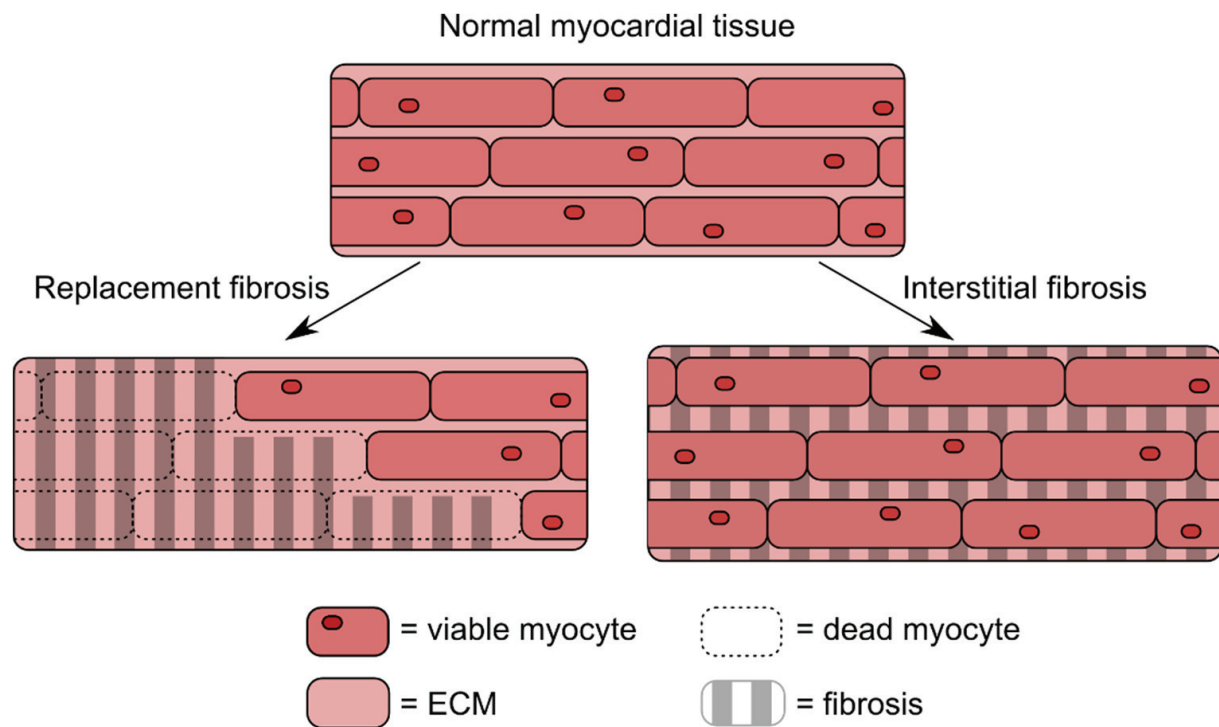
Normal myocardial tissue

Figure 1.1 Schematic drawing of two different types of fibrosis. Myocyte death leads to replacement fibrosis and interstitial fibrosis is characterized by an increase deposition of collagen and expansion of the ECM without myocyte death. See text for details.

Fibrosis can develop even in absence of myocyte death. If the equilibrium between collagen deposition and degradation is altered, this may result in excess deposition of collagen and expansion of the ECM. This type of fibrosis is called *interstitial fibrosis*,[10] Figure 1.1. In interstitial fibrosis, fibroblasts are mainly activated through TGF-β and angiotensin II but increased degradation by MMPs is also seen.[21] Mechanical stress or inflammation may also induce fibrosis by activating fibroblasts. If the location of the interstitial fibrosis is around vessels, it is called *peri-vascular fibrosis*. Another form of interstitial fibrosis is seen in HCM, called *plexiform fibrosis* and characterized by coarse bands of collagen in a bizarre and criss-cross architecture.[10] Infiltrative interstitial fibrosis is a subtype of fibrosis characterized by deposition of non-collagen proteins, such as amyloid protein in amyloidosis.[21]

Following myocardial infarction, both replacement and interstitial fibrosis is seen.[22] In HCM there is usually a mixture of plexiform, perivascular, interstitial and small foci of replacement fibrosis.[10] Interstitial fibrosis can be found in conditions with pressure or volume overload[21,23] and in metabolic disorders such as diabetes.[24] With increasing age there is also evidence of interstitial fibrotic remodeling.[25]

Assessment of fibrosis can be done with invasive endomyocardial biopsies but this method has several disadvantages. It is an invasive procedure with risks, e.g. perforation and prone to sampling error. Furthermore, the fibrosis may be missed if it is not uniform in the myocardium. With CMR, it is possible to non-invasively assess viability both in the acute stage following myocyte death and in the chronic stage with fibrotic remodeling without ionizing radiation. Myocardial viability and loss thereof will be further discussed in the pathophysiological context of ischemic heart disease and non-ischemic cardiomyopathy, particularly hypertrophic cardiomyopathy.

1.2 Ischemic heart disease

1.2.1 Pathophysiology

Ischemic heart disease (IHD) is a disease affecting the coronary arteries. In the healthy heart, epicardial coronary arteries supply oxygen-rich blood to the myocardium and the blood supply to the myocardium is controlled by constriction and dilation of arterioles. The maximum achievable increase in coronary blood flow is called the *coronary flow reserve* (CFR). Coronary blood flow can normally increase 3-5 times from rest due to heavy exercise or using pharmacological agents. However, with the presence of an impingement in the lumen diameter of a coronary artery, the blood flow distal to it will be decreased. In response, the arterioles will dilate at rest and have limited capability to dilate in response to increased metabolic demands during for example exercise. Hence, if oxygen delivered to the myocardium is not in relation to its demand, *myocardial ischemia* occurs. The blood flow supplying the myocardium can be partly blocked by a coronary stenosis or completely due to coronary occlusion. Coronary occlusion can be caused by vasospasm[26] of the coronary artery or embolism.[27] However, the most common pathophysiological reason for coronary occlusion and stenosis is an atherosclerotic plaque.

Atherosclerosis

The atherosclerotic process is an ongoing process in most humans. If a person develops hypercholesterolemia it can trigger the activation of the endothelium. This will enable infiltration of lipoproteins into the arterial intima layer and initiate an inflammatory response. Oxidation of the lipoproteins leads to activation of endothelial cells, which via blood platelets and local cytokine release, enable migration of leukocytes (monocytes and lymphocytes) into the intima layer of the vessel.[28] The differentiation of monocytes into macrophages, with up-regulation of scavenger-receptors, leads to an accumulation of oxidized lipoproteins which in turn transform the macrophage into a foam cell. Migration and proliferation of smooth muscle cells and deposition of ECM form a fibrous capsule covering the lipid-rich core of the plaque. However, if there is

degradation of ECM and abundant macrophages in relation to smooth muscle cells, the plaque is prone to rupture.[28,29] If the plaque ruptures, tissue factor within the plaque is exposed to the coagulation factors in the blood and a coronary thrombus can form. The majority of all fatal coronary thromboses are due to such plaque rupture.[30]

Furthermore, following a plaque rupture or plaque erosion, the cellular constituents of the plaque, e.g. atherothrombotic debris and platelet-leukocyte aggregates, can wash out into the coronary microcirculation resulting in downstream embolization, i.e. *coronary microembolization*.[31] Unstable plaques that have a thin fibrous capsule and a rich lipid core are prone to erode and/or rupture, which may lead to microembolization. From experimental studies it is evident that the major adverse effects of microembolization are impaired perfusion, edema and decreased regional contractility due to a triggered inflammatory response and local cytokine release, mainly TNF-α.[32] Microembolization can also occur during coronary interventions which is discussed further below.

The process of plaque rupture described above can be studied using an experimental setup mimicking the pathophysiology that follows a total coronary occlusion or microembolization in human. As shown in Figure 1.2, this is done by using invasive angiography and inflating a balloon-tipped catheter at the desired site of occlusion. This allows for complicated pathophysiology to be studied in a controlled setting.

Ischemic cascade

Once a coronary occlusion is established and ischemia follows, a series of cellular events are triggered that can potentially lead to cell death. This is called the *ischemic cascade,*[33] and is described below.

Normally the myocytes relax by pumping out Ca^{2+} from the cytosol into the sarcoplasmic reticulum or out of the cell utilizing adenosine triphosphate (ATP). When myocardial cells are deprived from oxygen the metabolism shifts almost instantly from aerobic to anaerobic glycolysis in order to produce ATP.[34] The high energy phosphate reserve within the cell, mainly CrP, is quickly depleted from ischemia onset.[35] This imbalance of ATP in the cell makes relaxation of the myocytes impaired, causing *diastolic dysfunction*.

As ischemia persists, the pH of the cells decreases, lowering the activity of cellular enzymes promoting normal homeostasis. The relative lack of ATP causes the membrane Na^+/K^+ pump to fail, which then accumulates sodium intracellularly and causes potassium to diffuse out of the cell. With increasing concentration of sodium, there is influx of water which causes cells to swell. In order to maintain normal pH, the Na^+/H^+ pump is activated and H^+ is pumped out of the cell. This in turn causes Ca^{2+} influx and accumulation in the cell. These events result in impaired contraction and *systolic dysfunction*. As the Ca^{2+} concentrations rise in the cell phospholipase A2 is activated, leading to degradation of phospholipids in the cell membrane and an increase in free fatty acids and lysophosholipids.[36,37] The latter two will disrupt the cell membrane and mediate inflammation. The rise in Ca^{2+} also activates proteases that

disrupt the cell membrane and the structural integrity of the cell is compromised. Reactive oxygen species (ROS) can form free radicals which further damage cellular constituents.[38] Edema occurs as the leakage of large molecules from blood vessels cause water influx by osmosis. Such edema can be detected by CMR as a marker of the ischemic area.
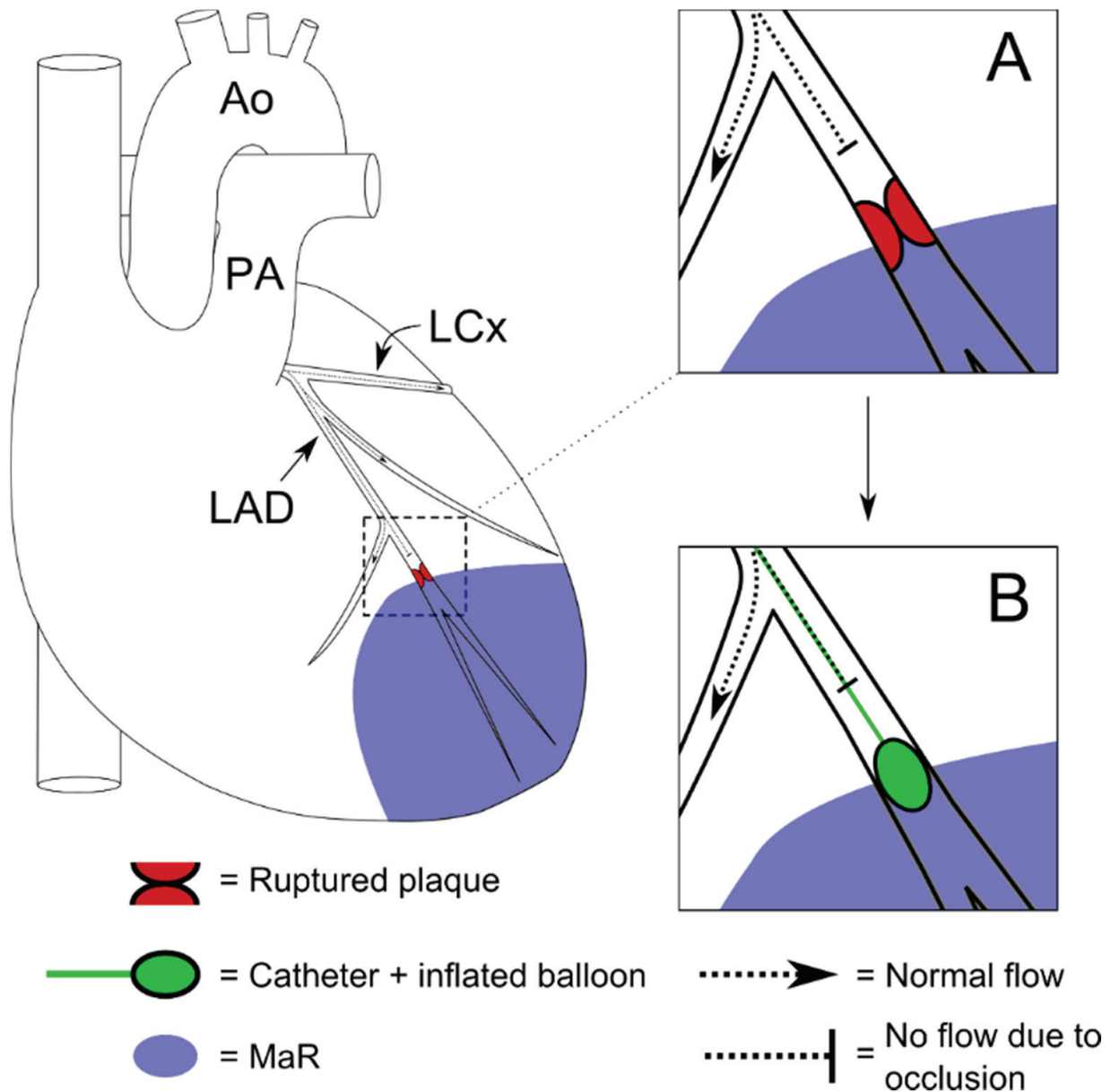
Figure 1.2 Schematic representation of a heart with occlusion in a coronary artery due to (A) a ruptured plaque causing total coronary occlusion and (B) a balloon tipped catheter that is positioned at a desired position in the coronary artery and subsequently the balloon is inflated causing total coronary occlusion. The balloon is defleated after a given time of occlusion. To study microembolization, the same setup is used with the difference that microemboli are delivered distal to the balloon occlusion. This setup (B) is used in the experimental work in the thesis. The blue area distal to the occlusion represent the myocardium at risk (MaR), that may become irreversible injured if the occlusion and resulting ischemia persist. Ao = aorta, PA = pulmonary artery, LAD = left anterior descending artery, LCx = left circumflex artery.

As the ion pumps in the cell malfunction, the resting membrane potential and the action potential rate are disrupted. These changes can be detected on the electrocardiogram (ECG). As degradation of cells continues, metabolites such as adenosine in the ischemic area will give rise to chest pain (angina pectoris).[39] All events except those affecting the structural integrity of the cell are reversible given restoration of blood flow. However, if blood flow is not restored and ischemia persists it will lead to irreversible cell rupture and necrosis, i.e. myocardial infarction, progressing from the sub-endocardium to the epicardium in a wavefront manner.[40] The infarct transmurality will progress with duration of ischemia, eventually involving the full thickness of the myocardial wall, called a *transmural MI*. If blood flow is restored, the result can be an MI that only involves a part of the myocardial wall, called a *subendocardial MI*.

Reperfusion injury

The area of the myocardium supplied by the coronary artery distal to the occlusion is called the *myocardium at risk* (MaR), Figure 1.2.[41] In order to prevent infarction of the entire MaR different reperfusion strategies have been adopted, both medical and mechanical. However, paradoxically, reperfusion itself can result in arrhythmias, microvascular obstruction and even lethal myocardial injury. Occurrence of cell death following reperfusion means that viable myocytes exist in part of the MaR at the time of restored blood flow.[42]

Following reperfusion several components interact to cause irreversible cell damage. Simplified, the process begins as the ATP-dependent ion pumps start up and instantaneously begin to correct for the intracellular acidosis. To do so, H^+ is exchanged for Na^+ which leads to a Ca^{2+} influx and consequently an overload of Ca^{2+}. This in turn affects the mitochondrial membrane, specifically the mitochondrial permeability transition pore (mPTP), which opens in response to Ca^{2+} overload and also other factors such as ROS. Opening of mPTPs for too long, however, will eventually lead to collapse of mitochondrial membrane potential, ceased ATP production and triggered apoptosis, eventually leading to cell death.[43] Second, the washout of molecules that has accumulated during the ischemic phase decreases the intracellular osmotic pressure, causing water influx and uncontrolled swelling of the cell. This may also lead to loss of cell membrane integrity and cell death.[43]

Microvascular obstruction – no reflow

Microvascular obstruction (MVO) is another reperfusion injury with clogging of the microvasculature in previous ischemic tissue seen after revascularization that can result in endothelial and myocyte cell death. This zone is also called a *no reflow zone*[44] and can be caused by microemboli of cell debris, thrombogenic and vasoconstrictor substances, neutrophils, erythrocytes and edema.[45]

1.2.2 Factors affecting final infarct size

The loss of myocardial viability described in the ischemic cascade and due to reperfusion injury are however modulated by several factors. First, duration and size of ischemia are important factors in determining final infarct size. It has been shown that the process of infarct evolution is species dependent. In human it takes approximately 5 hours for 50 % of the MaR to become irreversible injured after a coronary occlusion.[46] In contrast, this process to reach infarction in 50 % of the MaR is slower in pigs (37 min), rats (41 min) and dogs (3 hours).[46]

Second, final infarct size can also be affected due to ischemic preconditioning, first described in canines in the 1980s.[47] This implies that short durations of ischemia, hours or days, before a longer ischemic episode is cardioprotective.[48] The preconditioned myocardium has a lower energy demand and can therefore withstand ischemia for a longer duration before cell death occurs.

Third, presence and extent of collaterals can influence final MI size during ischemic conditions of coronary occlusion.[49] Collaterals are preexisting non-functional vessels that exist interconnected between coronary arteries, mainly in the sub-epicardium. During a process of transformation they can develop into functional vessels following coronary vasospasm, inflammation, shear stress, exercise and hypoxia. In patients with coronary artery disease the main driving force is hypoxia. The presence of collaterals in patients have been shown to reduce infarct size and mortality.[50,51] Collateralization has been shown to be species dependent and while dogs have similar collateral structure as humans, pigs and rats lack collaterals.[52] The difference in collateralization between species, in part, explains the archipelago type of infarct evolution seen in pigs compared to the wavefront appearance in dogs.

1.2.3 Diagnosing myocardial infarction

Clinical diagnosis of myocardial infarction

The diagnosis of acute MI is based on patient symptoms, ECG changes, sensitive biomarkers and imaging techniques.

Several biochemical markers can detect myocardial injury such as creatinine kinase MB (CK-MB), cardiac troponin I and T (cTnI and cTnT). These biomarkers leak out of the cell as the membrane integrity is lost due to coronary occlusion[53] or microinfarcts following reperfusion therapy.[54] CK-MB is a strict cytosolic protein whereas the troponins are found both in the cytosol and also bound to the tropomyosin complex in the sarcomere and are expressed almost exclusively in the myocardium. The preferred biomarker are the troponins due to high degree of myocardial specificity and clinical sensitivity.[55]

In 2012, the Third Universal definition of MI was proposed.[56] The proposed criteria for MI are mainly based on the detection of a rise or fall of cTn I or T taken as a blood sample, with one value being above the 99th percentile of the upper reference

limit. However, the rise of cTn should be accompanied by one out of five major criteria that meet the diagnosis of MI when there is evidence of myocardial necrosis consistent with acute myocardial ischemia.[56] Those five criteria are: 1) symptoms of ischemia; 2) new (or presumably new) significant ST-segment/T-wave changes or left bundle branch block (LBBB); 3) development of pathological Q waves on ECG; 4) new loss of viable myocardium or regional wall motion abnormality by imaging; and 5) identification of intracoronary thrombus by angiography or autopsy.

Different types of myocardial infarction

Myocardial infarction can be classified into five groups (1-5) based on clinical, pathological, prognostic differences and different treatment strategies, Table 1.1.

The most common MI in the clinical setting is type 1, with an underlying atherosclerotic plaque rupture, ulceration or dissection leading to necrosis. Myocardial infarction type 2 is defined as a condition other than coronary artery disease that contributes to an ischemic imbalance between myocardial oxygen supply and demand, i.e. vasospasm or endothelial dysfunction.[26,57] The diagnosis of MI can be difficult in the setting of sudden cardiac death. If there are symptoms suggestive of ischemia and new ischemic ECG changes, classification as a type 3 MI can be made. During percutaneous coronary intervention (PCI) or coronary artery by-pass grafting (CABG) there can be adverse periprocedural events, such as microembolization, as described earlier. Microembolization during PCI occur in nearly one third of all PCIs and can be seen as rise in biomarkers or changes on the electrocardiogram during PCI.[54,58] Microembolization can occur in patients treated with PCI both for an acute coronary syndrome or in patients with stable angina. PCI and CABG are classified as type 4 (a-c) and type 5 MI respectively with details provided in Table 1.1. The biomarker cut-off values for diagnosing MI are higher for type 4 and type 5 MI than for type 1-3. This reflects that a lower cut-off value would result in too many false-positive MI:s.

Furthermore, these elaborate definitions of MI can be of value in the setting of clinical trials as the pathophysiological basis for MI can be determined, rendering a more homogenous study population. In the controlled experimental studies of this thesis MI type I (study II, III) and MI type 4a (Study I) are examined.

Table 1.1. Classification of different types of myocardial infarction. Adapted with permission from Thygesen et al.[56]

Type	Description
1	**Spontaneous myocardial infarction** - Athersclerotic plaque rupture, ulceration, fissuring or dissection with resulting intraluminal thrombus in one or more coronary arteries or platelet emboli.
2	**Myocardial infarction secondary to an ischemic imbalance** - Myocardial necrosis due to non-coronary artery disease condition e.g. coronary endothelial dysfunction, coronary artery spasm, coronary embolism or anemia.
3	**Myocardial infarction resulting in death when biomarker values are unavailable** - Cardiac death with symptoms suggestive of myocardial ischemia and presumed new ischemic ECG changes or new LBBB, but without collected cardiac biomarkers.
4a	**Myocardial infarction related to percutaneous coronary intervention (PCI)** - Defined as elevation of cTn values >5 × 99th percentile if normal baseline values or a rise of cTn values >20% if baseline values are elevated and stable/falling + one of the five criteria mentioned in the main text above.
4b	**Myocardial infarction related to stent thrombosis** - Detected by coronary angiography or autopsy in the setting of myocardial ischemia and with a rise and/fall of cardiac biomarker >99th percentile.
4c	**Myocardial infarction related to restenosis** - Defined as ≥50% stenosis at coronary angiography or a complex lesion associated with a rise and/or fall of cTn values >99th percentile and no other significant obstructive coronary artery disease of greater severity following: (i) initially successful stent deployment or (ii) dilatation of a coronary artery stenosis with balloon angioplasty (<50%).
5	**Myocardial infarction related to coronary artery by-pass grafting (CABG)** - Elevation of cardiac biomarker values >10 × 99th percentile in patients with normal baseline cTn values. In addition, either (i) new pathological Q waves or new LBBB, or (ii) angiographic documented new graft or new native coronary artery occlusion, or (iii) imaging evidence of new loss of viable myocardium or new regional wall motion abnormality.

Pathology

On pathology, MI is defined as myocardial cell death due to prolonged ischemia. Cell death can be characterized by specific histology patterns, i.e. ultrastructure of the tissue, and classified as acute, healing or healed. Using specific staining techniques different cells can be visualized, e.g. collagen.

For a macroscopic evaluation of infarction, histochemical staining with triphenyltetrazolium chloride (TTC) is often used as a reference standard in experimental settings.[59] The myocardial tissue examined is soaked in a TTC solution. TTC will stain viable myocardium with intact mitochondrial respiration brick red. This is accomplished by a redox reaction, where TTC is reduced to triphenylformazan due to activity of dehydrogenases in the presence of an electron donor in a viable cell, such as NADH.[59] After cell death, there is a gradual loss of NADH from the tissue.

If TTC staining is performed too early after cell death, there might be residual NADH in the necrotic tissue which will then be stained. Infarct size may then be underestimated. The reperfusion time required for accurate depiction of infarct size varies among species.[60] For larger animals, 3 hours reperfusion is needed to allow accurate depiction of infarct size following 30 minutes of ischemia.[60]

Imaging

Different imaging techniques can be used to assess acute and chronic MI. Echocardiography, single photon emission computed tomography (SPECT) and CMR are the most frequently used but positron emission tomography (PET) and X-ray computed tomography (CT) can be utilized. Viability can be assessed with all techniques using either dobutamine stress assessing the contractile reserve on echocardiography or CMR, radioactive tracers for assessing perfusion and viability on SPECT and PET or using contrast enhancement for detection of fibrosis on CMR and CT. The reference method today for viability assessment is contrast-enhanced CMR.

1.2.4 Outcomes of myocardial infarction

Several factors determine the outcome of a myocardial infarction. Overall, ischemic heart disease is the most common cause of heart failure and the prognosis is often poor.[61]

Infarct transmurality is an important determinant for functional recovery after acute MI and after revascularization in chronic heart disease.[62,63] A large MI is also shown to predict worse left ventricular (LV) function,[64] occurrence of ventricular arrhythmias[65] and increased mortality.[66] Microvascular obstruction have been showed to reduce global LV function, yield larger MI size and promote adverse remodeling following MI.[67,68] Extravasation of blood may occur in MVO areas causing intra-myocardial hemorrhage, which, if present in an MI is an independent predictor of adverse LV remodelling.[45,67]

Microembolization can result in microinfarcts and impaired perfusion as well as decreased contractile function,[58,69] which can explain adverse outcomes following PCI without apparent complications.[54] One limitation of animals studies investigating microembolization has been the use of exogenous microemboli, however, they have been shown to cause an inflammatory and thrombotic response similar to that of endogenous microemboli.[58,69]

Furthermore, if there is good collateral flow and the duration of ischemia is short, the infarction may be very small or *aborted* with subsequent normalization of cardiac function. Another possible outcome following MI or severe ischemia is *stunning,* which is defined as post-ischemic dysfunction of viable myocardium.[70] Stunned myocardium may recover fully in function and usually does not benefit from revascularization.

In the setting of persistent reduced coronary blood flow, cardiac function can also be reduced. This state is called *hibernating myocardium* and is defined as dysfunctional but viable myocardium following reduced coronary perfusion and function may be restored if blood flow is improved or if the metabolic demands are reduced.[71] Thus, hibernating myocardium can recover its function following revascularization therapy and can be identified using CMR.[62]

Remodeling

The altered conditions in the ventricle after an MI can alter both the infarcted areas as well as remote viable myocardium in a process called *remodeling.* Following an acute MI there can be dilation and thinning of the infarcted area without additional necrosis which leads to infarct expansion.[72] This can result in an aneurysm formation which may lead to mechanical dyssynchrony.[64]

Remodeling may also take place in remote myocardium with secondary hypertrophy to compensate for the loss of function (*positive remodeling*). During the process of infarct healing, resorption of inflammation and edema, together with formation of a mature collagen scar can result in decrease of infarct size.[73]

Malignant arrhythmias

The increased risk of sudden cardiac death in IHD is often due to the development of ventricular tachycardia (VT) or ventricular fibrillation (VF). Lethal arrhythmias in IHD can occur at any time e.g. during coronary occlusion or during reperfusion,[74] or in the setting of chronic MI.[65] In the setting of chronic MI, the pathophysiology behind increased arrhythmogenesis is due to slow-conduction of the electrical signal in the borderzone of fibrotic areas. In these areas, where viable and fibrotic cells are intertwined, re-entry circuits form and can trigger VT or VF.[75] Using CMR to quantify the heterogeneous borderzone it has been shown that the heterogeneous borderzone is a predictor of ventricular arrhythmias[76-77] and mortality.[78-79] Microinfarcts have been proposed to create similar borderzones serving as an arrhythmia substrate.[80]

1.2.5 Therapy

Therapy following MI is initially targeted at re-vascularization of the occluded artery. Post MI, medical therapy aims at preventing adverse remodeling and improve outcome. Also, ICD-therapy can be used to prevent sudden cardiac death.

Revascularization

After a coronary occlusion, the blood flow can be restored by pharmacological or mechanical intervention and should be performed as early as possible.[81] Though blood flow can be restored spontaneously if the intrinsic fibrinolytic system is activated, therapeutic restoration of blood flow is yet of value.[82] Mechanical reperfusion is commonly performed by percutaneous coronary intervention (PCI) where a balloon is inflated at the site of occlusion followed by a stent to prevent re-occlusion. PCI has been proved superior to fibrinolytic treatment in several larger studies but since PCI is a not always available, fibrinolytic therapy may be a viable option.[82,83] Coronary artery by-pass grafting is used in patients with multivessel disease or in patients not suitable for PCI. Furthermore, during PCI there are several possibilities to prevent distal microembolization. In short, the protection devices can either be located downstream of the occlusion such as filter devices to catch and collect microemboli. It is also possible to aspirate thromboses in adjunct to angioplasty and stent deployment.[58] However, these devices may not be useful if the size of the microemboli is small for the device to catch.[32]

Targeting reperfusion injury

Studies have shown that modification of reperfusion conditions affect final infarct size[84] and that post-conditioning[85] resembles the cardioprotective effects of preconditioning.[47] It was recently shown that reperfusion injury actually exists in human, by performing repeated inflations/deflation of an angioplasty balloon following reperfusion which reduced MI size by 36 %.[86] Several different reperfusion therapies have been investigated trying to reduce infarct size.[87] Drugs targeting the mPTP have shown some initial promising results using cyclosporine A[88] but other trials have recently shown overall negative results.[89] Other approaches include inducing hypothermia in patients during ischemia, which have shown conflicting results in reducing MI size.[90,91]

In order to assess the potential benefit of a reperfusion therapy there is a need to first establish the ischemic region that potentially can become infarcted, i.e. the MaR, Figure 1.2. An accurate measure of the final infarct size is then needed to calculate myocardial salvage which is defined as how much of the MaR that has been saved by the reperfusion therapy. Both these measures can be obtained using CMR. Therefore, CMR has been used as a gold standard modality in recent reperfusion trials.[89,90] Calculation of myocardial salvage is described in chapter 3.4.

Medical therapy

To reduce infarct related mortality and adverse remodeling, several drugs are used in the post-MI period. Acetylsalicylic acid and platelet aggregation inhibitors are used to prevent re-occlusion and glycoprotein receptor IIb/IIIa inhibitors may be used to reduce thrombotic complications.[92] To further improve outcome drugs as angiotensin converting enzyme inhibitors, angiotensin receptor blockers, β-blockers and statins are used to prevent adverse remodeling.[93]

Implantable cardioverter defibrillator (ICD)

Ischemic heart disease patients with a history of sudden cardiac arrest or hemodynamically unstable VT may receive treatment with an implantable cardioverter defibrillator (ICD) as secondary preventive treatment.[94] For patients that are at risk for malignant arrhythmias or sudden cardiac death (SCD), ICD-therapy for primary prevention may be warranted.[94] The criteria for selecting patients for primary preventive ICD-treatment are mainly based on two large trials[95,96] which concluded that patients, both ischemic and non-ischemic cardiomyopathy with an LV ejection fraction < 35% are recommended for ICD-therapy. However, using this criteria many patients receiving an ICD never experience any arrhythmias but are subject to potential device complications. Thus, better characterization of individual risk in patients could improve cost-effectiveness and minimize potential complications. Using late gadolinium enhancement (LGE)-CMR for risk stratification has a pathophysiological basis since heterogeneous scar is potentially arrhythmogenic and it can be depicted using CMR.[97] This is further discussed in study V.

1.3 Hypertrophic cardiomyopathy

Cardiomyopathies with an etiology other than ischemic heart disease can be referred to as non-ischemic cardiomyopathy (NICM). Several definitions of cardiomyopathy has emerged in recent years, but the proposed definition from the European Society of Cardiology[98] in 2008 was:

> "a myocardial disorder in which the heart muscle is structurally and functionally abnormal, in the absence of coronary artery disease, hypertension, valvular disease and congenital heart disease sufficient to cause the observed myocardial abnormality".

Two of the most prevalent cardiomyopathies are dilated cardiomyopathy (DCM) and hypertrophic cardiomyopathy (HCM). DCM can be idiopathic or caused by a variety of etiologies such as: infectious diseases, alcohol consumption, chemotherapeutic agents, autoimmune and systemic disorders but can be hereditary as well. The hallmark of DCM is LV dilatation and systolic dysfunction in the absence of abnormal loading conditions (i.e. hypertension) or significant coronary artery disease. HCM will be covered in detail below.

1.3.1 Diagnosis of HCM

Hypertrophic cardiomyopathy was first described by Donald Teare, a British pathologist, in the 1950s.[99] He described the pathological findings in nine cases of sudden cardiac death in young people, as a septal bulge in the left ventricular cavity. This morphological description is still one of the hallmarks of the LV in HCM. Today, HCM is recognized as the most common hereditary cardiac disease with a prevalence of 0.2 % in the population.[100,101] HCM occurs from infancy to late in life, equally in both sexes and is present in all ethnicities.[102–104]

Patients with HCM can present with symptoms such as fatigue, exertional dyspnea, chest pain and systolic heart murmur. Chest pain can be caused by left ventricular outflow tract obstruction (LVOTO) or can be due to microvascular ischemia.[105–107] An abnormal ECG is found in a majority of patients with signs of LV hypertrophy (LVH). However, the first presentation may be a cardiac event as syncope or sudden cardiac death.[108] HCM is diagnosed using cardiac imaging techniques, such as echocardiography or CMR.

The clinical diagnosis of HCM is defined as an increase in LV wall thickness, in one or more LV segments, not explained by other factors such as hypertension, aortic stenosis or metabolic disorders. In adults the diagnostic criteria is an LV wall thickness ≥15 mm but in familial cases a cut-off of > 13 mm is used. In the pediatric population a deviation in LV wall thickness of Z-score > 2SD is diagnostic, where a Z-score is the number of standard devotions from the population mean.[109] Other criteria such as a hypertrophied wall vs. non-hypertrophied wall ratio of > 1.3 measured in asymmetric

HCM is also indicative of the diagnosis. Using echocardiography, wall thickness and ventricular function can be assessed. LV outflow tract obstruction can be assessed at rest and during pharmacological stress or provoked by the Valsalva maneuver. An LVOT gradient of > 50mmHg is considered hemodynamically important. However, echocardiography has limitations and can miss HCM when LVH is focal or apical.[109]

CMR has the potential to asses several characteristics of HCM not possible on echocardiography and is of value when good image quality on echocardiography is difficult to obtain. In one single examination CMR can depict the anatomy of the LV, fibrosis and assess perfusion.[110] CMR also allows for easier differentiation of conditions such as LV non-compaction or athletes heart.[111,112]

Positron emission tomography can also be used to detect perfusion or viability abnormalities in HCM.[113]

1.3.2 Phenotype and morphological features

Left ventricular hypertrophy in HCM patients usually manifests in young adulthood,[114] and can be found in various places of the LV,[115] Figure 1.3.

Asymmetric LV hypertrophy is the most common appearance in HCM. The most prevalent place (~ 70%) is the basal anterior septum, also called septal HCM with sigmoid contour (B in Figure 1.3). In this subset of HCM patients (~ 25 %), the hypertrophy in the basal septum can intermittently block the LV outflow and affect the mitral valve leaflets, leading to elongation and thickening of the leaflets. This can then result in a systolic anterior motion (SAM) of the mitral valve with septal contact, leading to a high pressure gradient due to LVOTO (black arrow in Figure 1.3 B).[116] This subtype can be referred to as obstructive HCM.

The second most common region for LVH is the mid-ventricular septum but not seldom involving adjacent LV segments then resulting in a reversed septal contour (C).[117] HCM can also present with mid-ventricular hypertrophy as seen in (D) with a narrowing of the LV wall towards the apex which can cause apical dilatation and aneurysm formation with concomitant fibrosis. This phenotype can progress into severe heart failure.[118]

In apical HCM (E) there is pronounced apical wall thickening and this type is more prevalent among the Japanese population,[119] and carries a better prognosis.

Symmetrical hypertrophy with a reduced LV cavity size as seen in (F) is rare in HCM.[115,117] This type can also be seen in athletes and patients with hypertension, aortic stenosis or amyloidosis.

A majority of HCM patients have hypertrophy in more than half of the total LV. However, in 10-20 % of patients hypertrophy can be focal and only present in a single LV segment[117] not affecting the LV mass. Thus, increased LVM is not a prerequisite for HCM but is associated with disease severity and adverse outcome.[120]

Another feature of HCM is fibrosis. The pattern of fibrosis is often located mid-wall in areas with hypertrophy but it can also be located in the ventricular septum or

areas of right ventricular insertion in the LV. The increased stiffness of the ventricle and reduced relaxation due to the adverse remodeling with hypertrophy and fibrosis can lead to diastolic dysfunction.[121] Furthermore, HCM patients have been shown to have an impaired coronary flow reserve (CFR) both in the adult HCM population[113,122] and in adolescents.[123]
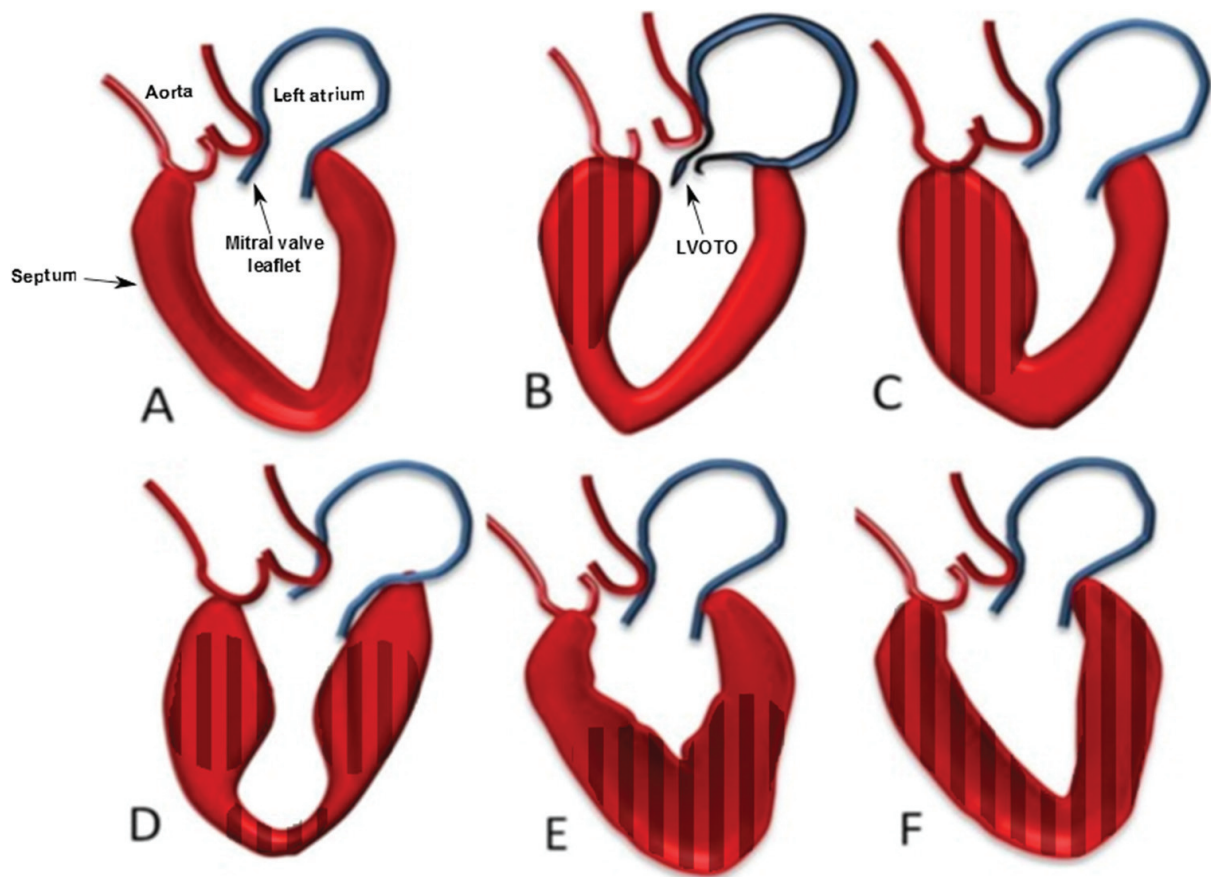

Figure 1.3 Schematic drawings of the left ventricle (LV). Panel (A) represents a normal LV, and panels B-F represent different types of left ventricular hypertrophy found in hypertrophic cardiomyopathy. Striped areas represent pathological areas of the ventricle in respective subtype. LVOTO = left ventricular outflow tract obstruction. See text for details. *Adapted from Noureldin et al.[124] and reprinted with permission under Creative Commons Attribution License (http://creativecommons.org/licenses/by/2.0).*

Individuals at risk and athletes

Genetic testing can be used to identify individuals with a known HCM mutation but without LVH, thus at risk of developing HCM. These subjects are often classified as genotype positive-phenotype negative.[125] Pathogenic mutations are only found in a subset of probands with fulminant HCM. However, if a gene mutation is present in the proband but not found in family member the risk of developing disease is low.[126] Since genotype positive individuals are at risk of developing LVH and/or fibrosis,[127] risk stratification in this phenotypically healthy group is important. It has been shown that genotype positive HCM risk individuals have normal perfusion but an impaired

oxygenation during stress,[128] which may potentially be a novel risk factor. Morphologic abnormalities such as crypts in the septum or free wall of the LV on CMR have also been described.[129,130] The prognostic significance is however unknown.[129,130] Athletes can sometimes also present with LVH mimicking HCM.[112] However, in athletes the LVH is often modest and the LV cavity size is normal/enlarged. In order to differentiate them from HCM patients, they can restrain from physical activity and see if the LVH regresses.

Genetics

HCM is inherited with an autosomal dominant Mendelian pattern with variable expressivity and incomplete penetrance.[126] Offspring run a 50 % chance inheriting a mutation in a gene but mutations can arise *de novo* as well. There are eleven known gene mutations as of 2015 but there is a large number of individual mutation often specific to families. All these genes encode proteins in the myocyte sarcomere. The most common gene mutations are located on the β-myosin heavy chain (MYH7) and myosin binding protein-C (MYBPC3) which account for 60 % of mutations.[126,131] Others include mutation of, for example, troponin T (TNNT2). The genetic mutations of the sarcomere does, however, not explain all features of HCM such as interstitial fibrosis, abnormal intramural arteries and mitral valve deformations. Thus, the penetrance and variability of phenotypic expression is influenced by other factors.

1.3.3 Histological hallmarks of HCM

There are several histological hallmarks of HCM. Myocytes are often organized in a chaotic manner, often described as *myocyte disarray*.[132] The disarray may be widely distributed in the LV wall. Myocyte disarray can however be present in non-HCM subjects, often where the right ventricle inserts into the LV. Therefore, at biopsy 5-10 % myocyte disarray is often required for HCM diagnosis.[132] Furthermore, the myocytes are often hypertrophied with nuclear enlargement and hyperchromasia. Another feature is dysplasia of small intramural coronary arteries with narrowing of the lumen due to intimal smooth muscle cell proliferation.[133,134] There is also evidence of a lower capillary density.[135] These changes described inherently have adverse effects on the microvasculature and may serve as a substrate for ischemia.[133,134] Furthermore, these alteration are histologically often found in areas of LVH but non-hypertrophied areas can be affected and contribute to ischemia and diastolic dysfunction.[136,137]

Another hallmark is interstitial and replacement fibrosis, sometimes as disorganized plexiform fibrosis, which can be focal or diffuse and often in hypertrophied areas.[106,133,136] Fibrosis can also be found around small vessels and in the media of the vessel wall as perivascular fibrosis.[138] The myocyte disarray, replacement and interstitial fibrosis may serve as an arrhythmic substrate for ventricular arrhythmias.[139]

1.3.4 Origin of fibrosis

The pathophysiological basis for development of fibrosis in HCM is not yet fully elucidated. One plausible explanation is that microvascular disease seen in HCM can possibly lead to loss of myocyte viability with following replacement fibrosis.[106,133,138] Perfusion studies on CMR have shown that areas of hypoperfusion, i.e. ischemia, correlates to the degree of LVH,[140] even when adjusting for presence of hyperenhancement (fibrosis) on LGE-CMR,[110,141] supporting that ischemia precedes replacement fibrosis. Furthermore, LV segments with fibrosis has been shown to have even lower perfusion than myocardium without fibrosis.[110,140,141]

However, it has been shown in preclinical models that profibrotic pathways that drive ECM expansion are activated before onset of overt disease.[142] Ho et al.[143] found increased collagen synthesis in genotype positive but phenotype negative subjects. Moreover, there is also data demonstrating a higher extracellular volume, suggestive of ECM expansion, in genotype positive but phenotype negative subjects compared to normal controls.[127] Thus, sarcomere gene mutations may alter the homeostasis in the ECM which results in fibrotic remodeling. Interestingly, it was shown in a PET/CMR study that 8 % of the patients with LGE had normal perfusion, suggesting that the microvasculature was intact despite presence of fibrosis.[144]

Taken together, there is evidence in the literature that the cause of fibrosis in HCM can be multifactorial.

1.3.5 Outcomes and therapy

HCM is generally compatible with normal life expectancy without adverse events and HCM patients survive as long as a sex and age matched general population.[145] Atrial fibrillation is the most common arrhythmia in HCM occurring in about 20 % of patients due to left atrial enlargement, increasing the risk for embolic stroke.[114] In spite of the good prognosis, there are several possible adverse outcomes in HCM such as heart failure and sudden cardiac death. Approximately 50 % of HCM patients develop some degree of heart failure, usually with preserved ejection fraction. The major determinants of heart failure are LVOTO, atrial fibrillation and diastolic dysfunction. Patients with LVOTO are treated with β-blockers, disopyramide and verapamil.[109] In patients with severe outflow gradient obstruction and heart failure, interventional therapy with septal myectomy or alcohol ablation can be beneficial.[146]

Patients with non-obstructive HCM usually have a benign clinical course. However, a minority of patients will progress into heart failure which can lead to adverse remodeling with LV dilatation and extensive fibrosis , so called *end stage HCM* or *burned out HCM*.[147] In these patients cardiac transplantation can be the only treatment option.

Sudden cardiac death is not very common in the adult HCM population.[3,148] However, in young people < 30 years of age and in competitive athletes, HCM is most

common cause of SCD.[2] Exercise restriction is often enforced in patients with risk factors for SCD. Only ICD-therapy has been shown to decrease mortality. The implantation of a secondary preventive ICD after cardiac arrest or sustained ventricular tachycardia is uncontroversial.[109] For primary preventive ICD therapy, there are several risk factors recognized such as: family history of SCD, unexplained syncope, abnormal exercise blood-pressure response, LVOT gradient, LVH, left atrial diameter and non-sustained VT.[109] In children the degree of LVH and syncope are the strongest risk markers for ICD therapy.[148] However, the use of prophylactic ICD-therapy is still a challenge as SCD occurs in patients without conventional markers of risk.

Recently, CMR has emerged as modality that can help with risk stratification. Hyperenhancement on LGE-CMR is found in around 60 % of HCM patients and presence of LGE has shown a relationship with increased cardiovascular mortality and heart failure in HCM but not in predicating risk of SCD.[149] Moreover, it has been shown that the amount of LGE is proportional to the risk for SCD.[150] However, even though lack of LGE is associated with a lower risk of SCD, these patients with no LGE still experience SCD.[150] Thus, there is still a need for better markers of risk stratification. Current ongoing large multicenter trials, such as the HCMR trial, aiming at finding novel markers of prognosis in HCM, will hopefully add new information in risk stratification of HCM patients.

1.4 Cardiac magnetic resonance imaging

Cardiac imaging can be performed using different modalities which all use different physical properties to depict cardiac anatomy and physiology. All modalities have their strengths and limitations and differ in availability and most can assess myocardial viability in some way. However, the focus in this chapter will be on cardiac magnetic resonance imaging (CMR) and the possibilities to assess myocardial viability. CMR is used as an acronym when referring to cardiac MRI, however when referring to technical aspects of the technique itself, the acronym MRI is used. Magnetic resonance imaging (MRI) is a modality that can obtain images of the body in any plane without ionizing radiation. In 1952 the Nobel Prize was awarded to Felix Bloch and Edward Purcell for discovering magnetic resonance by electromagnetic fields. Since then, three more Nobel prizes (in 1991, 2002 and 2003) have been awarded for developing the MRI technique.

1.4.1 The MRI system

An MRI system consists of three main components. First a strong magnetic field is needed. To produce a strong magnetic field the main magnet consists of metal wires wrapped around a circular bore. This wire is cooled using liquid Helium resulting in supraconduction. Applying an electrical current through the wires induces a magnetic field. The main magnetic field, B_0 is measured in units of Tesla (T). Normal field strengths for clinically used MRI are 1.5T or 3T. To define the magnetic field direction a reference coordinate system with three orthogonal axis (x, y and z) is used. The z-axis is defined to be parallel to B_0. Second, three gradient coils are built into the scanner and generates linear variations in the main magnetic field enabling spatial localization of the MR signal. Thirdly, there are two types of radiofrequency (RF) coils that transmit and receive radiofrequency pulses. The RF transmitter is mounted inside the scanner and transmit energy in radio-pulses at a specified frequency. The RF receiver coils detects the generated signal generated from the patient and is placed as close as possible to the patient.

MRI physics

The basis for MRI is that nuclei with an uneven mass number possess a spin and thereby a magnetic moment. The most widely used nucleus in clinical MRI is the hydrogen atom (^{1}H) due to its abundance in water and fat. The magnetic moments (i.e. spins) from protons are normally oriented in a random orientation. When placed inside a strong magnetic field, the spins will align with the field and start to precess at a specific angular frequency, called the *Larmor frequency*. The Larmor frequency differs from protons in different molecules and increases linearly with the applied magnetic field strength. This linear relationship is described by the so called gyromagnetic ratio,

defined as the increase in angular frequency per Tesla and is 42,58MHz/Tesla for [1]H. Hydrogen spins may align parallel or anti-parallel to the applied magnetic field, but a few more spins will align with the magnetic field as it requires less energy. This small difference is the basis for generating an MR-signal and causes a net magnetization vector (M) along the z-axis in the direction of the magnetic field. The number of spins aligned up with B_0 is proportional to the field strength, thus higher field strengths yield a stronger MR-signal. However, when M is aligned with the strong B_0–field it cannot be detected. In order to detect M it is tilted at an angle from B_0. This is performed by introducing an electromagnetic field, B_1, from the transmitting RF coil.

Radio frequency coils

In order to affect spins in the strong magnetic field, B_0, the RF pulse has to be transmitted at the Larmor frequency of the spin. If this is done the RF pulse and spin will be in resonance, hence the term *magnetic resonance* imaging. The transmission of the RF pulse causes the net magnetization vector to rotate away from its alignment with B_0 at an angle. This angel is called the flip angle. During and directly after an RF pulse can be divided into three nonzero vector components of M, one along the z-axis, M_z, and two orthogonal vectors in the xy plane, M_x and M_y. The components in the xy-plane induce a small current which can be detected by the RF receiver coils as the MR signal (echo).

Gradient coils

In order to spatially locate the MR signal, the gradient coils are used. Using the three components of the gradient system a specific slice can be chosen and the slice can be spatially encoded. The gradient coils are used to generate small linear variations in the main magnetic field which enables spatial encoding. By applying a slice selective gradient it is possible to excite only the specific slice of tissue where the Larmor frequency is in resonance with the RF pulses. In order to spatially encode the signal within the excited slice, a gradient in the y-direction is applied, in order to induce differences in spin frequencies prior to detecting the signal. This results in a phase shift which varies along the y-direction and is called *phase encoding*. A gradient applied in the x-direction during signal sampling causes a variation in spin frequency along the x-direction and is called *frequency encoding*. The signal detected by the RF receiver coil is acquired in the spatial frequency domain, k-space. The signal in k-space is encoded according to phase and frequency. With each signal sampled, one line of k-space is acquired. The number of lines and number sampling points in k-space determine the final spatial resolution of the image. The last step is to transform the raw data in k-space by Fourier transformation into anatomical images.

T1 and T2 relaxation

In order to describe the magnetic properties of tissue, the parameters T1 and T2 relaxation are used. Directly after the RF pulse has been applied, the net magnetization

vector starts to return to its original state. This is called *relaxation*. The relaxation for the longitudinal component (M_z) along the z-axis is called *T1 relaxation* and the decay of the transverse component (M_{xy}) is called *T2 relaxation*. Both T1 and T2 are time constants with different definitions. T1 is the duration of time it takes for 63 % of the M_z to recover. T2 is the time it takes for M_{xy} to decrease to 37 % of its value directly after the RF pulse. T1 is around 1100 ms and T2 is about 50 ms in healthy myocardium at 1.5T. T1 and T2 properties govern the way MR pulse sequence are designed, i.e. being T1 or T2 weighted, in order to visualize different tissues and pathophysiological processes.

1.4.2 Contrast agents

The contrast agents used in MRI are mostly paramagnetic and are based on gadolinium (Gd). The main effect of gadolinium is T1 shortening of the protons in its surrounding and thus it is not the Gd itself that emits a signal.[151] Gadolinium ions are toxic in their free form and therefore there is a need to couple it to a ligand. The most widely used ligands are DOTA and DTPA. These molecules are small (~ 0.8 kDa) and diffuse passively into the extracellular space but are excluded from normal myocardial cells. The Gd-chelate is eliminated by the kidneys with a half-life of about two hours.

1.4.3 Cardiac function

Cardiac function is assessed by using time-resolved imaging, also called cine imaging. Due to movement of the heart during respiration as well as intrinsic cardiac motion imaging is performed during breath-hold. For full coverage of the heart, multiple breath-holds are often needed, which can be a challenge in a clinical setting. ECG-gating can be used to account for the intrinsic movement. Usually retrospective ECG-gating is used which involves continuous and simultaneous acquisition of ECG and the MR signal. In patients with arrhythmias ECG-gating can be difficult. Real-time imaging is then an option which acquires all data for an image in one heartbeat. However, this kind of imaging limits both spatial and time-resolution. The currently used sequence for cine imaging is balanced steady state free precession (SSFP) which provides excellent contrast between the myocardium (appears dark) and the blood pool (appears bright) without the use of contrast agents. The signal in these images utilizes the ratio between T2 and T1. In these images cardiac volumes, mass and LV function can be assessed.

Regional function

The first method that was validated for assessing viability on MRI was dobutamine stress MRI.[152] In analogue with dobutamine stress on echocardiography, ventricular function is imaged at various doses of dobutamine. Ischemic myocardium may show a

biphasic response with increased contractility using low dobutamine doses and lower contractility at high doses.

Regional function can also be assessed using "tagged"-images. In these images a grid-pattern is used covering the heart and along the grid-lines the signal is cancelled in end-diastole. As the heart contracts the grid-lines are deformed more or less depending on the regional function. Moreover, it is possible to extract phase information from the MR signal acquired which can be used for velocity encoded imaging or phase sensitive contrast-enhanced imaging (PC-MRI). In PC-MRI, one anatomical image is collected (magnitude) and one velocity-image is collected (phase) where the gray scale in each volume element (voxel) is proportional to the velocity of the voxel. This enables the velocity of the myocardium as well as the blood to be measured.[153] Using both grid-tagging and PC-MRI myocardial strain can be calculated. Strain in the myocardium is defined as the deformation of a region of interest in the myocardium between end-diastole and end-systole. Strain is measured in three directions to depict the ventricular contraction: radial, circumferential and longitudinal.

1.4.4 Perfusion

MRI can be used to assess regional myocardial perfusion by measuring the inflow of a Gd-based contrast agent during the first passage through the vasculature in the myocardium, called first-pass-perfusion (FPP). If there is a stenosis or microvascular disease, perfusion will be decreased to that part of the myocardium. The contrast agent typically reaches the myocardium within 15 - 20 seconds of administration. The inflow of contrast agent is seen as hyperenhancement of the blood pool first, then the myocardium. Regions with low or no perfusion appear as hypoenhanced. Typically three short-axis slices are acquired simultaneously and the number of slices is limited by the heart rate in current techniques. Perfusion can be assessed at both rest and at stress using e.g. adenosine as a stress-agent. Adenosine is a natural occurring substance in the body and its main affect is vasodilation. Thus, if the vasculature already at rest is dilated in order to facilitate enough blood flow to the tissue due to disease, there is limited capability of further dilatation in response to adenosine. The diseased area will be seen as a hypoperfused (dark) area, due to less Gd, whereas normal tissue will look similar in rest and stress, see Figure 4.11.

Perfusion can be assessed semi-quantitatively in several ways. The basis is to evaluate the change in signal intensity in the myocardium and blood over time during the first pass of the contrast agent. Figure 1.4 shows three different ways to assess perfusion semi-quantitatively: (1) upslope (2) area under the curve and (3) time to peak signal intensity, see figure text for details. It is also possible to estimate absolute blood flow from FPP images by using advanced mathematical modeling.[154]

Global perfusion can also be assessed using CMR. This is done by using velocity encoded imaging (PC-MRI) and measuring the blood flow in the coronary sinus, the vein that drains the myocardium.[155]
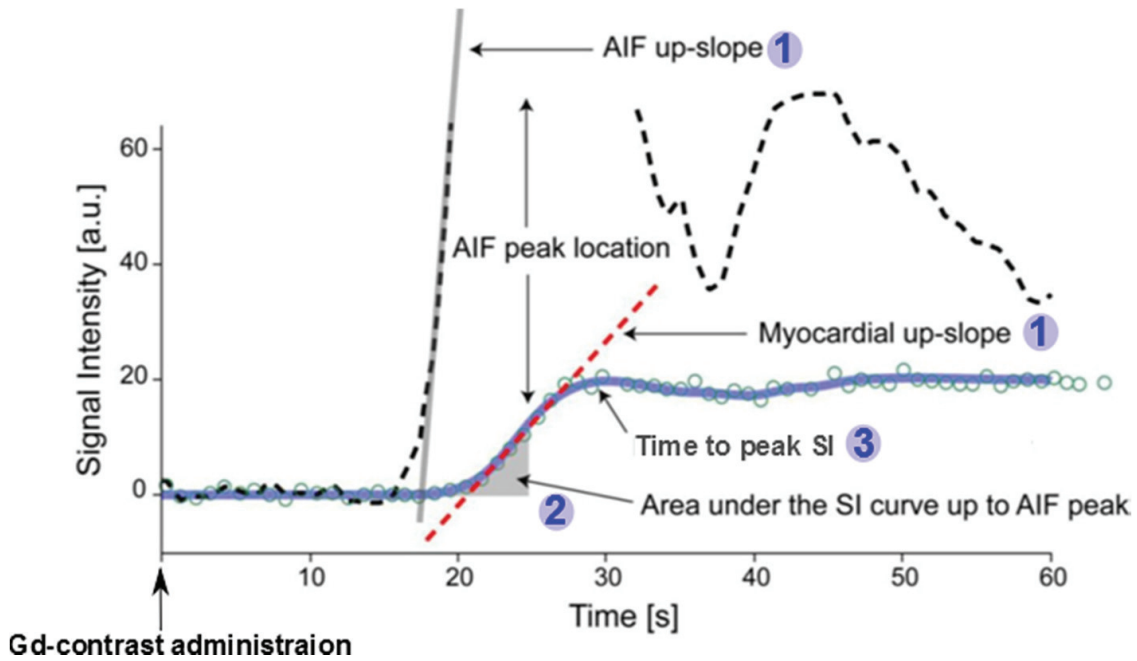
Figure 1.4 This figure shows the signal intensity (SI) in the myocardium (blue line) and blood pool (black striped line) as a function of time after administration of a Gd-contrast agent in first-pass-perfusion imaging. Three semi-quantitative measures of perfusion are shown: (**1**) The red line shows a fitting of the first derivative of the SI curve during the initial passage of contrast through the myocardium. This gives the intial rate of contrast. The upslope of myocardium is often normalized to the upslope of the blood pool (AIF) seen as the gray line. If images are aquired both during rest and stress, a ratio (stress/rest) can be calculated which yields an estimate of the perfusion flow reserve. This is not equal to the coronary flow reserve (CFR) but can under some circumstances be used as an estimate of it. The normalization to the blood pool is done to account for the altered hemodynamics that can occur between rest and stress. (**2**) Area under the curve can be calculated from a set point, e.g. foot of the sharp rise in SI to the peak of the first pass of contrast. (**3**) Time to peak SI is the time from the apperance of contrast (i.e. at the start of the sharp rise of the blue line) to the peak SI. A forth possibility is to measure the peak SI. *Figure adapted from Jerosch-Herold*[154] *and reprinted with permission under Creative Commons Attribution License (http://creativecommons.org/licenses/by/2.0).*

1.4.5 Edema

On MRI, T2-weighted imaging can be used to assess the ischemic, edematous, MaR following an MI.[156] T2w imaging has been validated in MI patients against SPECT and the methods showed good agreement.[157] Edema imaging can be used to differentiate acute from chronic MI. Recently a new method for assessing MaR has emerged using the same sequence used for cine imaging (SSFP) but acquiring images after contrast administration.[158] This sequence, contrast-enhanced SSFP has been validated against SPECT showing good agreement.[158] This new approach enables MR protocols to be shortened since contrast-enhanced SSFP images contain both information on function and MaR.

1.4.6 Fibrosis and myocardial infarction

Using MRI, fibrosis and myocardial infarction (acute and chronic) can be visualized both *in vivo* and *ex vivo* using the technique called *late gadolinium enhancement* (LGE). An example of an LGE –MRI image is shown in Figure 3.3. As previously mentioned, LGE-MRI is considered the reference method for assessing myocardial viability. This technique was pioneered in the 1970s by Charles Higgins group using CT to detect MI in canine hearts.[159] In the 1980s, MRI using Gd-based contrast agents were used for the first time in patients with MI.[160] With the advent of faster more clinically suited sequences the method became widely used.[161]

Pathophysiological basis of late gadolinium enhancement

Gadolinium-based contrast agents distribute in the extracellular space, as previously stated, and are excluded from normal viable cells with an intact cell membrane. The basis of LGE is that the amount of contrast agent is proportional to the distribution volume of the tissue, i.e. the amount of extracellular space.[162,163] Following acute MI, the infarcted myocardium has an increased distribution volume due to the loss of cell membrane integrity which allows Gd into the intracellular space of the infarcted myocytes and also due to edema and hemorrhage. Chronic infarction or areas with fibrotic remodeling due to other diseases with collagen deposition also exhibit Gd-enhancement.[164] This is due to that collagen has a small intracellular space and the collagen matrix has a large effective extracellular space, yielding a greater distribution volume for Gd than in viable myocardium.

Extracellular volume

It is possible to quantify the distribution volume, or extracellular volume (ECV) which are used synonymously. Quantifying ECV gives information about the composition of the tissue, i.e. if it is healthy or diseased. This can be done on MRI by using the reciprocal of the longitudinal relaxation time-constant T1, called R1. The change in $\Delta R1$ of pre and post contrast measurements of T1 is proportional to the concentration of Gd-DTPA. Extracellular volume can be calculated if a dynamic steady state between the blood and myocardium exists, i.e. tissue that has a contrast rate exchange which is faster than the renal clearance of contrast from the blood. This is apparent in the heart after approximately 5 minutes after contrast administration.[163] By measuring the hematocrit, the distribution volume of blood can be calculated as 1 - hematocrit. Thus, by calculating $\Delta R1$ for both blood and myocardium (by measuring T1 in the MR image), ECV can be calculated using Equation (1).

$$ECV = (1\text{-hematocrit}) \times \Delta R1_{myocardium} / \Delta R1_{blood}$$

By using specific MR pulse sequences, T1 in both the myocardium and blood pool can be estimated and mapped (T1 mapping) before and after contrast administration.

Using that T1 data, a pixel-based ECV-map can be rendered for the myocardium.[165] ECV can also be calculated using other strict extracellular tracers as well. For example, ^{99m}Tc-DTPA can be used by measuring the rate of radioactive decay following intravenous administration instead of T1. In study III in this thesis, ^{99m}Tc-DTPA is used to calculate ECV based on the same principles described here. The ECV in normal tissue has been shown to be 17 - 25 % in rat,[163,166] and around 25% in humans using T1 mapping on CMR.[167]

Imaging using late gadolinium enhancement

The name of the technique late gadolinium enhancement indicates that is temporal consideration made when using this image technique. There is also a difference in contrast kinetics in normal and non-viable myocardium with a delayed wash-out of contrast media from the non-viable myocardium.[168] In order to image the true non-viable area there has to be a steady-state between the blood and the extracellular space. Gadolinium in the non-viable myocardium is in a transient steady-state with the blood when imaging is performed approximately 5 - 30 minutes after contrast administration of 0.1 to 0.2 mmol/kg contrast.[163,169] This time delay for when images are acquired is the reason for the name *late* gadolinium enhancement. In clinical practice images are usually acquired between 10 - 30 minutes after 0.2 mmol/kg contrast administration. Imaging earlier than 5 minutes is called early gadolinium enhancement (EGE) imaging and is sensitive for demonstrating microvascular obstruction.[68]

In order to visualize the infarction, or area with loss of viability, an Inversion Recovery (IR) pulse sequence is used to enhance the difference between viable and non-viable myocardium.[161] The area with loss of myocardial viability will have a greater accumulation of gadolinium with a shorter T1 relaxation. This is utilized in the IR-sequence where the net magnetization vector is first flipped 180° followed by a delay, inversion time (TI), before image acquisition is performed. The TI can be adjusted to null the signal from a certain tissue which results in that tissue appearing dark in the images. This is used in LGE imaging where normal myocardium is nulled (dark) and the non-viable tissue appears bright. However, by using a phase-sensitive inversion recovery (PSIR) sequence it is not required to find the precise TI that nulls normal myocardium due to the incorporation of phase information, however image quality can improve if a TI is selected as in the IR-seqeunce.[170] LGE images are acquired during breath-hold in both short-axis and long-axis projections. This can be done either by a segmented two dimensional acquisition or a three-dimensional acquisition were the whole volume of interest is acquired. These two approaches (2D and 3D imaging) have different advantages and disadvantages which can be utilized in the clinical setting. Using 2D-LGE imaging will take longer time but the breath-holds will be shorter. Using 3D-LGE image acquisition is faster but with greater susceptibility to arrhytmias and aliasing. Novel techniques include single-shot acquisitions can be used for patients where breath-hold is difficult or in patients with severe arrhythmias. Thus, several factors affect the size of the non-viable area on LGE imaging: TI, Gd concentration and dose,[169] timing of imaging[171] and the elimination rate.

Validation of late gadolinium enhancement

Late gadolinium enhancement has been shown to correspond well to infarcted myocardium using histopathological staining with TTC in *ex vivo* canine hearts at day 1, 3 and 8 weeks following MI.[172] Subsequently, LGE has also been validated by others against TTC following MI, both *in vivo*[173,174] and *ex vivo*.[174] Further validation at high field strengths have shown LGE to correspond well to areas with fibrosis and also that the borderzone in chronic MI consists of viable and fibrotic myocytes intertwined.[97]

However, in acute MI, there is evidence that contrast-enhanced MRI overestimates infarct size compared to histopathological staining with TTC.[175,176] This has been attributed to a peri-infarction zone that hyperenhances on contrast-enhanced MRI but contains reversibly injured myocytes.[166,175] There is also evidence of a peri-infarction zone in patients following acute MI that diminishes during the first week.[177] One explanation for the hyperenhancement in the peri-infarction zone, i.e. increase in distribution volume for Gd acutely, has been edema. It has been shown, following acute MI in rat, that the fractional distribution volume or ECV in the salvaged MaR is higher than ECV in normal myocardium but lower than the EVC in the infarction.[166] Interestingly, the zone around the infarction with elevated ECV compared to normal tissue, per-infarction zone, contained viable myocytes assessed on autoradiography. This is further discussed in study III. However, here an important distinction in the nomenclature has to be made: the peri-infarction zone in the acute setting after MI has to be distinguished from the borderzone seen in chronic MI (intertwined viable and fibrotic cells). These two borderzones are different pathophysiological entities but are sometimes viewed as one entity in the literature.

Furthermore, in HCM, there is limited evidence that LGE corresponds to fibrosis.[178,179] Thus, in HCM, areas of LGE may represent other pathophysiological entities than replacement fibrosis such as edema, myocyte disarray or more diffuse interstitial fibrosis. This remains to be explored further.

Quantifying late gadolinium enhancement

Late gadolinium enhancement CMR has the ability to detect very small areas of irreversibly damaged myocardium. However, this requires a way to quantify it. Quantification can be done visually, manually or using a more or less sophisticated algorithm. In the experimental setting, both dichotomous threshold algorithms using different number of SDs to separate infarct from normal myocardium,[172] a FWHM algorithm,[173] and other more advanced algorithms have been validated.[174,180] Quantification of LGE in MI or HCM patients can be performed using different algorithms[181] such as threshold algorithms (2-5SD) or the FWHM algorithm[77,173] as well as other more elaborate algorithms that take partial volume and infarct heterogeneity into account are avaible.[180] Algorithms for LGE borderzone quantification are discussed in study V. However, the large number of algorithms is a source bias if not used appropriately.

Characteristic patterns of late gadolinium enhancement

Figure 1.5 shows typical patterns of LGE in different cardiac pathologies. This can be used for differential diagnosis. Due to the infarct evolution from sub-endocardium to epicardium, the LGE pattern seen in MI is either subendocardial to some extent or transmural. In non-ischemic cardiomyopathies the spectrum is wider. Dilated cardiomyopathy usually presents with a mid-wall pattern of LGE. Hypertrophic cardiomyopathy, as discussed earlier, often have mid-wall LGE in hypertrophied areas and at the insertion points for the right ventricle. In myocarditis typically an epicardial LGE pattern is seen. In diseases such as sarcoidosis, Anderson-Fabrys and Chagas disease, the LGE pattern can be mid-wall or epicardial. Amyloidosis and systemic sclerosis can present with a global endocardial LGE pattern.
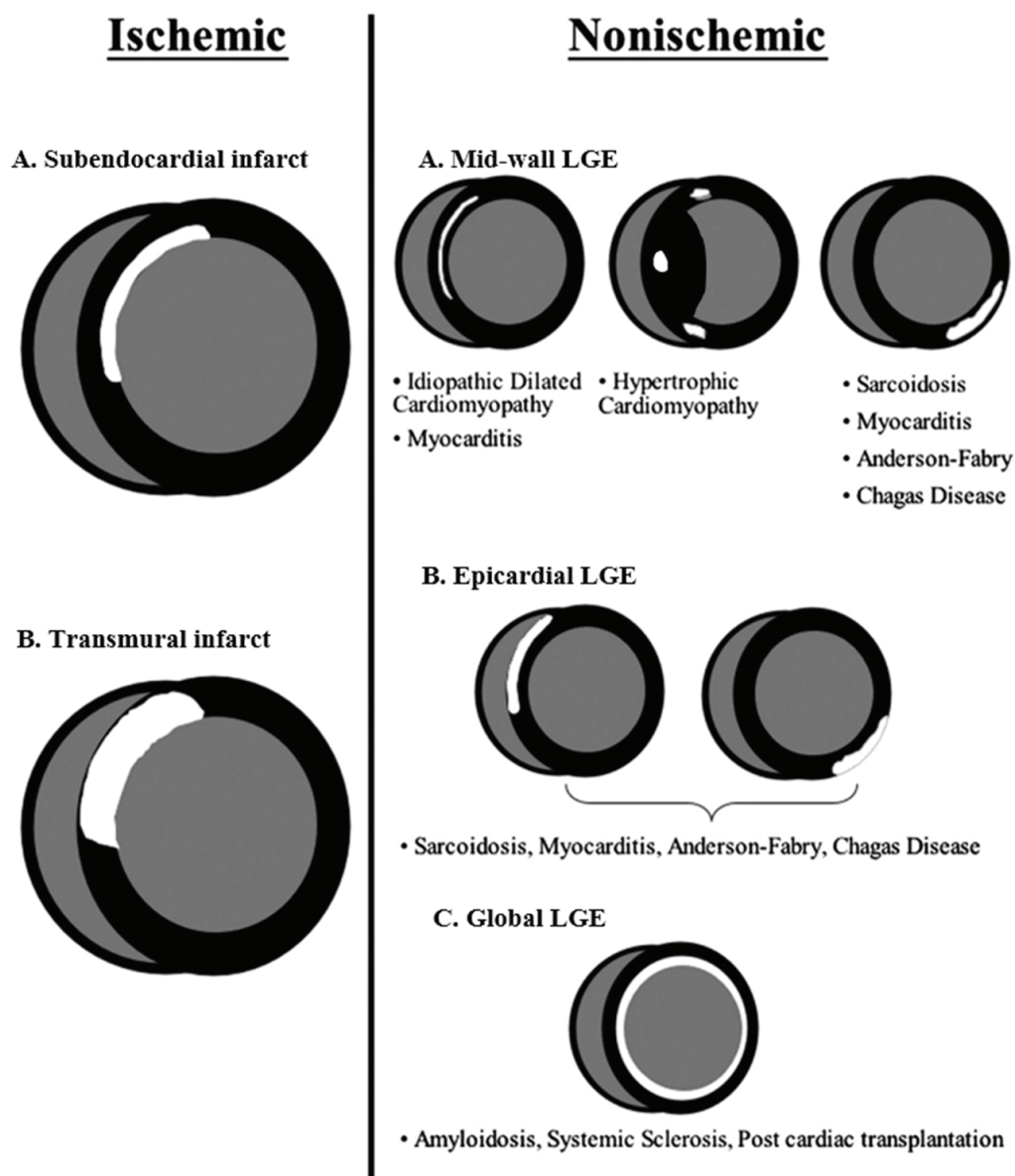

Figure 1.5 Different types of LGE patterns (white) in ischemic and non-ischemic cardiomyopathy are shown in schematic short-axis slices of the heart. *Reprinted and adapted from Mahrholdt et al.[182] with permisson from Oxford University Press.*

2. Aims of the work

The general aim of this thesis was to investigate how magnetic resonance imaging can be used for diagnosis, prognosis and for understanding the pathophysiological mechanisms behind ischemic and non-ischemic cardiomyopathy.

The specific aims for each study were:

I.   To examine whether coronary microemboli have long term deleterious effects on LV function and to study whether the perfusion and LGE patterns differ between small and large microemboli in the acute stage.

II.   To determine the agreement between 2D-PSIR and 3D-IR for measurement of infarct size in patients and to compare both sequences with a reference high resolution T1w sequence in an experimental model.

III. To investigate if the reported overestimation by MRI versus TTC remain after seven days in an experimental pig model and elucidate the mechanism behind hyperenhancement of the peri-infarction zone early after acute myocardial infarction.

IV.   To measure if regional perfusion is decreased in young patients with HCM and in HCM-risk subjects and also to determine if hypoperfused areas of myocardium are larger than areas with fibrosis.

V.   To determine if the size and heterogeneity of LGE can predict appropriate ICD-therapy in ischemic and non-ischemic cardiomyopathy patients and if a newly developed weighted borderzone algorithm has similar predictive value as previously reported heterogeneity algorithms.

3. Materials and Methods

The protocols and procedures were approved by the ethics committee at Lund University (study II-V) and by the Institutional Committee on Animal Research at University California San Francisco (study I). Patients were recruited at Lund University Hospital (study II, IV, V). Subjects in study II and study IV provided written informed consent while the ethics committee at Lund University provided a waiver of individual consent for the clinical patients in study V.

3.1 Human studies (Study II, IV and V)

In *study II*, patients (n = 26) with a documented ST-elevation myocardial infarction (STEMI) treated with PCI and referred for viability assessment on CMR were prospectively included.

In *study IV*, patients < 30 years of age were identified and recruited at the Departments of Pediatric and Adult Cardiology at Lund University Hospital and referred for a stress CMR examination. Participants were defined as either HCM patients or HCM-risk subjects using the following criteria: i) HCM (n = 12): LV wall thickness exceeding 13 mm (subjects >18 years of age) or > 3 SD on Z-score (pediatric patients) on echocardiography with confirmed increased wall thickness and/or fibrosis on CMR, ii) HCM-risk (n = 15): either a HCM gene mutation or first degree relatives with HCM, but without signs of LVH or LGE on CMR. Exclusion criteria were: LV outflow tract obstruction, LVH due to other causes including congenital heart disease, malformation syndromes, neuromuscular and metabolic disorders. Gender and age-matched controls were included (n = 9).

In *study V*, patients (n = 115) with systolic heart failure undergoing primary or secondary prophylactic treatment with ICD between 2002 – 2013 at Lund University Hospital and who had undergone a CMR examination were retrospectively included. Patients were divided into either ischemic cardiomyopathy (ICM) and non-ischemic cardiomyopathy (NICM).[183] Criteria for ICM were (i) history of MI in medical record, (ii) previous PCI or CABG, or (iii) significant angiographic stenosis: ≥ 70% in > 1 epicardial artery or ≥ 50% in left main or proximal LAD. Patients not fulfilling the criteria for ICM were classified as NICM. Patient outcome was appropriate ICD-therapy for ventricular tachycardia or ventricular fibrillation (defined as anti-tachycardia pacing, shock or both).

3.2 Animal studies (Study I, II, III)

Study I. An overview of the experimental protocol in study I is shown in Figure 3.1. Animals were anesthetized using a mixture of isoflurane (2 – 5%) and Oxygen. Farm pigs (33 ± 1 kg) underwent baseline CMR before subsequent microembolization. CMR was then performed at one hour and 7 – 8 weeks after microembolization for detection of the effects on myocardial function, perfusion and viability. A hybrid X-ray and CMR system, was used to place a catheter in the LAD artery, to deliver the microemboli and to quantify the LV function. A 3F-catheter (Infusion Catheter: Cook, Chicago, Ill.) was placed distal to the first diagonal of the LAD under X-ray guidance. With the catheter in place the animal was moved to the MR-scanner where an intra-arterial injection of diluted Gd-DOTA (10ml 10%, Dotarem, Guerbet, France) was performed. LGE imaging immediately after injection was used to delineate the area at risk (AAR).[184] Microembolization was performed through the 3F catheter using an infusion of 250 000 microemboli with a diameter between 40 – 120 μm (Embosphere, Biosphere Med, Rockland, MA). Animals were euthanized using saturated potassium chloride. The hearts were excised and sliced into 10 mm thick slices for histopathology.
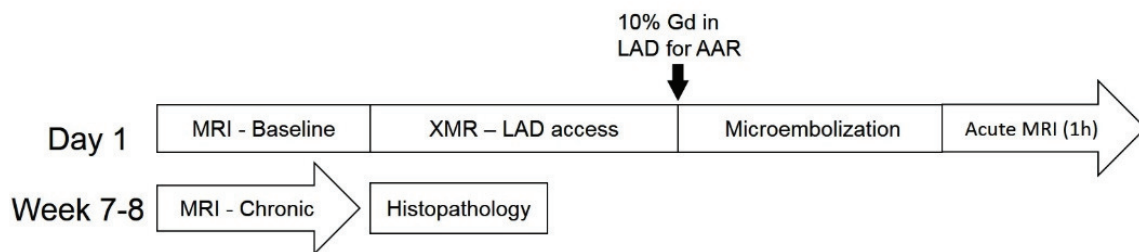

Figure 3.1 Overview of the experimental protocol in study I. See text for details.

Study III. An overview of the experimental protocol in study III is shown in Figure 3.2. After overnight fasting with free access to water, pigs (weighing 30 - 40 kg) were pre-medicated with ketamine 15 mg/kg (Ketaminol, Intervet, Danderyd, Sweden) and xylazin 2 mg/kg intramuscularly (Rompun, Bayer AG, Leverkusen, Germany). Anesthesia was induced with thiopental 12.5 mg/kg (Pentothal, Abbot, Stockholm, Sweden) and maintained with infusion of 10 mcg/kg/h fentanyl (Fentanyl, Pharmalink AB, Stockholm, Sweden), 0.5 mg/kg/h midazolam and 10 mg/kg/h ketamin during instrumentation, transportation and imaging. Pigs were subjected to 40-minutes LAD occlusion. The balloon-occlusion was placed either after the first or after the second diagonal branch of the LAD followed by six hours (n = 9) or seven days (n = 9) of reperfusion. After reperfusion in-vivo imaging was performed with 0.2 mmol/kg Gd-DOTA (Dotarem) administrated intravenously before LGE-CMR. An additional 0.2 mmol/kg Gd-DOTA was administered 41 ± 7 minutes following the first contrast injection as well as 1000 megabecquerel of ^{99m}Tc-DTPA 15 minutes prior explantation. Pigs were euthanized with potassium chloride and the hearts explanted and suspended in a plastic container with the atria excised and filled with balloons containing

50

deuterated water in the ventricles for *ex vivo* imaging. The hearts were then cast in a solution of 2 % agarose (Sigma Aldrich, Stockholm, Sweden) and sliced into 5 mm thick slices. For each animal, two to four consecutive slices with infarct by TTC were chosen, and 2 mm cylindrical biopsies were taken from four regions. One biopsy per slice was taken in remote myocardium, 3-4 biopsies in myocardium at risk (MaR) defined as part of the salvaged myocardium (i.e. with 4-6 mm proximity to the infarct), 2-3 biopsies in the peri-infarction zone within the salvaged myocardium defined as the myocardium adjacent to the solid infarct (approximately 2 mm from the TTC-negative tissue) and one biopsy in the infarction. Biopsies were analyzed in a gamma counter and with light microscopy.

In study II, animals followed the same initial protocol as in study III but were euthanized following four hours of reperfusion after administration of 0.2 mmol/kg Gd–DOTA 30 minutes prior explantation of the heart. Whole heart e*x-vivo* imaging was performed after explantation, as described above.

3.3 Magnetic resonance imaging

Imaging was performed on a 1.5 T MR system (Philips Achieva, Best, Netherlands or Siemens Magnetom Vision, Erlangen, Germany). In study I, an XMR, a hybrid x-ray (Integris V5000, Philips Medical Systems, Best, the Netherlands) and CMR (Achieva I/T) system, was used. *Ex vivo* imaging was performed using a simulated ECG with heart rate 60/min using a head coil. Images were analyzed using the software Segment v1.7 or above with the exception of Tagged MRI which was analyzed using the HARP software (Diagnosoft Inc, Palo Alto, CA).

3.3.1 Left ventricular function and mass

Left ventricular (LV) function was assessed, with the patient or animal in supine position, by cine imaging in breath hold both in short axis and long axis projections. The cine images were acquired using either a steady state free precession (SSFP) sequence
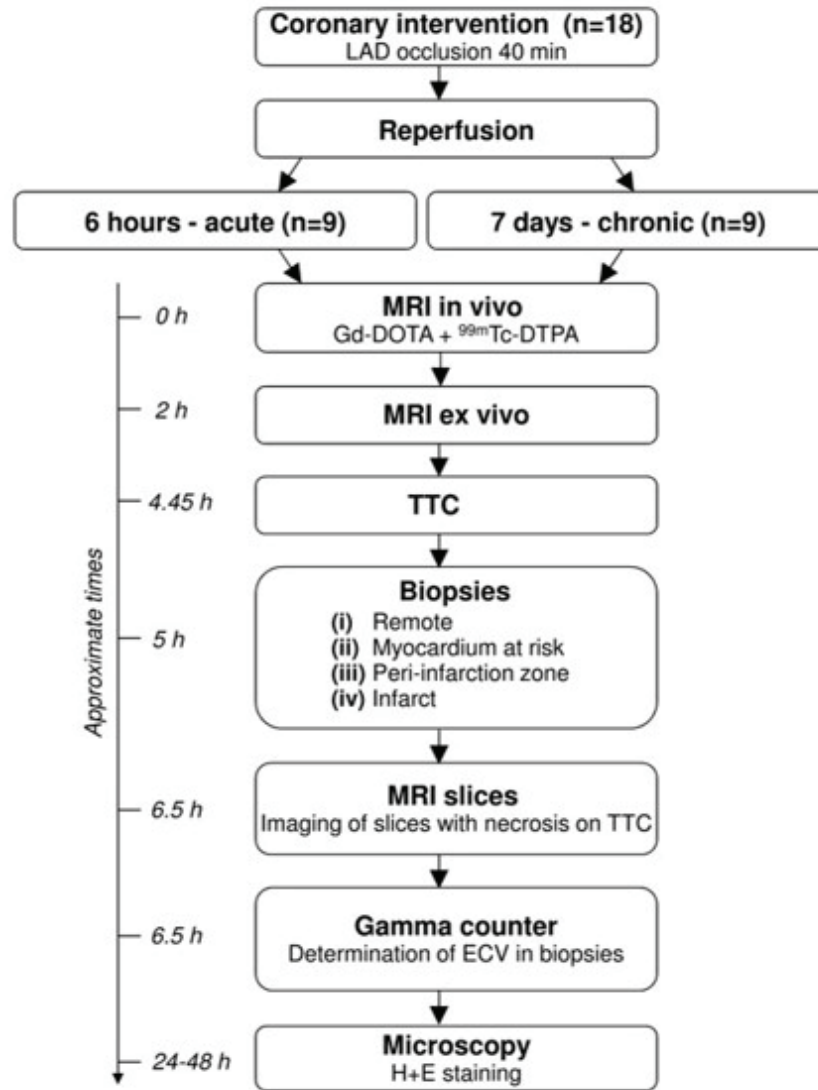
Figure 3.2 Overview of the experimental protocol in study III. See text for details.

(Philips) or a cine gradient recalled-echo (GRE) sequence (Siemens). The cine SSFP sequence was retrospectively ECG-gated (TE/TR = 1.4/2.9 ms; flip angle 60°; image resolution 1.5 × 1.5 × 8 mm and no slice gap). The cine GRE sequence was prospectively ECG-triggered (image resolution 1.6 × 1.6 × 8 mm; slice gap 2 mm and temporal resolution 50 ms).

In study I, cine images were acquired using a SSFP sequence with slightly different parameters (TR/TE/flip angle = 3.5 ms/1.75 ms/70°, spatial resolution 1.0 × 1.0 × 10 mm). Phase contrast MR images for quantification of longitudinal strain were acquired in three long-axis views with a phase contrast velocity encoded fast-field echo sequence (TR/TE/flip angle = 23.4 ms/4.8 ms/15°, spatial resolution 1.6 × 1.6 × 7 mm, VENC = 20 cm/s). Tagged MR images for circumferential strain in the short-axis plane were acquired using a tagged turbo-field echo-planar sequence (TR/TE = 35/6.1 ms, flip angle 25°, spatial resolution 1.0 ×1.0 ×10 mm).

3.3.2 Perfusion

In study IV first-pass perfusion (FPP) images were acquired in three short axis-slices at basal, midventricular and apical levels. Regional perfusion imaging was performed with a balanced Turbo Fast Field Echo (TFE) sequence in breath hold (TR/TE = 2.7/1.4, flip angle 50°, acquired spatial resolution 2 x 2 x 10 mm reconstructed to 1.4 x 1.4 x 10 mm and SENSE factor 3). Images were acquired during the first pass of a bolus of Gd-DOTA (0.05 mmol/kg, injection rate 5 ml/s) followed by a saline flush (injection rate 5 ml/s). Images were acquired during both adenosine (140 μg/kg/min) hyperemia and at rest. In study I, FPP images were acquired during administration of 0.1 mmol/kg Gd-DOTA with an injection rate of 3 ml/min. Four short-axis slices were acquired with a saturation-recovery gradient-echo sequence (TR/TE = 4.5/2.2 ms, flip angle = 20°, image resolution $1.0 \times 1.0 \times 10$ mm).

3.3.3 Late gadolinium enhancement and edema

In vivo. Late gadolinium enhancement (LGE) *in vivo* imaging was performed using a 2D-IR GRE (Siemens) or a 2D-PSIR and/or 3D IR GRE sequence (Philips). Images were triggered by ECG and acquired during mid diastole. The 2D sequence was acquired slice by slice during breathold whereas the 3D sequence was acquired five slices per breathold. Short-axis slices covering the entire LV and three long-axis projections were collected 10 - 30 minutes after administration of 0.2 mmol/kg of gadolinium based contrast agent.

Typical image parameters for the 2D-IR (Siemens) were: TE 3.4 ms, effective repetition time every second heartbeat, flip angle 25°, slice gap 2 mm, slice thickness 8 mm and in-plane resolution 1.6×1.6 mm. The 2D-PSIR sequence (Philips) had similar parameters except: TE 4 ms, no slice gap and in-plane resolution 1.4×1.4 mm. The 3D-IR sequence parameters were (Philips): TE 1.3 ms, effective repetition time every heartbeat, flip angle 15°, slice gap 0 mm, slice thickness 8 mm and inplane resolution 1.5×1.5 mm. The inversion time was chosen to optimally null the myocardium.

In study I, LGE images were acquired after 5 – 10 minutes, because of faster wash-in and wash-out of Gd in microinfarcts, after an additional 0.05 mmol/kg Gd-DOTA injection using a 2D IR GRE sequence (TR/TE = 5 ms/2 ms, flip angle 15°, shot interval 2RR intervals, spatial resolution $1.1 \times 1.1 \times 4$ mm), following the perfusion imaging. A T2-weighted short tau inversion recovery (T2-STIR) sequence was used to assess MaR *in-vivo* (TE 100 ms, repetition time 2 heart beats, number of averages 2, TI 180 ms, image resolution 1.5×1.5 mm, slice thickness 8 mm, slice gap 2 mm).

Ex vivo. Sequence parameters for e*x vivo* imaging (short-axis) with 2D-PSIR and 3D-IR were the same as *in vivo,* but with a spatial resolution for 2D-PSIR of $0.6 \times 0.6 \times 4$ mm and for 3D-IR of $1 \times 1 \times 4$ mm. In study II and III a high resolution T1w *ex vivo* sequence was performed.[172] Acquisition typically resulted in 200 - 220 image slices

per heart with an acquisition time of 30 - 40 minutes. Typical sequence parameters were: TE/TR = 3.2/20 ms, flip angle 70°, slice gap 0 mm, spatial resolution 0.5 × 0.5× 0.5 mm. For *ex vivo* MaR imaging a T2-weighted turbo spin echo (T2-TSE) sequence was used (TE 60 ms, repetition time 2 heart beats, number of averages 2, black blood inversion delay 574 ms, slice thickness 4 mm, slice gap 0 mm and no parallel imaging).

Ex-vivo imaging of the TTC stained-slices with apparent necrosis was performed with the same T1w sequence as described above.

3.4 Image analysis

3.4.1 Left ventricular function and mass

Left ventricular mass (LVM), LV ejection fraction (LV-EF), end-diastolic volume (EDV) and end-systolic volume (ESV) and regional end-diastolic LV wall thickness were determined by first manually delineating the endocardium and epicardium in short-axis cine images at both end systole and end diastole. LVM was calculated by multiplying the myocardial volume measured by planimetry with the myocardial density (1.05 g/ml). In study II and III LVM was calculated on LGE-CMR *in vivo* and contrast-enhanced T1w images *ex vivo* by delineating the endo- and epicardium. For all image analysis, the delineation of the endocardium included papillary muscles and trabeculations as LV volume.

In study I, systolic wall thickening in percent was quantified by dividing the difference in wall thickness in systole and diastole by the thickness in diastole and multiplying by 100 as a measure of radial strain.

PC-strain images were analyzed by a semi-automated method where the myocardial contours are manually drawn on the end-diastolic time frame followed by an automated myocardial contour tracking. A strain tensor was calculated from the velocity information and decomposed into the longitudinal direction for quantification of longitudinal circumferential strain.[153] Cine, Tagging and PC-strain images were correlated with FPP and LGE images to define regions of microinfarcts and remote myocardium.

3.4.2 Perfusion

In study IV, FPP images were delineated by semi-automatically tracing the endocardium and epicardium in all time frames. The slices were divided according to the American Heart Association 17-segment model[185] with the apex being left out. The delineated contours were contracted by ten percent both endo- and epicardially to account for partial volume and interaction with the blood pool. Upslope ratio

(stress/rest) normalized for the LV arterial input function was used to assess perfusion.[154] Co-registration between cine, LGE and perfusion short-axis images was performed to identify segments that were hypertrophied (LVH+) or of normal wall thickness (LVH-), hyperenhanced on LGE (LGE+) or not (LGE-). The upslope analysis was performed on a segmental basis and also on a per subject level by averaging all segments with the same tissue classification. An assessment of the hypoperfused area (expressed as an average percentage of the short-axis LV surface area for all perfusion slices) at rest and stress was performed and compared to the hyperenhanced region on the corresponding LGE short-axis slice.

In study I, FPP images at rest were used to determine max upslope, peak signal intensity and time to peak in the LV blood pool, areas of microinfarcts and remote myocardium.
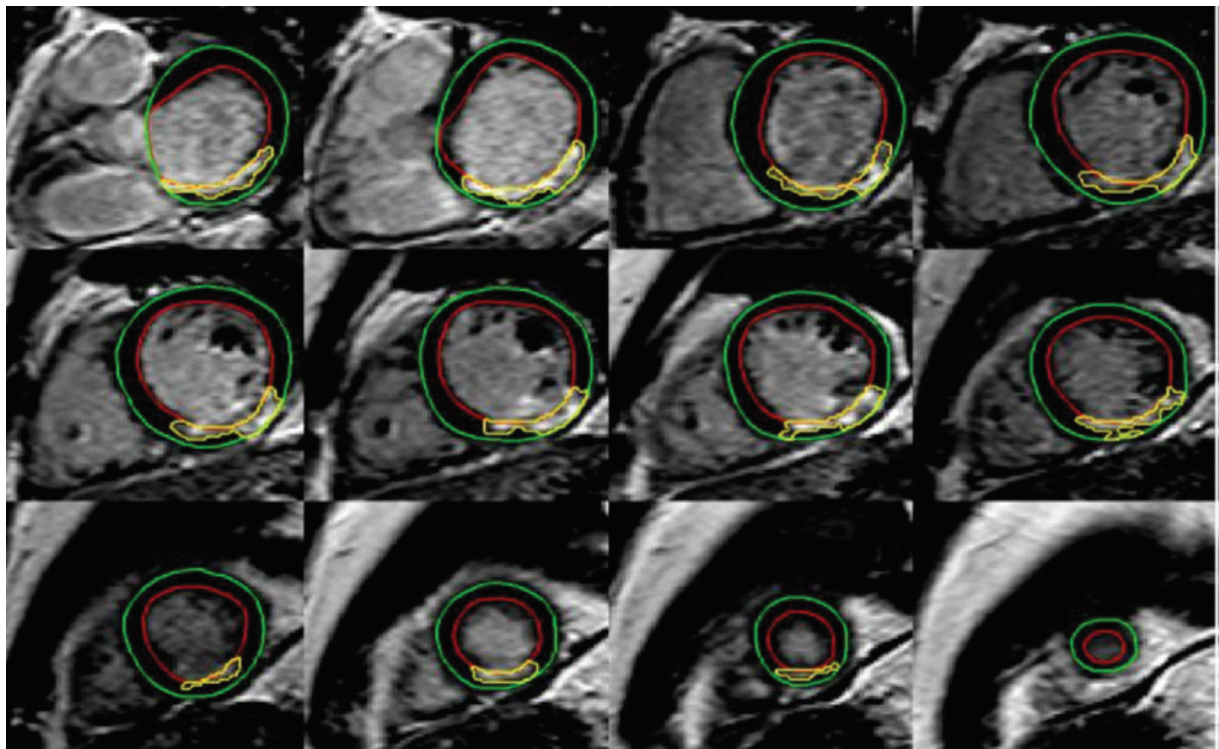

Figure 3.3 Example of delineation of LGE images in a patients with a myocardial infarction. Short-axis images are shown from base (top left corner) to apex (bottom right corner). Green line = epicardium, red line = endocardium, yellow line = infarction.

3.4.3 Late gadolinium enhancement and myocardium at risk

Total hyperenhancement on LGE images was quantified on short-axis images after delineating the endocardial and epicardial borders using a weighted semi-automatic algorithm[180] with manual corrections where necessary, Figure 3.3. In study V, both total, core and the LGE borderzone was quantified using three different algorithms (i)

weighted semi-automatic algorithm,[180] (ii) a modified full-width half-maximum (FWHM) algorithm,[77] and (iii) a 2-3 SD threshold method,[79] shown in Figure 4.14. In study I, the total size of the microinfarcts were quantified on LGE-images by selecting regions with > 3SD above the signal intensity of remote myocardium.

In study II and III, on contrast-enhanced high resolution T1w images, scarred myocardium was quantified using a threshold in signal intensity of 8 SD above normal remote myocardium.[180]

Ex-vivo MR images of TTC-stained slices were analyzed on both basal and apical sides using the same threshold methodology as for *ex vivo* whole heart analysis. The outermost layer of the *ex-vivo* MRI slices was identified using a novel off-line post processing method, enabling direct comparison with photographed TTC slices.

Manual corrections were also applied when necessary. Areas of microvascular obstruction, if present, were included as infarction. Myocardial infarct size was express as either as volume in milliliters, grams, percentage of the LVM or percentage of slice area. The LGE borderzone was expressed as a percentage of total scar.

In-vivo T2-STIR and *ex vivo T2-TSE* images were manually delineated.[186] Using MaR from *ex vivo* T2-TSE, the myocardial salvage index, 1-(infarct size/MaR), was calculated both acutely and at seven days using infarct size from both *ex-vivo* high resolution T1w MRI and TTC. Maximal wall thickness in infarcted and remote myocardium was measured on *in-vivo* LGE images in short axis slices. An example of delineations of *in vivo LGE*, *ex vivo* T1w and *ex vivo* T2w images is shown in Figure 3.4.

Mean infarct transmurality was also calculated by assessing the radial extent of the infarction between the endocardial and epicardial borders around the circumference at 4.5° intervals of short-axis LGE images.

3.5 Histopathology

In study I, myocardial slices (10 mm) were soaked for 15 min in 2% triphenyltetrazolium chloride (TTC). Representative tissue samples were taken from the areas with microinfarcts and remote myocardium and stained with hematoxylin-eosin (H+E) or Masson's trichrome.
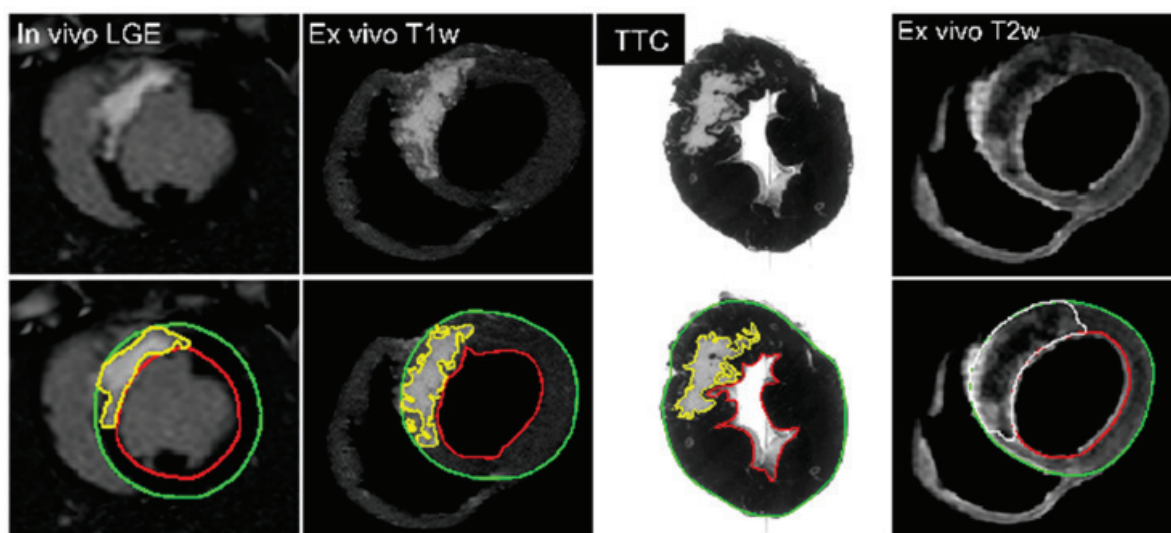
Figure 3.4 Example of infarct delineation in a short-axis slice on *in vivo* LGE, *ex vivo* T1w, TTC and of myocardium at risk on a *ex vivo* T2w image in one pig with acute MI. Green line = epicardium, red line = endocardium, yellow line = infarction, white line = myocardium at risk.

Histopathology was used to confirm the delivery of microemboli to the target region, as well as to establish formation of scarred lesions at 7 - 8 weeks. In study III, myocardial slices (5mm) were incubated in TTC dissolved in a buffer (pH 8.5) for five minutes at 35-37°C. Slices were photographed in blue light for analysis of infarction. Furthermore, TTC stained slices were analyzed by manually delineating the endocardium and epicardium, Figure 3.4. The infarct was delineated manually on both apical and basal sides and the infarct size was calculated as a mean of the infarcted surface area on the apical and basal side of the slice multiplied with the slice weight.

Representative formalin-fixed biopsies from remote, salvaged MaR, peri-infarction zone and infarction were stained with H+E and examined under light microscopy.

3.6 Extracellular volume analysis

Extracellular volume (ECV) from biopsies containing ^{99m}Tc-DTPA was calculated using a gamma counter. Since ^{99m}Tc-DTPA distributes in the extracellular space similar to Gd-DOTA,[163] ECV was calculated using Equation 1.

$$(1) \quad ECV = (counts_{biopsy} / weight_{biopsy}) / (counts_{plasma} / weight_{plasma})$$

The average ECV for each region was calculated in each animal and subsequently used in the analysis. However, the LV slices were stained with TTC and rinsed in water prior to punching biopsies, which may wash out ^{99m}Tc-DTPA from the surface of the slices.

Therefore, ECV from biopsies taken were corrected for ECV from remote myocardium (21 ± 1%) obtained from four pigs without any intervention, imaging or TTC staining. This design assured that biopsies were taken in desired regions of the myocardium. ECV on microscopy in remote and salvaged MaR was analyzed by a manually set threshold to differentiate the extracellular space from viable myocytes and calculated as (extracellular space/total area) × 100.

3.7 Statistical analysis

Calculations and statistics were performed using Graph Pad Prism 5.0 software (Graph Pad Software, Inc., La Jolla, CA, USA) or IBM SPSS Statistics (version 22, Armonk, New York, USA). Differences with a $P < 0.05$ were considered statistically significant. Results are expressed as either mean ± SEM, mean ± SD or median and range as appropriate. For normally distributed data paired and unpaired t-test were used to assess variance between data. Variance in data not normally distributed was assessed by the Mann-Whitney test or Wilcoxon matched pairs test.

Correlation between variables was assessed by linear regression analysis using the Pearson and Spearman's rank-order correlation for normal and not normally distributed data respectively. Differences between two methods was assessed using Bland-Altman plots with the difference plotted against the average of the methods.

In study III, when using TTC as reference standard for MRI infarct size, bias was calculated as (MRI-TTC)/TTC × 100. A random intercept mixed model was also performed to correct for multiple observations (i.e. slice by slice analysis) within animals.

In study IV, the Kruskal-Wallis test with Dunn's post hoc test was used to compare parameters between different groups and myocardial segments.

In study V, ANOVA with Student's t-test as post-hoc test was used to assess continuous variables Event-free time was assessed by Kaplan Meier curves using the log-rank test stratified by median borderzone. Univariate Cox-regression analysis was used to assess the hazard ratio for LGE characteristics and LV-EF on the primary endpoint. Hazard ratio was expressed as risk increase (or decrease, as appropriate) per 1% increase in scar or borderzone volume.

4. Results and Comments

4.1 Coronary microembolization (Study I)

Microembolization has been shown to contribute to the pathophysiological injury during ST-elevation myocardial infarction (STEMI)[187] and coronary interventions for stable angina.[188] The long-term effects of microemboli on regional left ventricular (LV) strain and global LV function in experimental models have not been examined by MRI. Furthermore, there is no data on the effects of small-sized microemboli on perfusion and viability. Therefore, we examined the long-term effects of microemboli on LV-function and also if perfusion and LGE patterns differed at the acute stage between small (40 – 120 μm) and large (100 – 300 μm), previously studied,[69,189] microemboli.

Table 4.1 shows that the small microemboli caused severe global LV dysfunction at the acute phase, which completely recovered at 7 – 8 weeks. There was no difference in the global LV function parameters at one hour between small and large microemboli.[69,189] Homogenous infarcts cause a more severe decline in cardiac function at 7 – 8 weeks compared to microemboli.[190]

Table 4.1 Global LV function for small and large microemboli. Data from large size microemboli and homogenous infarct are shown as comparison. *indicates P < 0.05 compared to baseline MRI. indicates † P < 0.05 compared to microinfarcts at 7 – 8 weeks caused by the 40 – 120 μm sized microemboli.§ indicates that this data is erroneous in appended Paper I, Table II for 100-300 μm microemboli, correct data is shown here.

	Baseline 40 – 120 μm	1 hour 40 – 120 μm	7 – 8 weeks 40 – 120 μm	1 hour [§ 69,189] 100 – 300 μm	7-8 weeks[190] homogenous infarct
Total infarct size (% LVM)		0.1 ± 0.0	6.6 ± 0.5	1.4 ± 0.2	13.2 ± 1.4 †
EF (%)	49.5 ± 2.6	32.5 ± 2.8*	47.5 ± 3.2	29.3 ± 0.8	37.0 ± 0.96 †
EDV/kg	2.14 ± 0.03	2.40 ± 0.06*	1.92 ± 0.10	2.54 ± 0.15	2.41 ± 0.09 †
ESV/kg	1.08 ± 0.06	1.62 ± 0.09*	1.00 ± 0.08	1.79 ± 0.12	1.51 ± 0.06 †
Heart rate (bpm)	84 ± 6	81 ± 4	88 ± 5	78 ± 4	88 ± 5
Weight (kg)	33.1 ± 1.3	33.1 ± 1.3	47.7 ± 2.4	33.8 ± 1.2	53.3 ± 1.0

Small microemboli resulting in microinfarction caused persistent decline in both longitudinal (Figure 4.1), circumferential (Figure 4.2) and radial strain assessed by systolic wall thickening (Figure 4.3). In areas of microinfarction, there was a partial recovery of longitudinal and radial strain at 7 - 8 weeks. However, circumferential strain showed a persistent decline over the course of 7 - 8 weeks. There was also an acute effect on regional strain in remote myocardium not subjected to microembolization with partial recovery at 7 - 8 weeks (Figure 4.1 - 4.3). The decline in remote regional wall function indicates a global effect of microembolization on LV function. These acute changes in remote myocardium could be linked to the concomitant changes in LV dimensions. However, the long-term effects of microembolization on LV function are probably caused by myocyte and interstitial remodeling resembling ischemic cardiomyopathy.[191]

Microinfarcts were detected at one hour as a perfusion defect on first-pass perfusion both visually and semi-quantitatively. The maximum upslope was lower in areas with microinfarcts compared to remote myocardium, the maximum signal intensity was lower and the time to peak was longer. No perfusion defect was detected by visual assessment at 7 - 8 weeks and semi-quantitative parameters revealed a minor decrease in regional perfusion in areas with microinfarcts. The perfusion results at one hour were similar to those published earlier for large microemboli.[69]

At one hour after microembolization, microinfarcts were not visible on LGE and quantitative analysis revealed negligible areas of enhancement but at 7 – 8 weeks LGE showed clear differential enhancement in the microembolized region. However, the LGE patterns did not differ at one hour or the follow-up phase between small and large microemboli.[69]

The LGE and first-pass perfusion findings are in line with those of Breuckmann et al.[192] where LGE was increasingly detected with longer delays (up to eight hours) in imaging after microembolization. Moreover, our study showed that first-pass perfusion discloses a perfusion defect at one hour after microembolization greater than that of the resulting microinfarcts at 7 - 8 weeks. Thus, the early perfusion defect is not only caused by mechanical obstruction of microvessels but can also be attributed to regional inflammation caused by the microembolization.[58]

At long-term follow up, however, the findings of LGE and first pass perfusion are reversed; LGE is clearly present but the perfusion defect is too subtle to be visualized. However, the perfusion defect can be detected by semi-quantitative assessment. Similar recovery of perfusion has earlier been observed in continuous macro infarction using perfusion SPECT.[193] Taken together, the perfusion and LGE findings of the present study are also in line with results from large emboli at subacute imaging (1 week).[69]
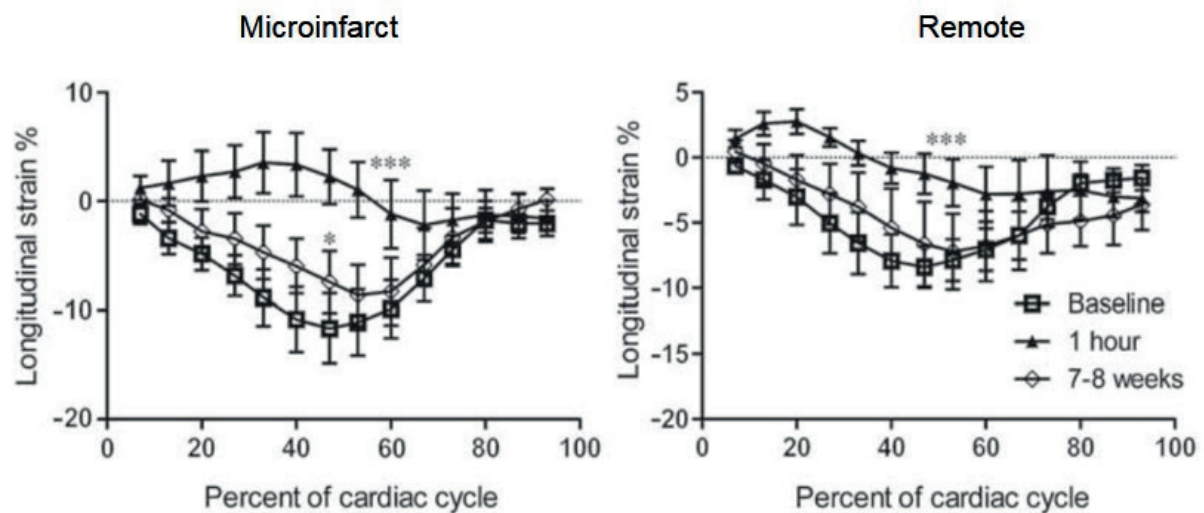
Figure 4.1 Longitudinal strain over the cardiac cycle decreased from baseline to one hour in both the area with microinfarcts (left) and remote myocardium(right). There was a partial recovery at 7 – 8 weeks for both areas. In the area with microinfarct there was still a minor reduction of longitudinal strain at 7 – 8 weeks compared to baseline. * $P < 0.05$ and *** $P < 0.001$ compared to baseline.
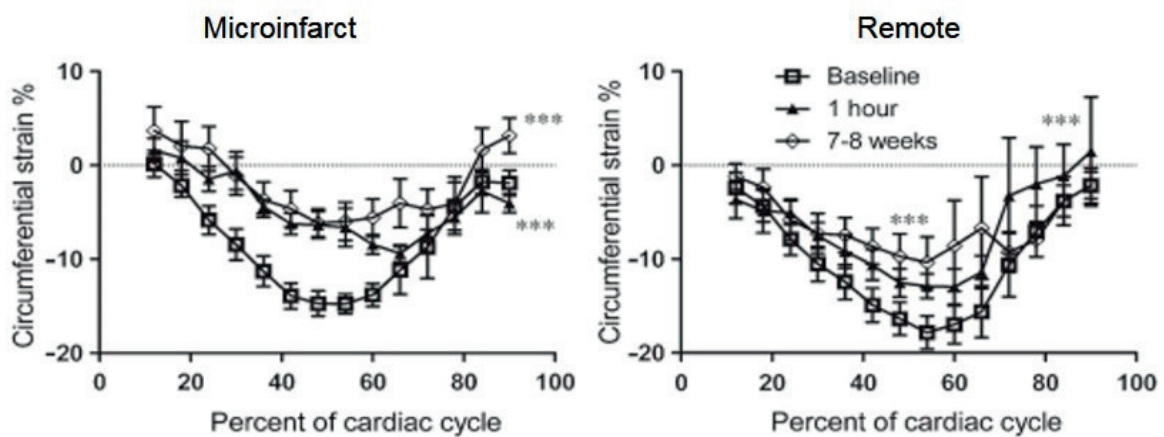

Figure 4.2 Circumferential strain over the cardiac cycle showed a persistent decline over the course of 7 – 8 weeks in both the area with microinfarcts (left) and remote myocardium (right). ***indicates $P < 0.001$ compared to baseline.
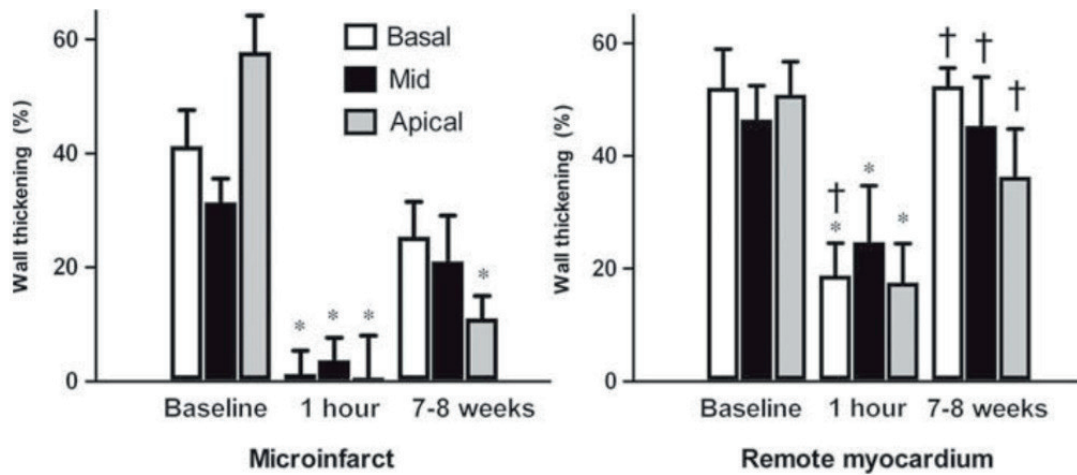
Figure 4.3 Systolic wall thickening in the area with microinfarcts (left) and remote myocardium (right) in three short axis slices through the embolized myocardium. At one hour, systolic wall thickening was reduced in areas with microinfarcts and remote myocardium in all slices through the embolized region. At 7 – 8 weeks, there was no difference in wall thickening compared to baseline in remote myocardium and a partial recovery of the function in areas with microinfarcts. However, wall thickening was decreased in areas with microinfarcts compared to remote myocardium at 7 – 8 weeks. *indicates $P < 0.05$ compared to baseline and † $P < 0.05$ compared to the area with microinfarcts within the same slice.

The findings of this experimental study warrant longitudinal studies on viability, perfusion and regional function in patients, for example undergoing coronary interventions for acute coronary syndrome and stable angina. The results of this study suggest that CMR may have the potential to determine the benefits of these devices and therapies.

4.2 Validation of 2D and 3D LGE for infarct quantification (Study II)

Both 2D- and 3D-LGE MRI sequences are used in clinical practice and in clinical and experimental studies for infarct quantification both *in vivo* and *ex vivo*. Previous studies have compared infarct quantification with different 2D-IR and 3D-IR sequences and have shown good agreement both in patients[194,195] and *in vivo* in animals.[195,196] However, 3D-IR has not been validated against 2D-PSIR in patients or compared to a high resolution T1 weighted (T1w) reference sequence *ex vivo*. Therefore, we investigated the agreement between a 2D-PSIR and 3D-IR sequence for measurement of infarct size in patients with acute and chronic MI. We also compared 2D-PSIR and 3D-IR with a reference high resolution T1w sequence in an experimental infarct model. Figure 4.4 shows an example of infarct quantification using 2D-PSIR and 3D-IR, respectively.

Figure 4.5 demonstrates a strong correlation and low bias for infarct size on 2D-PSIR and 3D-IR in absolute volume of infarct. Infarct size as part of the LVM also showed a low bias for the sequences (bias 0.16 ± 2.0%). The interobserver variability for infarct volume was similar for 2D-PSIR (-0.78 ± 2.8 ml) and 3D-IR (0.95 ± 2.9 ml). Furthermore, mean infarct transmurality did not differ between the two sequences (bias 0.52 ± 8.4) and there was good agreement of LV volumes for both sequences (bias = 5.5 ± 21 ml). The acquisition time was on average five times longer on 2D-PSIR (225 vs 45 seconds).
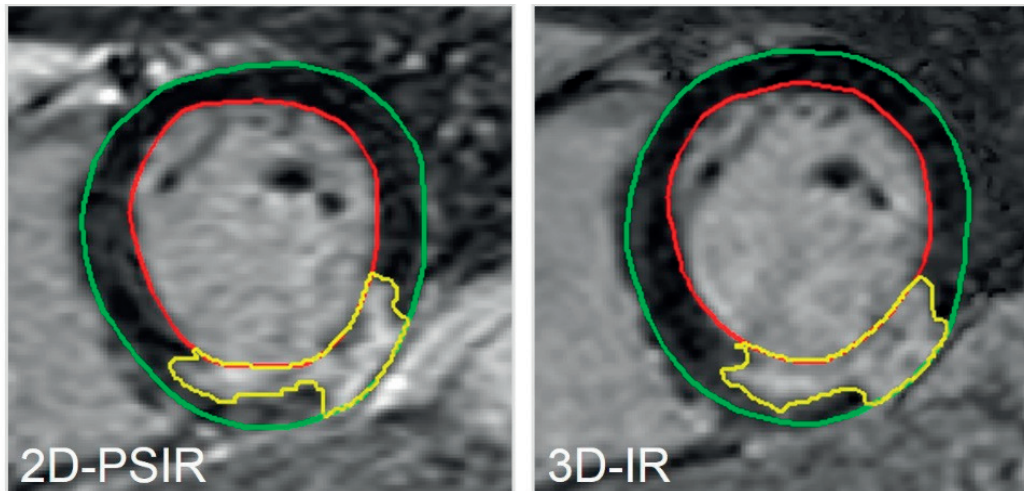

Figure 4.4 Representative short axis LGE-image in one patient with myocardial scarring. Left panel shows 2D-PSIR and right panel shows 3D-IR. Red line = endocardium, green line = epicardium and yellow line = infarction.

Previous studies comparing infarct size in patients using different 2D- and 3D-LGE sequences have shown good agreement using both a semiautomatic algorithm,[194] as in the current study, and visual assessment[197] for LGE-quantification. Furthermore, our results support previous findings by *Dewey* et al. [196] that showed good agreement between quantified infarct volumes comparing a 2D-IR and a single breath-hold 3D IR sequence (bias 0.3 ± 3.1 ml). Also, our findings are in line with *Goetti* et al.[194] who compared 2D- and 3D-IR GRE in patients with both acute, sub-acute and chronic infarction and found good agreement in all three groups with a mean difference of 0.26 ± 2.9 g infarct.
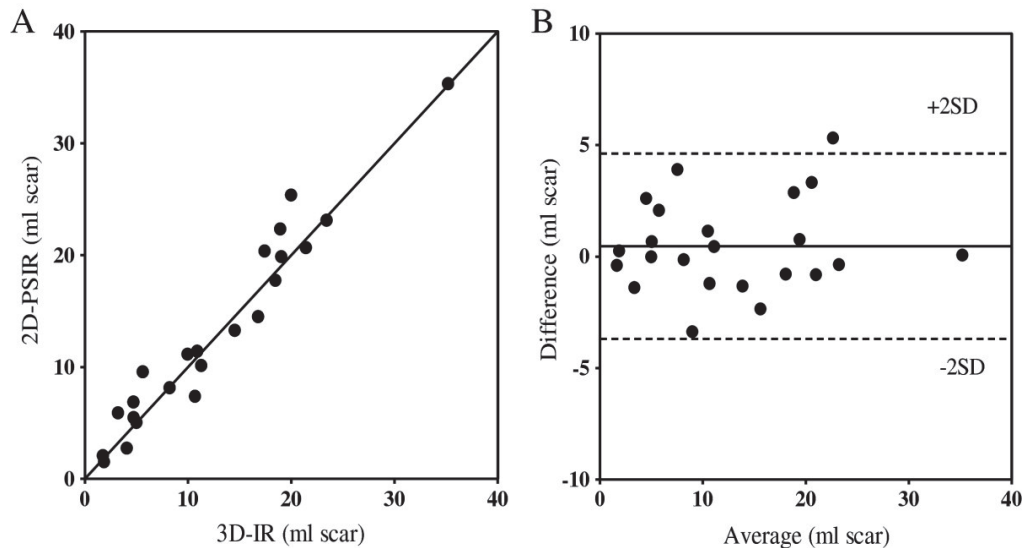
Figure 4.5 Patient infarct quantification. Agreement between 2D-PSIR and 3D-IR in absolute infarct volume in patients. (**A**) 2D-PSIR versus 3D-IR (r = 0.97) and the line of identity (**B**) The limits of agreement between the two LGE-techniques. The difference between the two methods was 0.47 ± 2.1 ml scar. Solid line = mean difference; dashed lines = ± 2 SD.

Figure 4.6 demonstrates that 2D-PSIR and 3D-IR sequences, *ex vivo,* correlated and showed a low bias for infarct size as part of the LVM. However, both LGE sequences overestimated infarct size compared to the high resolution T1w sequence when used *ex vivo.*
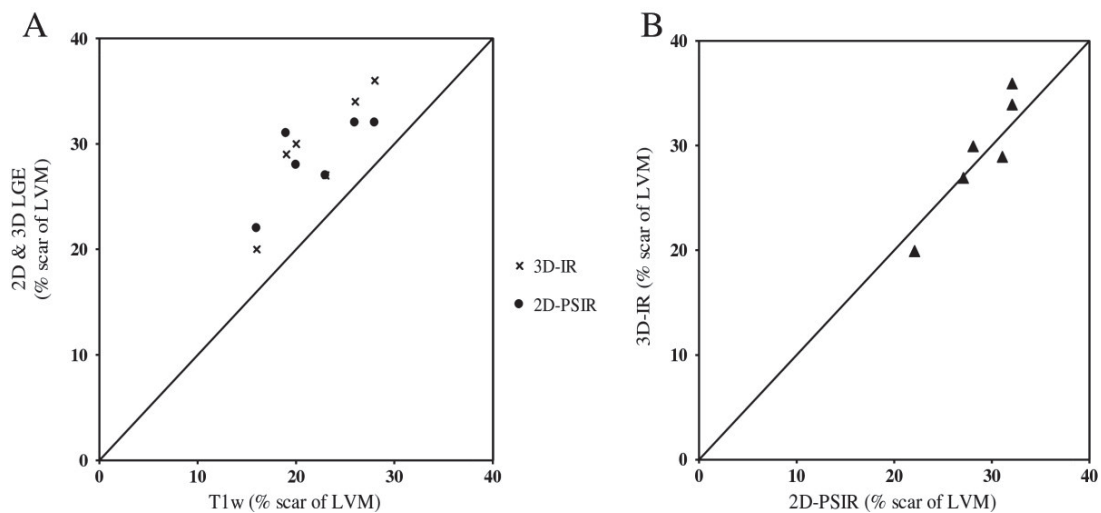

Figure 4.6 Ex vivo infarct quantification. (**A**) Agreement between the high resolution T1 weighted sequence compared to 2D-PSIR and 3D-IR ex vivo. The bias was 6.7 ± 3.0% for the 2D-PSIR sequence and 7.3 ± 2.7% for the 3D-IR sequence (*P* < 0.05 for both). (**B**) Agreement between the 2D-PSIR and 3D-IR sequence ex vivo. Each black triangle represents one pig. The bias was 0.67 ± 2.4% and r = 0.93. Solid line = line of identity in both panel A and B.

Previous studies in pigs comparing 2D and 3D LGE have besides showing good agreement for *in vivo* imaging also performed histopathological analysis.[195,196] Those studies showed good agreement with histochemical TTC staining in infarct transmurality and volume quantification using visual assessment.[195,196]

In our study, we found an overestimation of infarct volume with both 2D- and 3D LGE compared to the high-resolution T1w sequence. Furthermore, the *ex vivo* T1w reference sequence used in the current study has been validated against histopathology with TTC-staining.[172] The difference from previous studies[195,196] can possibly be attributed to the use of an objective semi-automatic method, 8SD threshold algorithm,[180] for infarct quantification as compared to visual assessment. Further work in study III also compared the *ex vivo* T1w sequence to histopathology with TTC as reference standard both in acute MI and at seven days.

The implication of this study is that infarct size quantification in patients with both acute and non-acute infarcts on LGE-MRI using two different sequences, 2D PSIR and 3D IR, can be pooled together. This may be beneficial for patient recruitment in the setting of a multi-center study providing the use of similar MR-scanners.

4.3 MRI overestimates AMI compared with histopathology (Study III)

The overestimation of infarct size by LGE-MRI compared to histopathology with TTC, due to a reversibly injured peri-infarction zone that hyperenhances early after acute MI, has been controversial.[172,175] We sought to investigate if the reported overestimation by MRI versus TTC remains after seven days in an experimental pig model and further elucidate the mechanism behind hyperenhancement of the peri-infarction zone early after acute MI.

In pigs with acute MI, infarct size measured on MRI *in vivo* did not differ from *ex-vivo* imaging. However, infarct size quantified on *ex-vivo* MRI was larger compared with quantification of necrosis using TTC in whole hearts ($11.8 \pm 3.4\%$ vs. $9.4 \pm 3.0\%$, $P = 0.008$). This overestimation (bias: $27 \pm 22\%$) is demonstrated in Figure 4.7 A-B.

In contrast to the findings acutely, there was no significant difference in infarct size between *in-vivo*, *ex-vivo* MRI and TTC at seven days. Thus, there was no overestimation of infarct size by *ex-vivo* MRI vs. TTC at this time point (bias:$-5.8 \pm 15\%$, Figure 4.7 C-D). A larger area of hyperenhancement on MRI compared to the corresponding necrotic area on TTC indicates an increased distribution volume for Gd-DOTA in the peri-infarction zone acutely.
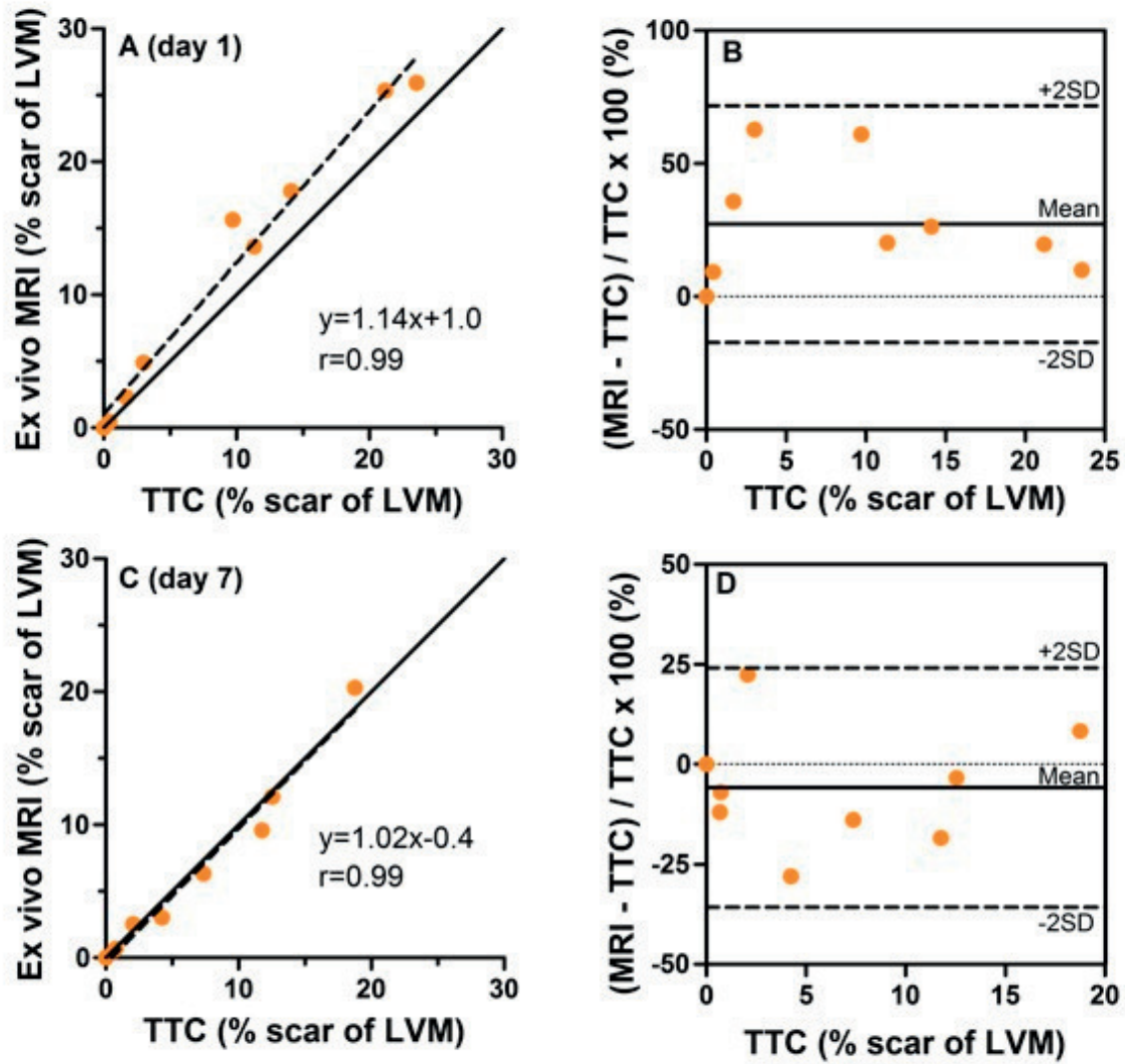
Figure 4.7 Whole heart infarct quantification with *ex vivo* MRI and TTC (**A**) *Ex vivo* MRI versus TTC as reference standard in AMI. (**B**) Bias in AMI: 27 ± 22%. (**C**) *Ex-vivo* MRI versus TTC at seven days. (**D**) Bias at seven days: -5.8 ± 15%. Thus, infarct size is overestimated by *ex-vivo* MRI acutely but not at seven days. Left panels: solid lines = line of identity, dashed lines = linear regression.
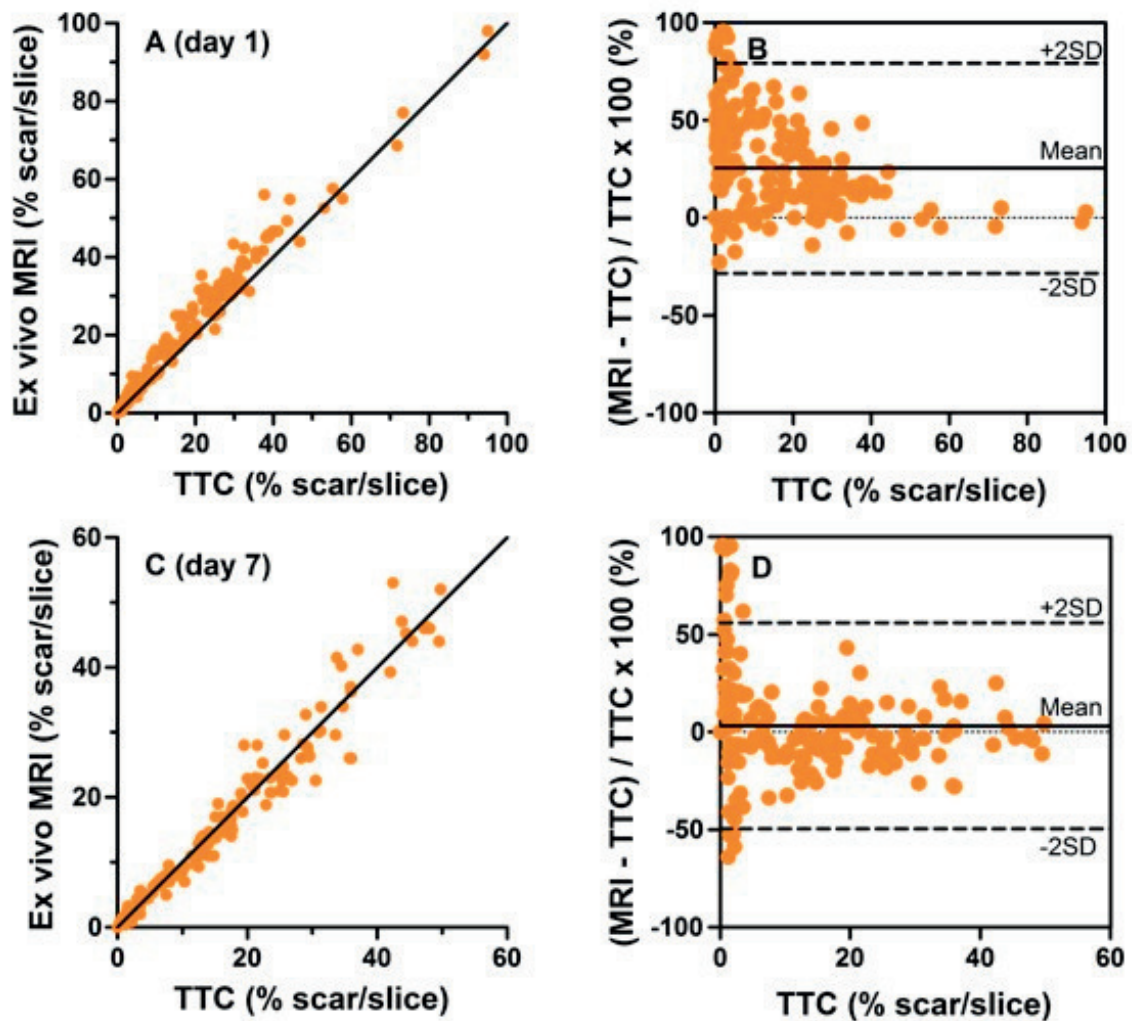
Figure 4.8 Slice-by-slice comparison of infarct size between *ex-vivo* MRI and TTC. (**A**) *Ex-vivo* MRI versus TTC as reference standard in AMI. (**B**) Bias in AMI: 26 ± 27%. (**C**) *Ex vivo* MRI and TTC at seven days. (**D**) Bias in MI at seven days: 3.2± 26%. *Ex-vivo* MRI overestimated infarct size compared to TTC acutely but not at seven days. Left panels: solid lines = line of identity.

These findings are in line with previous experimental studies demonstrating an overestimation of infarct size in acute MI with *ex-vivo* MRI compared to TTC-staining.[175,176,198] In contrast, *Kim* et al.[172] showed a close agreement of infarct size on *ex-vivo* MRI and TTC at one day, three days and at eight weeks after infarction and concluded that hyperenhanced areas on MRI can be equated with irreversibly injured myocardium. However, they did not exclude the possibility of enhancement of a peripheral region surrounding the infarction that resolves by 24 hours.

Furthermore in the current study, a slice-by-slice comparison between corresponding *ex-vivo* MRI and TTC slices also showed an overestimation of infarct size acutely, demonstrated in Figure 4.8 A-B. Also, in line with the whole heart findings, corresponding *ex-vivo* MRI and TTC stained slices showed a low bias at seven days seen in Figure 4.8 C-D. A comparison between *ex-vivo* MRI and corresponding

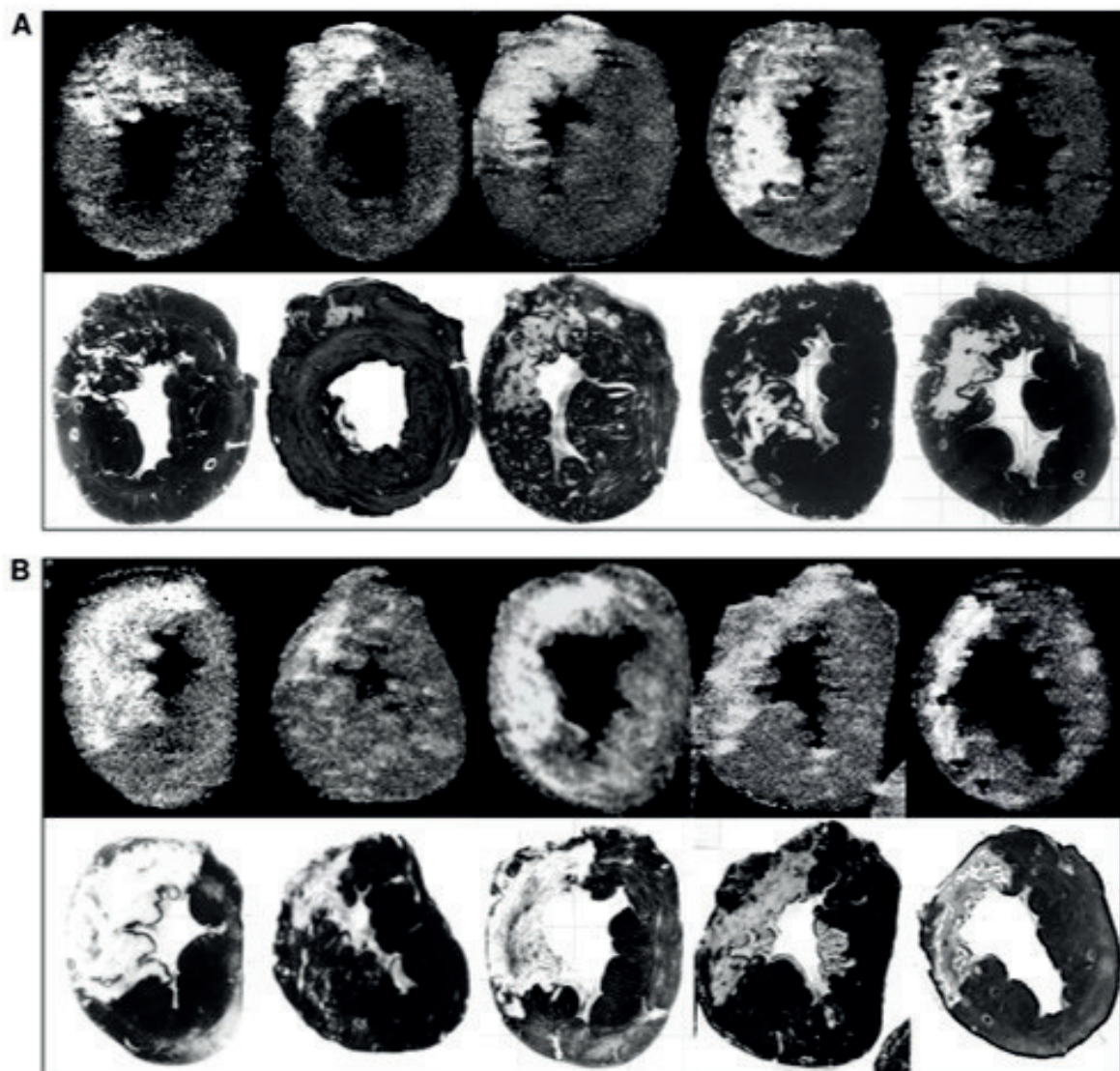TTC slices in five animals after acute MI and MI after seven days, respectively, are shown in Figure 4.9.

Figure 4.9 Corresponding MRI (top row) and TTC (bottom row) slices acutely (**A**) and at seven days (**B**) after re-scanning the photographed TTC stained slices. Note the hyperenhanced areas (white) on MRI without apparent necrosis (bright areas) on the corresponding TTC slices acutely, not seen at seven days.

Furthermore, myocardial salvage index with infarct size on *ex-vivo* MRI was significantly smaller than with infarct size on TTC acutely, but at seven days there was no significant difference. However, the ratio between infarct size on TTC and myocardium at risk was constant over seven days. This highlights that if myocardial salvage in cardioprotective clinical trials is assessed too early after infarction it may render false negative results due to the overestimation of infarct size acutely.

Figure 4.10 demonstrates differences in ECV between different regions at the two time points. There was no statistically significant difference in ECV acutely compared to seven days in salvaged MaR. There was, however, a significant decrease in the peri-

infarction zone. A decrease of ECV in the infarction was also seen over seven days, which is likely attributed to resorption of edema and possibly to infiltration of inflammatory cells. Furthermore, ECV in the peri-infarction zone was significantly higher than in salvaged MaR acutely but not at seven days.

These results are in line with data demonstrated by *Arheden* et al.[163,166] who showed an increased ECV in the salvaged MaR compared to normal myocardium, similar to the present study.

Also, in the current study, ECV by planimetry of microscopy images was higher in salvaged MaR compared to remote myocardium acute and at seven days demonstrating independently that the elevated ECV in salvaged myocardium remained at seven days. This is in line with the biopsy findings in the present study and previous work in humans[157] and provides independent pathophysiological evidence for the validity to use T2-weighted MRI or T1-mapping before and after contrast providing ECV-maps to quantify MaR during the first week after acute MI.[199]

This study implies that the overestimation of infarct size early after MI with *in-vivo* and *ex-vivo* contrast enhanced MRI compared to histochemical staining with TTC can be attributed to an increased ECV with corresponding contrast enhancement in the TTC-negative peri-infarction zone. However, no difference in infarct size was seen at seven days between *in-vivo* and *ex-vivo* MRI compared with TTC. The better agreement between methods at seven days compared with acutely is likely explained by a decrease in ECV in the TTC-negative peri-infarction zone. These results are valid both for whole heart comparison as well as for a direct slice-by-slice comparison between hyperenhanced areas on MRI and necrosis/scar on TTC utilizing novel methodology.
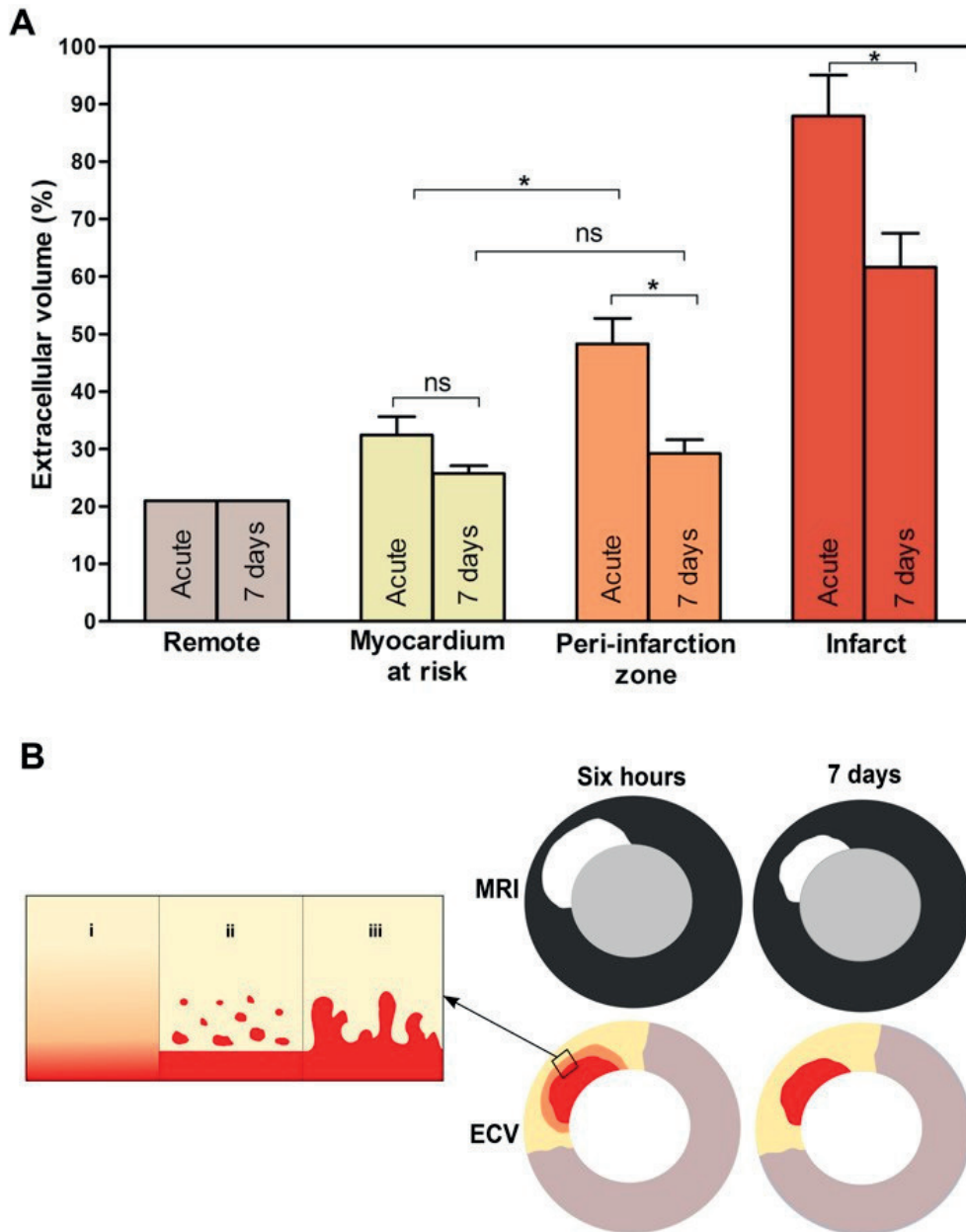
Figure 4.10 (**A**) ECV acutely and at seven days after MI are shown for: remote myocardium, salvaged myocardium at risk, peri-infarction zone and infarction. A significant decrease of ECV in the peri-infarction zone was seen over seven days. Furthermore, there was a significant difference in ECV between the salvaged myocardium at risk and peri-infarction zone acutely, however no significant difference was seen at seven days (**B**) Schematic drawing of a LV short-axis slice in AMI at six hours and at seven days. Acutely the hyperenhanced area on MRI (white) is larger compared to at seven days. This is explained by an ECV gradient between salvaged myocardium at risk (yellow) and the peri-infarction zone (orange). The ECV in the zone closest to the infarction (red), the peri-infarction zone which hyperenhances on MRI acutely, decreases during seven days to the same level as the rest of salvaged myocardium at risk. The blow up shows three possible pathophysiological explanations to the findings of an increased ECV in the peri-infarction zone: (*i*) severe edema (*ii*) archipelago like pattern and (*iii*) peninsula like pattern. *$P < 0.05$.

4.4 Regional stress induced ischemia in HCM patients (Study IV)

The relationship between left ventricular hypertrophy, perfusion abnormalities and fibrosis are unknown in young patients with hypertrophic cardiomyopathy. Since mounting evidence suggests causal relationship between myocardial ischemia and major adverse cardiac events, we sought to investigate whether regional myocardial perfusion is decreased in young HCM-patients and in individuals at risk for HCM and the relation to fibrosis.

Figure 4.11 shows representative perfusion images at rest and stress as well as corresponding LGE images in all three groups. No perfusion deficits were observed in HCM-risk subjects or in normal controls. In two HCM patients (18 %) a perfusion deficit was found at rest and in eight patients (73 %) during adenosine. Interestingly, one of these patients showed hypoperfusion during adenosine without any LGE in any segment with hypertrophy. The remaining patients with perfusion deficits (n = 7) had at least one LVH+LGE+ segment.
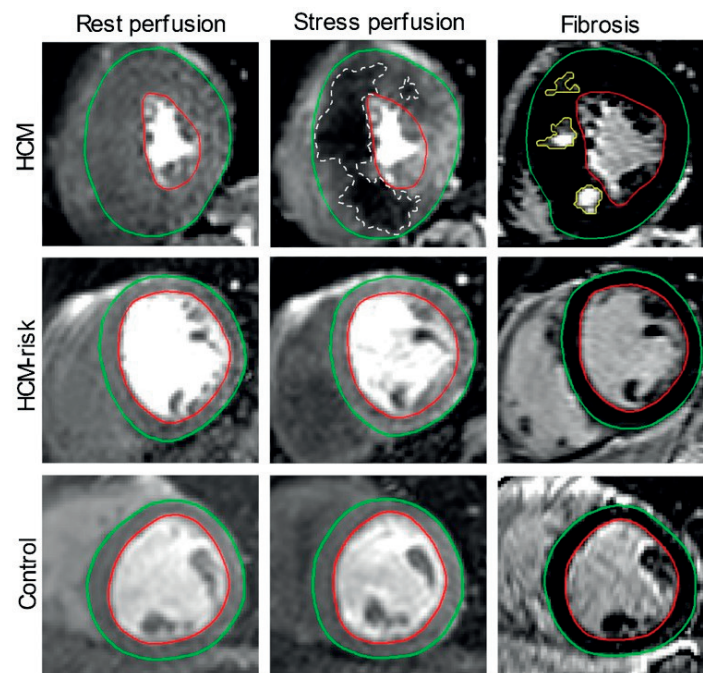
Figure 4.11 Short-axis first-pass perfusion images of the LV at rest (left column), adenosine stress (middle column) and corresponding late gadolinium enhancement (LGE)-CMR image for determining fibrosis (right column) in one patient with hypertrophic cardiomyopathy (HCM), one HCM-risk subject and in one healthy control. In the HCM patient the extent and severity of hypoperfused areas (white dashed line) was larger at adenosine stress compared to rest. The extent of hypoperfused areas at adenosine stress was also larger compared to fibrosis on LGE-CMR (yellow line) suggesting ischemia as the precursor of fibrosis. Green line = epicardium, red line = endocardium.

No hyperenhancement on LGE was present in HCM-risk subjects or controls. However, eight HCM patients (73 %) showed hyperenhancement on LGE with an average of 2.9 % scar of LVM. Of these, seven patients also had hypoperfused myocardium during adenosine.

Figure 4.12 shows semi-quantitative analysis of perfusion. Analysis on a segmental level in HCM patients showed that LVH+LGE- segments had decreased perfusion compared to LVH-LGE- segments. Furthermore, segments with LVH+LGE+ showed even lower perfusion compared to LVH+LGE-. These findings, that perfusion is lower in LVH+LGE- segments and even lower in LVH+LGE+ segments, has to our knowledge previously not been reported in young HCM patients. In cohorts with older HCM patients, similar degree of hypoperfusion in areas with LVH was found regardless of the presence of fibrosis.[110,128]
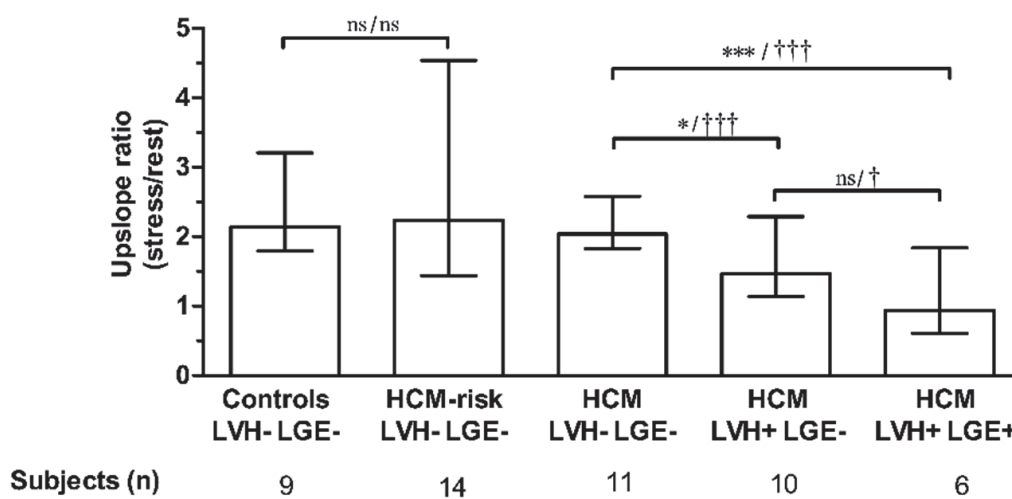

Figure 4.12 Regional myocardial perfusion expressed as upslope ratio (median, range) in normal controls, patients at risk of hypertrophic cardiomyopathy (HCM-risk) and HCM patients. There was a significant difference between the LVH-LGE- segments compared to both LVH+LGE and LVH+ LGE+ segments in HCM patients. Segments that were LVH+ LGE+ had lower perfusion than LVH+ LGE- segments and was statistically significant on segmental analysis but not averaged on a per patient basis. No difference in regional perfusion was seen between HCM-risk subjects and controls. *$P < 0.05$, ***$P < 0.001$ per patient analysis; † $P < 0.05$, ††† $P < 0.001$ on segmental analysis.

Our group has previously shown global hypoperfusion using flow measurements in the coronary sinus in young HCM-patients.[123] The present study extends these results showing that regional hypoperfusion is linked to both LVH and fibrosis. The perfusion deficits found in HCM patients ranged from subendocardial to transmural but fibrosis was predominantly found in the mid-mural and in hypertrophied segments, similar to previous studies.[117,200] Our results with the perfusion deficits mainly manifesting at adenosine stress show the importance and added value of performing myocardial perfusion at both rest and stress.

Young subjects at risk for HCM showed no difference in myocardial perfusion compared controls, which supports previous findings in the same cohort on global perfusion.[123] Genotype positive subjects with no sign of HCM morphology at age 18

have been shown to have a more benign clinical course. Demonstrating a normal perfusion during adenosine stress may provide a more sensitive and accurate way to correctly classify these subjects as true phenotype negative as compared to only wall thickness. This however remains to be proven by further studies.

Furthermore, the relation between hypoperfusion and fibrosis is demonstrated in Figure 4.13. The area of hypoperfused myocardium in HCM patients during adenosine was significantly larger compared to rest and was in all patients larger compared to the area of hyperenhancement on LGE ($P < 0.05$). This suggests that ischemia may play a primary role in the pathogenesis of fibrosis in HCM.
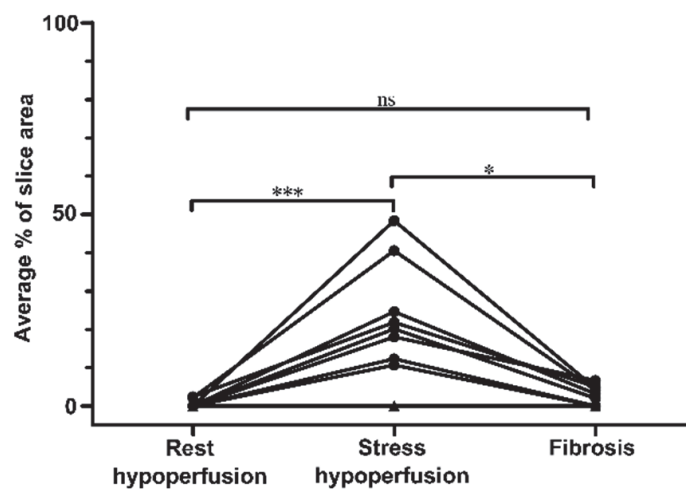

Figure 4.13 Areas of hypoperfusion in HCM-patients at rest, adenosine stress and fibrosis determined as hyperenhancement on LGE-CMR expressed as an average % of slice area in all patients with HCM. Areas of hypoperfusion at adenosine stress are significantly larger than hypoperfused areas at rest and fibrotic areas. Black triangles = three patients overlapping with no perfusion deficits or fibrosis on LGE. *$P < 0.05$, *** $P < 0.001$.

Moreover, as discussed in previous chapters, there is evidence suggesting that pathways involved in fibrosis and collagen deposition are activated in HCM before the onset of pathological evidence of disease.[127] In our study we found one patient with fibrosis and no evidence of ischemia in a lateral wall with borderline hypertrophy. In the hypertrophied inferior and inferoseptal wall of the same patient a clear area of hypoperfusion at stress was visible with fibrosis in the same area within the hypoperfused area. This split image could represent two different pathophysiological explanations for fibrosis in HCM and similar findings have also been reported by others.[201]

This study in young patients with HCM showed the benefit of performing an MRI scan to assess function, fibrosis and perfusion with adenosine stress, in the same session. This diagnostic scheme may allow the clinician to risk stratify and perhaps assess whether a more aggressive primary prevention with e.g. implantable cardioverter defibrillator is warranted or whether medical therapy suffice.

4.5 LGE borderzone for prediction of appropriate ICD-therapy (Study V)

A heterogeneous LGE borderzone on CMR has been proposed as an independent predictor of ventricular arrhythmias. The heterogeneous LGE borderzone has previously been analyzed by methods based on both threshold algorithms[79] and full-width half-maximum (FWHM) algorithms.[77] We have developed and validated a weighted semi-automatic algorithm for infarct measurement with the potential to quantify the borderzone. Thus, we hypothesized that a heterogeneous LGE borderzone is related to appropriate ICD therapy and investigated if weighted borderzone algorithm has similar predictive value as those previously reported. An example of the three algorithms applied in one ICM and one NICM patient is shown in Figure 4.14.
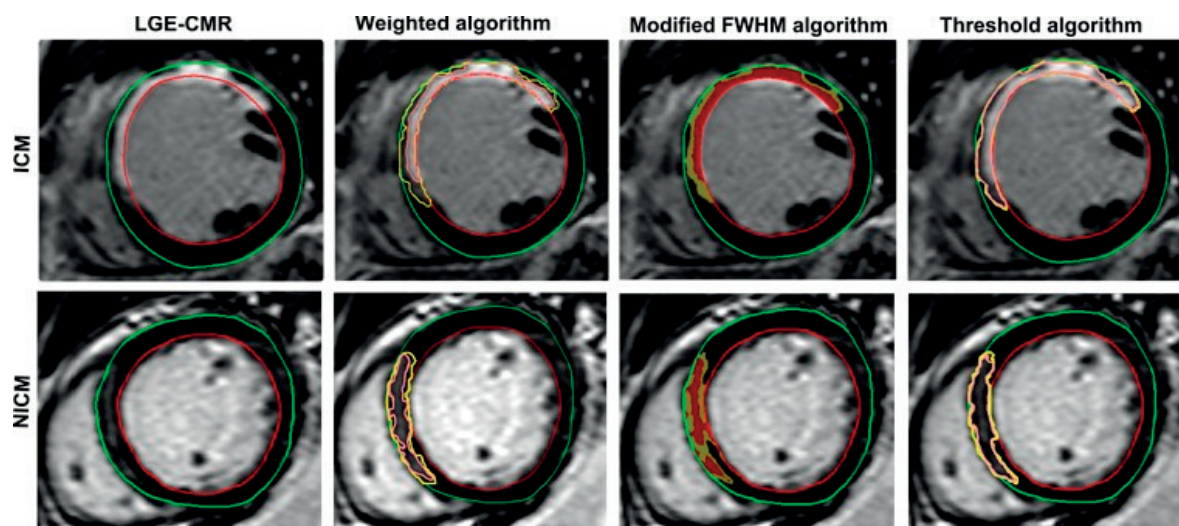

Figure 4.14 Representative short axis LGE-CMR images from one patient with ischemic cardiomyopathy (ICM), top row, and from one patient with non-ischemic cardiomyopathy (NICM), bottom row, evaluated for borderzone with three different methods (i) weighted borderzone algorithm (ii) modified FWHM algorithm and (iii) 2-3SD threshold algorithm. The borderzone in methods (i) and (iii) is defined as the area between the yellow (total LGE) and pink line (LGE core) and in method (ii) as the yellow area outside the red area (LGE core). Red line = endocardium, green line = epicardium.

In the current study, LV ejection fraction was not predictive of increased likelihood of ICD-therapy in pooled (ICM+NICM patients) analysis (HR = 1.02, P = 0.23). Also, neither total nor core LGE predicted an increased likelihood of appropriate ICD-therapy using the weighted borderzone or modified FWHM algorithm. However, LGE borderzone predicted increased ICD-therapy rate when using the weighted borderzone and modified FWHM algorithm (HR 1.07, P = 0.03 and HR 1.03, P = 0.048 respectively) but not when using the threshold algorithm (HR 0.98, P = 0.40).

Figure 4.15 illustrates that patients with large LGE borderzone had significantly more ICD-therapies compared to patients with small borderzone, using both the

weighted borderzone and the modified FWHM algorithm. The threshold algorithm, however, did not show any significant difference between the groups.

When performing subgroup analysis in ICM patients, both the weighted and modified FWHM algorithm predicted an increased ICD-therapy rate (HR 1.13, P = 0.0001 and 1.04, P = 0.02 respectively) but not the threshold algorithm.

In analysis of NICM patients alone, LGE borderzone did not predict ICD-therapy. These results in NICM patients support previous reports which also demonstrated that a larger borderzone in NICM patients did not predict ICD-therapy.[202]

In further subgroup analysis we found that ICM patients with primary preventive ICD and with a large borderzone showed higher rates of ICD-therapy using the weighted borderzone algorithm and modified FWHM algorithm but not using the threshold algorithm (Figure 4.16). Moreover, LGE borderzone assessed by the weighted algorithm and modified FWHM algorithm had the highest predictive value for ICD-therapy in this subgroup (HR 1.16, P = 0.003 and HR 1.14, P = 0.008, for respective algorithm). It is noticeable that the hazard ratio (HR 1.16) is higher than ejection fraction (HR 0.97), which is currently the major guideline criterion for implanting a primary preventive ICD. Furthermore, in these patients with primary preventive ICD, no other LGE characteristics predicted increased rate of ICD therapy.

Our results suggest that the new borderzone and modified FWHM algorithm may be used interchangeably for LGE borderzone quantification to predict ICD-therapy in patients eligible for primary preventive ICD-therapy. Furthermore, our results support previous findings that LGE borderzone can predict ventricular arrhythmias in ICM patients with primary preventive ICD.[203,204] In contrast, however, a study assessing LGE characteristics in 55 ICM patients with primary preventive ICD using three different methods (2 out of 3 used in the current study), borderzone did not add any predictive value over total LGE size for predicting ventricular arrhythmias.[205] One possible explanation for such divergent results is that the follow-up time was shorter (24 months) compared to our study.

Lastly, many patients undergo a CMR-examination when ICD-implantation is considered to determine the etiology of heart failure. The identification and characterization of the arrythmogenic borderzone is therefore available without further cost in these patients and may aid in the risk-stratification of ventricular arrhythmias. Therefore our findings should be confirmed in larger multicenter prospective studies, preferably a randomized controlled trial, in order to determine which specific algorithm is the most accurate for prediction of arrhythmic events, and further consolidate the role for LGE-CMR based evaluation in clinical risk stratification.

Figure 4.15 Kaplan-Meier curves demonstrating the differences in appropriate ICD-therapy in ischemic and non-ischemic cardiomyopathy patients. Patients were divided by median (%) extent of borderzone and there was no difference in follow up time between the patients with small (yellow line) and large (blue line) borderzone. Patients with larger borderzone had significantly more ICD-therapy compared to patients with small borderzone, using both the weighted borderzone and modified FWHM algorithm. The threshold algorithm did not show a difference between the groups.
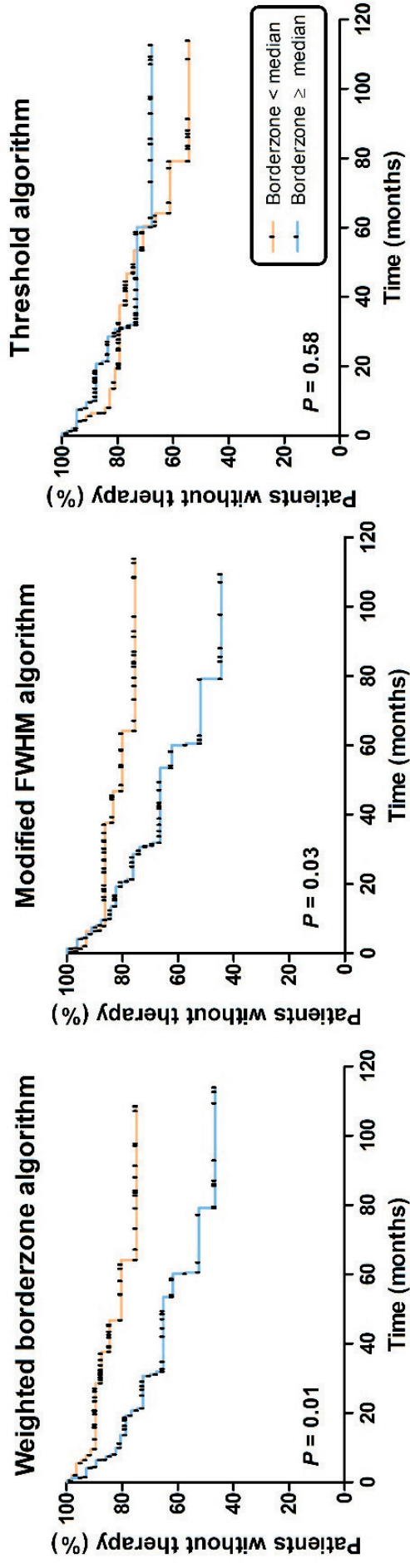
Figure 4.16 Kaplan-Meier curves demonstrating the differences in appropriate ICD-therapy in ischemic cardiomyopathy patients with primary preventive ICD. Patients were differentiated by median borderzone (%) and follow up time was similar for patients with small (yellow line) and large borderzone (blue line) . Patients with larger borderzone had significantly more ICD therapy compared to patients with small borderzone, using the weighted borderzone and modified FWHM algorithm. The threshold algorithm did not show a difference between the groups.
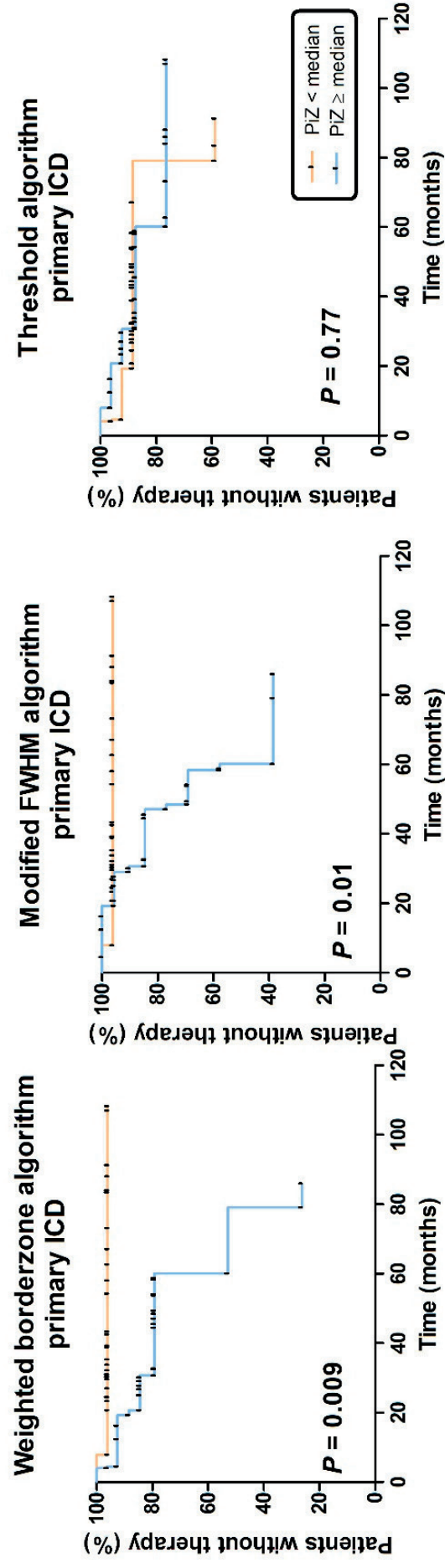
Conclusions

The major conclusion of each study was:

I.   Coronary microembolization causes long-term, regional left ventricular dysfunction and that even small microemboli, which may escape the distal protective devices, influence cardiac function. Furthermore, the perfusion and LGE patterns did not differ between small and large microemboli at the acute stage.

II.   Infarct quantification with a 2D-PSIR and a 3D-IR sequence shows good agreement in patients which allows for the sequences to be used interchangeably. Both LGE-sequences optimized for *in vivo* use yield an overestimation of infarct size *ex vivo*.

III.   *In-vivo* and *ex-vivo* contrast enhanced MRI consistently overestimates infarct size acutely compared to histopathology with TTC. This overestimation acutely may be explained by an ECV gradient in salvaged myocardium immediately adjacent to the infarct, the peri-infarction zone, which shows contrast enhancement on MRI. This gradient in ECV seen acutely could be due to severe edema, an admixture of viable and necrotic cells, peninsulas of necrotic tissue or a combination thereof. Thus, these results highlight the importance of performing MRI infarct quantification acutely within a consistent narrow time period when using infarct size in clinical trials.

IV.   Regional perfusion is decreased in hypertrophied compared to non-hypertrophied myocardium and is lowest in fibrotic myocardium in young patients with HCM but does not discriminate HCM-risk subjects from controls. Stress-induced hypoperfused regions exceed regions with LGE indicating that hypoperfusion precede fibrosis and may be a more sensitive marker of diseased myocardium in HCM.

V.   A heterogeneous LGE borderzone using two of the evaluated algorithms predicts appropriate ICD-therapy to a larger extent than ejection fraction, total and core LGE size. The discrimination of appropriate ICD-therapy was highest in ICM patients with primary prevention ICD. Thus, LGE borderzone size may be a risk marker in ICM patients considered for primary prevention ICD-therapy.

Acknowledgments

I would like to extend my greatest appreciation to everyone who has supported me throughout my time as a PhD-student. I especially wish to express my gratitude to:

My supervisor, **Marcus Carlsson**, for being a great mentor and an academic role-model and always having your door open for me.

My co-supervisor, **Håkan Arheden**, for academic guidance, excellent leadership training and inspiring thoughts and discussions on personal development.

My co-supervisor, **Henrik Engblom**, for great support, endless enthusiasm and a lot of fun during late night experiments.

My co-supervisor, **Petru Liuba**, for great support and discussions about pediatric cardiology.

Professor **Maythem Saeed** for letting me come to San Francisco and be part of the exciting experiments.

Einar Heiberg for invaluable help and support when the matters got technical and together with **Helen Fransson** and **Nisse Lundahl** providing an excellent image analysis software.

Mikael Kanski for being a great friend and always being there, also for having an absolute great sense of humor, especially during many late night experiments.

David Nordlund for all the exciting discussions and teaching me the invasive part of the experiments.

Professor **Anthony Aletras** for unparalleled MR expertise and providing out-of the box insights to projects.

Sebastian Bidhult for numerous interesting and helpful discussions on MRI.

Rasmus Borgquist for exciting collaboration and statistical help.

Professor **Katherine Wu** for great insights and excellent feedback.

Eva Fernlund for help in recruiting patients.

Tom Gyllenhammar, for many interesting discussions and collaborations

Kerstin Brauer and **Karin Larsson** for all the administrative help and support.

Elisabet Englund for help with histology and interesting pathophysiological discussions

Joey Ubachs, for showing me the ropes when I was new in the group and all the fun during conferences.

To all my colleagues in the Cardiac MR Group and at the Department of Clinical Physiology for friendship, support, and providing a great culture to work in: **Katarina Steding-Ehrenborg**, **Johannes Töger**, **Jane Tufvesson**, **Per Arvidsson**, **Jonas Jögi**, **Erik Hedström**, **Magnus Hansson**, **Bo Hedén**, **Karin Markenroth-Bloch**, **Christos Xanthis**, **Henrik Mosén**, **Ellen Ostenfeld**, **Shahnaz Akil**, **Pia Sjöberg**, **Mariam Al-Mashat**, **Fredrik Hedéer**, **Sverrir Stephensen**, **Giorgos Kantasis**, **Ulrika Pahlm-Webb**, **Eva Persson**, **Helen Almquist**, **Carina Ljungberg**, **Ann-Helen Arvidsson**, **Christel Carlander**, **Reza Farazdaghi**, **Lotta Åkesson** and **Johanna Koul** and all those who I might have forgotten to mention.

This thesis would have not been possible without the help and support from my colleagues at the Department of Cardiology, especially: Professor **David Erlinge**, **Sasha Koul**, **Jesper van der Pals** and **Uzma Chaudhry**.

To all my friends who have been supportive and understanding during periods with long hours.

To my parents, **Barbara** and **Ted**, for all your love and always believing in me and supporting my choices in life.

Finally, **Louise**, for your unconditional love and for being there by my side.

Bibliography

1. Mozaffarian D, Benjamin EJ, Go SA, et al. Heart Disease and Stroke Statistics--2015 Update: A report from the American Heart Association. Circulation. 2014;131:e29-e322.

2. Maron BJ. Sudden death in young athletes. N Engl J Med. 2003;349:1064–75.

3. Elliott PM, Poloniecki J, Dickie S, et al. Sudden death in hypertrophic cardiomyopathy: identification of high risk patients. J Am Coll Cardiol. 2000;36:2212–8.

4. Weber KT. Cardiac interstitium in health and disease: the fibrillar collagen network. J Am Coll Cardiol. 1989;13:1637–52.

5. Weber KT, Brilla CG. Pathological hypertrophy and cardiac interstitium. Fibrosis and renin-angiotensin-aldosterone system. Circulation. 1991;83:1849–65.

6. Jugdutt BI. Ventricular remodeling after infarction and the extracellular collagen matrix: When is enough enough? Circulation. 2003;108:1395–403.

7. Camelliti P, Borg TK, Kohl P. Structural and functional characterisation of cardiac fibroblasts. Cardiovasc Res. 2005;65:40–51.

8. Woodiwiss AJ, Tsotetsi OJ, Sprott S, et al. Reduction in myocardial collagen cross-linking parallels left ventricular dilatation in rat models of systolic chamber dysfunction. Circulation. 2001;103:155–60.

9. Ferrari R. Healthy versus sick myocytes: Metabolism, structure and function. Eur Heart J, Suppl. 2002;4:1–12.

10. Anderson K, Sutton M, Lie J. Histopathological types of cardiac fibrosis in myocardial disease. J Pathol. 1971;128:79.

11. Dobaczewski M, Gonzalez-Quesada C, Frangogiannis N. The extracellular matrix as a modulator of the inflammatory and reparative response following myocardial infarction. J Mol Cell Cardiol. 2010;48:504–11.

12. Frangogiannis NG. The immune system and cardiac repair. Pharmacol Res. 2008;58:88–111.

13. Dobaczewski M, Bujak M, Zymek P, Ren G, Entman ML, Frangogiannis NG. Extracellular matrix remodeling in canine and mouse myocardial infarcts. Cell Tissue Res. 2006;324:475–88.

14. Villarreal F, Omens J, Dillmann W, Risteli J, Nguyen J, Covell J. Early degradation and serum appearance of type I collagen fragments after myocardial infarction. J Mol Cell Cardiol. 2004;36:597–601.

15. Dewald O, Ren G, Duerr GD, et al. Of mice and dogs: species-specific differences in the inflammatory response following myocardial infarction. Am J Pathol. 2004;164:665–77.

16. Cleutjens JP, Verluyten MJ, Smiths JF, Daemen MJ. Collagen remodeling after myocardial infarction in the rat heart. Am J Pathol. 1995;147:325–38.

17. Gabbiani G. The myofibroblast in wound healing and fibrocontractive diseases. J Pathol. 2003;200:500–3.

18. Serini G, Bochaton-Piallat ML, Ropraz P, et al. The fibronectin domain ED-A is crucial for myofibroblastic phenotype induction by transforming growth factor-β1. J Cell Biol. 1998;142:873–81.

19. Schellings MWM, Pinto YM, Heymans S. Matricellular proteins in the heart: Possible role during stress and remodeling. Cardiovasc Res. 2004;64:24–31.

20. Lerman RH, Apstein CS, Kagan HM, et al. Myocardial healing and repair after experimental infarction in the rabbit. Circ Res. 1983;53:378–88.

21. Kong P, Christia P, Frangogiannis NG. The pathogenesis of cardiac fibrosis. Cell Mol Life Sci. 2014;71:549–74.

22. Volders PGA, Willems IE, Cleutjens J, et al. Interstitial collagen is increased in the non-infarcted human myocardium after myocardial. J Mol Cell Cardiol. 1993;25:1317–23.

23. Berk BC, Fujiwara K, Lehoux S. ECM remodeling in hypertensive heart disease. J Clin Invest. 2007;117:568–75.

24. Asbun J, Villarreal FJ. The pathogenesis of myocardial fibrosis in the setting of diabetic cardiomyopathy. J Am Coll Cardiol. 2006;47:693–700.

25. Biernacka A, Frangogiannis NG. Aging and cardiac fibrosis. Aging Dis. 2011;2:158–73.

26. Bertrand ME, LaBlanche JM, Tilmant PY, et al. Frequency of provoked coronary arterial spasm in 1089 consecutive patients undergoing coronary arteriography. Circulation. 1982;65:1299–306.

27. Prizel KR, Hutchins GM, Bulkley BH. Coronary artery embolism and myocardial infarction. Ann Intern Med. 1978;88:155–61.

28. Young IS, Mceneny J. Lipoprotein oxidation and atherosclerosis. Biochem Soc Trans. 2001;29:358–62.

29. Libby P. Molecular basis of the acute coronary syndromes. Circulation. 1995;91:2884–50.

30. Falk E, Shah P, Fuster V. Coronary plaque disruption. Circulation. 1995;92:657–71.

31. Virmani R, Burke AP, Farb A, Kolodgie FD. Pathology of the unstable plaque. Prog Cardiovasc Dis. 2002;44:349–56.

32. Skyschally A, Leineweber K, Gres P, Haude M, Erbel R, Heusch G. Coronary microembolization. Basic Res Cardiol. 2006;101:373–82.

33. Nesto RW, Kowalchuk GJ. The ischemic cascade: temporal sequence of hemodynamic, electrocardiographic and symptomatic expressions of ischemia. Am J Cardiol. 1987;59:23C – 30C.

34. Jennings RB, Reimer KA. The cell biology of acute myocardial ischemia. Annu Rev Med. 1991;42:225–46.

35. Jennings RB, Schaper J, Hill ML, Steenbergen C, Reimer KA. Effect of reperfusion late in the phase of reversible ischemic injury. Changes in cell volume, electrolytes, metabolites, and ultrastructure. Circ Res. 1985;56:262–78.

36. Gissel H. The role of Ca2+ in muscle cell damage. Ann NY Acad Sci. 2005;1066:166–80.

37. Duncan CJ. The role of phospholipase A2 in calcium-induced damage in cardiac and skeletal muscle. Cell Tissue Res. 1988;253:457–62.

38. Levraut J, Iwase H, Shao Z-H, Vanden Hoek TL, Schumacker PT. Cell death during ischemia: relationship to mitochondrial depolarization and ROS generation. Am J Physiol Heart Circ Physiol. 2003;284:H549–58.

39. Sylvén C. Mechanisms of pain in angina pectoris-A critical review of the adenosine hypothesis. Cardiovasc Drugs Ther. 1993;7:745–59.

40. Reimer KA, Jennings RB. The "wavefront phenomenon" of ischemic cell death. II. Transmural progression of necrosis within the framework of ischemic bed size. Lab Invest. 1979;40:633-44.

41. Lowe JE, Reimer KA, Jennings RB. Experimental infarct size as a function of the amount of myocardium at risk. Am J Pathol. 1978;90:363–79.

42. Matsumura K, Jeremy RW, Schaper J, Becker LC. Progression of myocardial necrosis during reperfusion of ischemic myocardium. Circulation. 1998;97:795–804.

43. Hausenloy D, Yellon D. The mitochondrial permeability transition pore: its fundamental role in mediating cell death during ischaemia and reperfusion. 2003;35:339–41.

44. Kloner RA, Ganote CE, Jennings RB. The "no reflow" phenomenon after temporary coronary occlusion in the dog. J Clin Invest. 1974;54:1496–508.

45. Hamirani YS, Wong A, Kramer CM, et al. Effect of microvascular obstruction and intramyocardial hemorrhage by CMR on LV remodelling and outcomes after

myocardial infarction: a systematic review and meta-analysis. J Am Coll Cardiol Img. 2014;7:940-52.

46.   Hedström E, Engblom H, Frogner F, et al. Infarct evolution in man studied in patients with first-time coronary occlusion in comparison to different species - implications for assessment of myocardial salvage. J Cardiovasc Magn Reson. 2009;11:38.

47.   Murry CE, Jennings RB, Reimer KA. Preconditioning with ischemia: a delay of lethal cell injury in ischemic myocardium. Circulation. 1986;74:1124–36.

48.   Yellon D, AM A, Pugsley W. Preconditioning the human myocardium. Lancet. 1993;342:276–7.

49.   Schaper W, Görge G, B W, Schaper J. The collateral circulation of the heart. Prog Cardiovasc Dis. 1988;31:57–77.

50.   Charney R, Cohen M. The role of the coronary collateral circulation in limiting myocardial ischemia and infarct size. Am Heart J. 1993;126:937–45.

51.   Williams DO, Amsterdam EA, Miller RR, Mason DT. Functional significance of coronary collateral vessels in patients with acute myocardial infarction: relation to pump performance, cardiogenic shock and survival. Am J Cardiol. 1976;37:345–51.

52.   Maxwell M, Hearse D, Yellon D. Species variation in the coronary collateral circulation during regional myocardial-ischemia - a critical determinant of the rate of evolution and extent of myocardial-infarction. 1987;737–46.

53.   Jaffe AS, Babuin L, Apple FS. Biomarkers in acute cardiac disease. The present and the future. J Am Coll Cardiol. 2006;48:1–11.

54.   Selvanayagam JB, Porto I, Channon K, et al. Troponin elevation after percutaneous coronary intervention directly represents the extent of irreversible myocardial injury: Insights from cardiovascular magnetic resonance imaging. Circulation. 2005;111:1027–32.

55.   Morrow DA, Cannon CP, Jesse RL, et al. National Academy of Clinical Biochemistry Laboratory Medicine Practice Guidelines: Clinical characteristics and utilization of biochemical markers in acute coronary syndromes. Circulation. 2007;115:356–76.

56.   Thygesen K, Alpert JS, Jaffe AS, et al. Third universal definition of myocardial infarction. Eur Heart J. 2012;33:2551–67.

57.   Suwaidi JA, Hamasaki S, Higano ST,. Long-term follow-up of patients with mild coronary artery disease and endothelial dysfunction. Circulation. 2000;101:948–54.

58.   Heusch G, Kleinbongard P, Böse D, Levkau B, Haude M, Schulz R, et al. Coronary microembolization: From bedside to bench and back to bedside. Circulation. 2009;120:1822–36.

59.   Fishbein MC, Meerbaum S, Rit J, et al. Early phase acute myocardial infarct size quantification: Validation of the triphenyl tetrazolium chloride tissue enzyme staining technique. Am Heart J. 1981;101:593–600.

60.   Birnbaum Y, Hale SL, Kloner RA. Differences in reperfusion length following 30 minutes of ischemia in the rabbit influence infarct size as measured by triphenyltetrazolium chloride staining. J Moll Cell Cardiol. 1997; 29:657-66.

61.   Kashani A, Giugliano RP, Antman EM, et al. Severity of heart failure, treatments, and outcomes after fibrinolysis in patients with ST-elevation myocardial infarction. Eur Heart J. 2004;25:1702–10.

62.   Kim R, Wu E, Rafael A, Chen E, et al. The use of contrast-enhanced magnetic resonance imaging to identify reversible myocardial dysfunction. N Engl J Med. 2000;343:1445–53.

63.   Choi KM, Kim RJ, Gubernikoff G, Vargas JD, Parker M, Judd RM. Transmural extent of acute myocardial infarction predicts long-term improvement in contractile function. Circulation. 2001;104:1101–7.

64.   Pfeffer MA, Braunwald E. Ventricular remodeling after myocardial infarction. Experimental observations and clinical implications. Circulation. 1990;81:1161–72.

65.   Scott PA, Rosengarten JA, Curzen NP, Morgan JM. Late gadolinium enhancement cardiac magnetic resonance imaging for the prediction of ventricular tachyarrhythmic events: A meta-analysis. Eur J Heart Fail. 2013;15:1019–27.

66.   Bello D, Einhorn A, Kaushal R, et al. Cardiac magnetic resonance imaging: Infarct size is an independent predictor of mortality in patients with coronary artery disease. Magn Reson Imaging. 2011;29:50–6.

67.   Ganame J, Messalli G, Dymarkowski S, et al. Impact of myocardial haemorrhage on left ventricular function and remodelling in patients with reperfused acute myocardial infarction. Eur Heart J. 2009;30:1440–9.

68   Wu KC, Zerhouni EA, Judd RM, et al. Prognostic significance of microvascular obstruction by magnetic resonance imaging in patients with acute myocardial infarction. Circulation. 1998;97:765–72.

69.   Carlsson M, Wilson M, Martin AJ, Saeed M. Myocardial microinfarction after coronary microembolization in swine: MR imaging charcterization. Radiology. 2009;250:703–4.

70.   Braunwald E, Kloner RA. The stunned myocardium: prolonged, postischemic ventricular dysfunction. Circulation. 1982;66:1146–9.

71.   Leor J, Kloner RA. The hibernating myocardium. Am Heart J. 1988;117:211-21.

72.   Weisman HF, Bush DE, Mannisi JA, Weisfeldt ML, Healy B. Cellular mechanisms of myocardial infarct expansion. Circulation. 1988;78:186–201.

73. Fieno DS, Hillenbrand HB, Rehwald WG, et al. Infarct resorption, compensatory hypertrophy, and differing patterns of ventricular remodeling following myocardial infarctions of varying size. J Am Coll Cardiol. 2004;43:2124–31.

74. Campbell RW, Murray A, Julian DG. Ventricular arrhythmias in first 12 hours of acute myocardial infarction. Natural history study. Br Heart J. 1981;46:351–7.

75. Janse M, Wit A. Electrophysiological mechanisms of ventricular arrhythmias resulting from myocardial ischemia and infarction. Physiol Rev. 1989;69:1049–169.

76. Roes SD, Borleffs CJW, van der Geest RJ, et al. Infarct tissue heterogeneity assessed with contrast-enhanced MRI predicts spontaneous ventricular arrhythmia in patients with ischemic cardiomyopathy and implantable cardioverter-defibrillator. Circ Cardiovasc Imaging. 2009;2:183–90.

77. Schmidt A, Azevedo CF, Cheng A, et al. Infarct tissue heterogeneity by magnetic resonance imaging identifies enhanced cardiac arrhythmia susceptibility in patients with left ventricular dysfunction. Circulation. 2007;115:2006–14.

78. Watanabe E, Abbasi SA, Heydari B, et al. Infarct tissue heterogeneity by contrast-enhanced magnetic resonance imaging is a novel predictor of mortality in patients with chronic coronary artery disease and left ventricular dysfunction. Circ Cardiovasc Imaging. 2014;7:887-894.

79. Yan AT, Shayne AJ, Brown KA, et al. Characterization of the peri-infarct zone by contrast-enhanced cardiac magnetic resonance imaging is a powerful predictor of post-myocardial infarction mortality. Circulation. 2006;114:32–9.

80. Appelbaum E, Manning WJ. Science to practice: can the combination of resting first-pass myocardial perfusion and late gadolinium-enhanced cardiovascular MR imaging help identify myocardial infarction resulting from coronary microembolization? Radiology. 2009;250:609–11.

81. Steg PG, James SK, Atar D, et al. ESC Guidelines for the management of acute myocardial infarction in patients presenting with ST-segment elevation. Eur Heart J. 2012;33:2569–619.

82. Keeley EC, Boura JA, Grines CL. Primary angioplasty versus intravenous thrombolytic therapy for acute myocardial infarction: a quantitative review of 23 randomised trials. Lancet. 2003;361:13–20.

83. Bonnefoy E, Steg PG, Boutitie F, et al. Comparison of primary angioplasty and pre-hospital fibrinolysis in acute myocardial infarction (CAPTIM) trial: a 5-year follow-up. Eur Heart J. 2009;30:1598–606.

84. Forman M, Perry J, Wilson B, et al. Demonstration of myocardial reperfusion injury in humans: results of a pilot study utilizing acute cornary angioplasty with perfluorochemical in anterior myocardial infarction. J Am Coll Cardiol. 1991;18:911–8.

88

85. Zhao Z-Q, Corvera JS, Halkos ME, et al. Inhibition of myocardial injury by ischemic postconditioning during reperfusion: comparison with ischemic preconditioning. Am J Physiol Heart Circ Physiol. 2003;285:H579–88.

86. Staat P, Rioufol G, Piot C, et al. Postconditioning the human heart. Circulation. 2005;112:2143–8.

87. Fröhlich GM, Meier P, White SK, Yellon DM, Hausenloy DJ. Myocardial reperfusion injury: Looking beyond primary PCI. Eur Heart J. 2013;34:1714–24.

88. Piot C, Croisille P, Staat P. Effect of cyclosporine on reperfusion injury in acute myocardial infarction. N Engl J Med. 2008;473–81.

89. Atar D, Arheden H, Berdeaux A, et al. Effect of intravenous TRO40303 as an adjunct to primary percutaneous coronary intervention for acute ST-elevation myocardial infarction: MITOCARE study results. Eur Heart J. 2014;36:112–9.

90. Erlinge D, Götberg M, Lang I, et al. Rapid endovascular catheter core cooling combined with cold saline as an adjunct to percutaneous coronary intervention for the treatment of acute myocardial infarction. J Am Coll Cardiol. 2014;63:1857–65.

91. Götberg M, Olivecrona GK, Koul S, et al. A pilot study of rapid cooling by cold saline and endovascular cooling before reperfusion in patients with ST-elevation myocardial infarction. Circ Cardiovasc Interv. 2010;3400–7.

92. Patrono C, Bachmann F, Baigent C, et al. Expert consensus document on the use of antiplatelet agents: The task force on the use of antiplatelet agents in patients with atherosclerotic cardiovascular disease of the european society of cardiology. Eur Heart J. 2004;25:166–81.

93. Van De Werf F, Bax J, Betriu A, et al. Management of acute myocardial infarction in patients presenting with persistent ST-segment elevation. Eur Heart J. 2008;29:2909–45.

94. Russo AM, Stainback RF, Bailey SR, et al. 2013 appropriate use criteria for implantable cardioverter-defibrillators and cardiac resynchronization therapy. J Am Coll Cardiol. 2013;61:1318–68.

95. Bardy G, Lee K, Mark D, Poole J. Amiodarone or an implantable cardioverter-defibrillator for congestive heart failure. N Engl J Med. 2005;352:225–37.

96. Moss AJ, Zareba W, Hall WJ, et al. Prophylactic implantation of a defibrillator in patients with myocardial infarction and reduced ejection fraction. N Engl J Med. 2002;346:877–83.

97. Schelbert EB, Hsu L, Anderson SA, Mohanty BD. Late gadolinium enhancement cardiac magnetic resonance identifies post infarction myocardial fibrosis and the border zone at the near cellular level in ex vivo rat heart. Circ Cardiovasc Imaging. 2012;3:743–52.

98.   Elliott P, Andersson B, Arbustini E, et al. Classification of the cardiomyopathies: a position statement from the european society of cardiology working group on myocardial and pericardial diseases. Eur Heart J. 2008;29:270–6.

99.   Teare D. Asymmetrical hypertrophy of the heart in young adults. Br Heart J. 1958;20:1–8.

100.   Maron BJ, Gardin JM, Flack JM, Gidding SS, Kurosaki TT, Bild DE. Prevalence of hypertrophic cardiomyopathy in a general population of young adults. Echocardiographic analysis of 4111 subjects in the CARDIA study. Circulation. 1995;92:785–9.

101.   Semsarian C, Ingles J, Maron MS, Maron BJ. New perspectives on the prevalence of hypertrophic cardiomyopathy. J Am Coll Cardiol. 2015;65:1249–54.

102.   Maron BJ, Carney KP, Lever HM, et al. Relationship of race to sudden cardiac death in competitive athletes with hypertrophic cardiomyopathy. J Am Coll Cardiol. 2003;41:974–80.

103.   Maron BJ. Hypertrophic cardiomyopathy: An important global disease. Am J Med. 2004;116:63–5.

104.   Olivotto I, Maron MS, Adabag SA, et al. Gender-related differences in the clinical presentation and outcome of hypertrophic cardiomyopathy. J Am Coll Cardiol. 2005;46:480–7.

105.   Olivotto I, Cecchi F, Gistri R, et al. Relevance of coronary microvascular flow impairment to long-term remodeling and systolic dysfunction in hypertrophic cardiomyopathy. J Am Coll Cardiol. 2006;47:1043–8.

106.   Basso C, Thiene G, Corrado D, Buja G, Melacini P, Nava A. Hypertrophic cardiomyopathy and sudden death in the young: pathologic evidence of myocardial ischemia. Hum Pathol. 2000;31:988–98.

107.   Maron MS, Olivotto I, Maron BJ, et al. The case for myocardial ischemia in hypertrophic cardiomyopathy. J Am Coll Cardiol. 2009 ;54:866–75.

108.   Corrado D, Basso C, Schiavon M, Thiene G. Screening for hypertrophic cardiomyopathy in young athletes. N Engl J Med. 1998;339:364–9.

109.   Elliott PM, Anastasakis A, Borger MA, et al. 2014 ESC guidelines on diagnosis and management of hypertrophic cardiomyopathy: the task force for the diagnosis and management of hypertrophic cardiomyopathy of the European society of cardiology (ESC). Eur Heart J. 2014;35:2733–79.

110.   Petersen SE, Jerosch-Herold M, Hudsmith LE, et al. Evidence for microvascular dysfunction in hypertrophic cardiomyopathy: New insights from multiparametric magnetic resonance imaging. Circulation. 2007;115:2418–25.

111.   Kelley-Hedgepeth A, Towbin JA, Maron MS. Overlapping phenotypes: Left ventricular noncompaction and hypertrophic cardiomyopathy. Circulation. 2009;119:588–9.

112.   Maron BJ. Distinguishing hypertrophic cardiomyopathy from athlete's heart physiological remodelling: clinical significance, diagnostic strategies and implications for preparticipation screening. Br J Sports Med. 2009;43:649–56.

113.   Camici P, Chiriatti G, Lorenzoni R, et al. Coronary vasodilation is impaired in both hypertrophied and nonhypertrophied myocardium of patients with hypertrophic cardiomyopathy: a study with nitrogen-13 ammonia and positron emission tomography. J Am Coll Cardiol. 1991;17:879–86.

114.   Maron BJ, Ommen SR, Semsarian C, Spirito P, Olivotto I, Maron MS. Hypertrophic cardiomyopathy: present and future, with translation into contemporary cardiovascular medicine. J Am Coll Cardiol. 2014;64:83–99.

115.   Klues HG, Schiffers A, Maron BJ. Phenotypic spectrum and patterns of left ventricular hypertrophy in hypertrophic cardiomyopathy: Morphologic observations and significance as assessed by two-dimensional echocardiography in 600 patients. J Am Coll Cardiol. 1995;26:1699–708.

116.   Schulz-Menger J, Abdel-Aty H, Busjahn A, et al. Left ventricular outflow tract planimetry by cardiovascular magnetic resonance differentiates obstructive from non-obstructive hypertrophic cardiomyopathy. J Cardiovasc Magn Reson. 2006;8:741–6.

117.   Maron MS, Maron BJ, Harrigan C, et al. Hypertrophic cardiomyopathy phenotype revisited after 50 years with cardiovascular magnetic resonance. J Am Coll Cardiol. 2009 ;54:220–8.

118.   Hughes SE. The pathology of hypertrophic cardiomyopathy. Histopathology. 2004;44:412–27.

119.   Moon JCC, Fisher NG, McKenna WJ, Pennell DJ. Detection of apical hypertrophic cardiomyopathy by cardiovascular magnetic resonance in patients with non-diagnostic echocardiography. Heart. 2004;90:645–9.

120.   Olivotto I, Maron MS, Autore C, et al. Assessment and significance of left ventricular mass by cardiovascular magnetic resonance in hypertrophic cardiomyopathy. J Am Coll Cardiol. 2008;52:559–66.

121.   Factor SM, Butany J, Sole MJ, Wigle ED, Williams WC, Rojkind M. Pathologic fibrosis and matrix connective tissue in the subaortic myocardium of patients with hypertrophic cardiomyopathy. J Am Coll Cardiol. 1991;17:1343–51.

122.   Cecchi F, Olivotto I, Gistri R, Lorenzoni R, Chiriatti G, Camici PG. Coronary microvascular dysfunction and prognosis in hypertrophic cardiomyopathy. N Engl J Med. 2003;349:1027–35.

123. Gyllenhammar T, Fernlund E, Jablonowski R, et al. Young patients with hypertrophic cardiomyopathy, but not subjects at risk, show decreased myocardial perfusion reserve quantified with CMR. Eur Heart J Cardiovasc Imaging. 2014;15:1350–7.

124. Noureldin RA, Liu S, Nacif MS, et al. The diagnosis of hypertrophic cardiomyopathy by cardiovascular magnetic resonance. J Cardiovasc Magn Reson. 2012;14:1–13.

125. Gray B, Ingles J, Semsarian C. Natural history of genotype positive-phenotype negative patients with hypertrophic cardiomyopathy. Int J Cardiol. 2011;152:258–9.

126. Maron BJ, Maron MS, Semsarian C. Genetics of hypertrophic cardiomyopathy after 20 years: clinical perspectives. J Am Coll Cardiol. 2012;60:705–15.

127. Ho CY, Abbasi SA, Neilan TG, et al. T1 measurements identify extracellular volume expansion in hypertrophic cardiomyopathy sarcomere mutation carriers with and without left ventricular hypertrophy. Circ Cardiovasc Imaging. 2013;6:415–22.

128. Karamitsos TD, Dass S, Suttie J, et al. Blunted myocardial oxygenation response during vasodilator stress in patients with hypertrophic cardiomyopathy. J Am Coll Cardiol.2013;61:1169–76.

129. Child N, Muhr T, Sammut E, et al. Prevalence of myocardial crypts in a large retrospective cohort study by cardiovascular magnetic resonance. J Cardiovasc Magn Reson. 2014;16:66.

130. Maron MS, Rowin EJ, Lin D, et al. Prevalence and clinical profile of myocardial crypts in hypertrophic cardiomyopathy. Circ Cardiovasc Imaging. 2012;5:441–7.

131. Niimura H, Bachinski L, Sangwatanaroj S, et al. Mutations in the gene for cardiac myosin-bidning protein c and late-onset familial hypertrohic cardiomyopathy. N Engl J Med. 1998;338:1248–57.

132. Maron BJ, Roberts WC. Quantitative analysis of cardiac muscle cell disorganization in the ventricular septum of patients with hypertrophic cardiomyopathy. Circulation. 1979;59:689–706.

133. Maron BJ, Wolfson JK, Epstein SE, Roberts WC. Intramural ("small vessel") coronary artery disease in hypertrophic cardiomyopathy. J Am Coll Cardiol. 1986;8:545–57.

134. Tanaka M, Fujiwara H, Onodera T, et al. Quantitative analysis of narrowings of intramyocardial small arteries in normal hearts, hypertensive hearts, and hearts with hypertrophic cardiomyopathy. Circulation. 1987;75:1130–9.

135 Johansson B, Mörner S, Waldenström A, Stål P. Myocardial capillary supply is limited in hypertrophic cardiomyopathy: a morphological analysis. Int J Cardiol. 2008;126:252–7.

136. Shirani J, Pick R, Roberts WC, Maron BJ. Morphology and significance of the left ventricular collagen network in young patients with hypertrophic cardiomyopathy and sudden cardiac death. J Am Coll Cardiol. 2000;35:36–44.

137.   Spirito P, Maron BJ. Relation between extent of left ventricular hypertrophy and diastolic filling abnormalities in hypertrophic cardiomyopathy. J Am Coll Cardiol. 1990;15:808–13.

138.   St John Sutton MG, Lie JT, Anderson KR, O'Brien PC, Frye RL. Histopathological specificity of hypertrophic obstructive cardiomyopathy. Myocardial fibre disarray and myocardial fibrosis. Br Heart J. 1980;44:433–43.

139.   Varnava A, Elliot P, Mahon N, Davies M, WJ M. Relation between myocyte disarray and outcome in hypertrophic cardiomyopathy. J Am Coll Cardiol. 2001;88:275–9.

140.   Ismail TF, Hsu L-Y, Greve AM, Gonçalves C, Jabbour A, Gulati A, et al. Coronary microvascular ischemia in hypertrophic cardiomyopathy - a pixel-wise quantitative cardiovascular magnetic resonance perfusion study. J Cardiovasc Magn Reson. 2014 16:49.

141.   Tyan C, Armstrong D, Scholl D, et al. Stress hypoperfusion and tissue injury in hypertrophic cardiomyopathy: spatial characterization using high-resolution 3-tesla magnetic resonance imaging. 2013;6:229-38.

142.   Kim JB, Porreca GJ, Song L, et al. Polony multiplex analysis of gene expression (PMAGE) in mouse hypertrophic cardiomyopathy. Science 2007;316:1481–4.

143.   Ho CY, López B, Coelho-Filho OR, et al. Myocardial fibrosis as an early manifestation of hypertrophic cardiomyopathy. N Engl J Med. 2010;363:552–63.

144.   Bravo PE, Zimmerman SL, Luo H-C, et al. Relationship of delayed enhancement by magnetic resonance to myocardial perfusion by positron emission tomography in hypertrophic cardiomyopathy. Circ Cardiovasc Imaging. 2013;6:210–7.

145.   Maron BJ, Casey SA, Poliac LC, Gohman TE, Almquist AK, Aeppli DM. Clinical course of hypertrophic cardiomyopathy in a regional United States cohort. JAMA. 1999;281:650–5.

146.   Agarwal S, Tuzcu EM, Desai MY. Updated meta-analysis of septal alcohol ablation versus myectomy for hypertrophic cardiomyopathy. J Am Coll Cardiol. 2010;55:823-34.

147.   Harris KM, Spirito P, Maron MS, et al. Prevalence, clinical profile, and significance of left ventricular remodeling in the end-stage phase of hypertrophic cardiomyopathy. Circulation. 2006;114:216–25.

148.   Maron BJ, Spirito P, Ackerman MJ, et al. Prevention of sudden cardiac death with implantable cardioverter-defibrillators in children and adolescents with hypertrophic cardiomyopathy. J Am Coll Cardiol. 2013;61:1527–35.

149.   Green JJ, Berger JS, Kramer CM, Salerno M. Prognostic value of late gadolinium enhancement in clinical outcomes for hypertrophic cardiomyopathy. J Am Coll Cardiol Img 2012;5:370–7.

150. Chan RH, Maron BJ, Olivotto I, et al. Prognostic value of quantitative contrast-enhanced cardiovascular magnetic resonance for the evaluation of sudden death risk in patients with hypertrophic cardiomyopathy. Circulation. 2014;130:484–95.

151. Weinmann H, Brasch R, Press W, Wesbey G. Characteristics of gadolinium-DTPA complex: a potential NMR contrast agent. AJR Am J Roentgenol. 1983;142:519–624.

152. Pennell DJ, Underwood SR, Manzara CC, et al. Magnetic resonance imaging during dobutamine stress in coronary artery disease. Am J Cardiol. 1992;70:34–40.

153. Bergvall E, Cain P, Arheden H, Sparr G. A fast and highly automated approach to myocardial motion analysis using phase contrast magnetic resonance imaging. J Magn Reson Imaging. 2006;23:652–61.

154. Jerosch-Herold M. Quantification of myocardial perfusion by cardiovascular magnetic resonance. J Cardiovasc Magn Reson. 2010;12:57.

155. Lund GK, Wendland MF, Shimakawa A, et al. Coronary sinus flow measurement by means of velocity-encoded cine MR imaging: validation by using flow probes in dogs. Radiology. 2000;217:487–93.

156. Aletras AH, Tilak GS, Natanzon A, et al. Retrospective determination of the area at risk for reperfused acute myocardial infarction with T2-weighted cardiac magnetic resonance imaging: Histopathological and displacement encoding with stimulated echoes (DENSE) functional validations. Circulation. 2006;113:1865–70.

157. Carlsson M, Ubachs JFA, Hedström E, Heiberg E, Jovinge S, Arheden H. Myocardium at risk after acute infarction in humans on cardiac magnetic Resonance. quantitative qssessment during follow-up and validation with single-photon emission computed tomography. J Am Coll Cardiol Img. 2009;2:569–76.

158. Sörensson P, Heiberg E, Saleh N, et al. Assessment of myocardium at risk with contrast enhanced steady-state free precession cine cardiovascular magnetic resonance compared to single-photon emission computed tomography. J Cardiovasc Magn Reson. 2010;12:25.

159. Doherty PW, Lipton MJ, Berninger WH, Skioldebrand CG, Carlsson E, Redington RW. Detection and quantitation of myocardial infarction in vivo using transmission computed tomography. Circulation. 1981;63:597–606.

160. Eichstaedt HW, Felix R, Dougherty FC, Langer M, Rutsch W, Schmutzler H. Magnetic resonance imaging (MRI) in different stages of myocardial infarction using the contrast agent gadolinium-DTPA. Clin Cardiol. 1986;9:527–35.

161. Simonetti OP, Kim RJ, Fieno DS, et al. An improved MR imaging technique for the visualization of myocardial infarction. Radiology. 2001;218:215–23.

162.   Tong CY, Prato FS, Wisenberg G et al. Techniques for the measurement of the local myocardial extraction efficiency for inert diffusible contrast agents such as gadopentate dimeglumine. Magn Reson Med. 1993;30:332–6.

163.   Arheden H, Saeed M, Higgins CB, et al. Measurement of the distribution volume of gadopentetate dimeglumine at echo-planar MR imaging to quantify myocardial infarction: comparison with 99mTc-DTPA autoradiography in rats. Radiology. 1999;211:698–708.

164.   Flacke SJ, Fischer SE, Lorenz CH. Measurement of the gadopentetate dimeglumine partition coefficient in human myocardium in vivo: normal distribution and elevation in acute and chronic infarction. Radiology. 2001;218:703–10.

165.   Kellman P, Wilson JR, Xue H, Ugander M, Arai AE. Extracellular volume fraction mapping in the myocardium, part 1: evaluation of an automated method. J Cardiovasc Magn Reson. 2012;14:63.

166.   Arheden H, Saeed M, Higgins CB, et al. Reperfused rat myocardium subjected to various durations of ischemia: estimation of the distribution volume of contrast material with echo-planar MR imaging. Radiology. 2000;215:520–8.

167.   Kellman P, Wilson JR, Xue H, et al. Extracellular volume fraction mapping in the myocardium, part 2: initial clinical experience. J Cardiovasc Magn Reson. 2012 ;14:64.

168.   Kim RJ, Chen E-L, Lima JAC, Judd RM. Myocardial Gd-DTPA kinetics determine MRI contrast enhancement and reflect the extent and severity of myocardial injury after acute reperfused iInfarction. Circulation. 1996;94:3318–26.

169.   Wagner A, Mahrholdt H, Thomson L, et al. Effects of time, dose and inversions time for acute myocardial infarct size measurements based on magnetic resonance imaging-delayed contrast enhancement. J Am Coll Cardiol. 2006;16:2027-33.

170.   Kellman P, Arai AE, McVeigh ER et al. Phase-sensitive inversion recovery for detecting myocardial infarction using gadolinium-delayed hyperenhancement. Magn Med Reson. 2002;47:372–83.

171.   Oshinski JN, Yang Z, Jones JR, et al. Imaging time after Gd-DTPA injection is critical in using delayed enhancement to determine infarct size accurately with magnetic resonance imaging. Circulation. 2001;104:2838–42.

172.   Kim RJ, Fieno DS, Parrish TB, et al. Relationship of MRI delayed contrast enhancement to irreversible injury, infarct age, and contractile function. Circulation. 1999;100:1992–2002.

173.   Amado LC, Gerber BL, Gupta SN, et al. Accurate and objective infarct sizing by contrast-enhanced magnetic resonance imaging in a canine myocardial infarction model. J Am Coll Cardiol. 2004;44:2383–9.

174.   Hsu L-Y, Natanzon A, Kellman P, Hirsch GA, Aletras AH, Arai AE. Quantitative myocardial infarction on delayed enhancement MRI. Part I: Animal validation of an automated feature analysis and combined thresholding infarct sizing algorithm. J Magn Reson Imaging. 2006;23:298–308.

175.   Saeed M, Lund G, Wendland MF, Bremerich J, Weinmann H-J, Higgins CB. Magnetic resonance characterization of the peri-infarction zone of reperfused myocardial infarction with necrosisspecific and extracellular nonspecific contrast media. Circulation. 2001;103:871–6.

176.   Choi SI, Jiang CZ, Lim KH, et al. Application of breath-hold T2-weighted, first-pass perfusion and gadolinium-enhanced T1-weighted MR imaging for assessment of myocardial viability in a pig model. J Magn Reson Imaging. 2000;11:476–80.

177.   Engblom H, Hedstrom̈ E, Heiberg E, Wagner GS, Pahlm O, Arheden H. Rapid initial reduction of hyperenhanced myocardium after reperfused first myocardial infarction suggests recovery of the peri-infarction zone one-year follow-up by MRI. Circ Cardiovasc Imaging. 2009;2:47–55.

178.   Moravsky G, Ofek E, Rakowski H, et al. Myocardial fibrosis in hypertrophic cardiomyopathy: accurate reflection of histopathological findings by CMR. J Am Coll Cardiol. 2013;6:587–96.

179.   Moon JCC, Reed E, Sheppard MN, et al. The histologic basis of late gadolinium enhancement cardiovascular magnetic resonance in hypertrophic cardiomyopathy. J Am Coll Cardiol. 2004 ;43:2260–4.

180.   Heiberg E, Ugander M, Engblom H, et al. Automated quantification of myocardial infarction from MR images by accounting for partial volume effects: animal, phantom and human study. Radiology. 2008;246:581–8.

181.   Schulz-Menger J, Bluemke DA, Bremerich J, et al. Standardized image interpretation and post processing in cardiovascular magnetic resonance: Society for Cardiovascular Magnetic Resonance (SCMR) board of trustees task force on standardized post processing. J Cardiovasc Magn Reson. 2013;15:35.

182.   Mahrholdt H, Wagner A, Judd RM, Sechtem U, Kim RJ. Delayed enhancement cardiovascular magnetic resonance assessment of non-ischaemic cardiomyopathies. Eur Heart J. 2005;26:1461–74.

183.   Felker GM, Shaw LK, O'Connor CM. A standardized definition of ischemic cardiomyopathy for use in clinical research. J Am Coll Cardiol. 2002;39:210–8.

184.   Carlsson M, Saeed M. Intracoronary injection of contrastmedia maps the territory of the coronary artery. An MRI technique for assessing the effects of locally delivered angiogenic therapies. Acad Radiol. 2008;15:1354–9.

185.   Cerqueira MD. Standardized myocardial segmentation and nomenclature for Ttomographic imaging of the heart: A statement for healthcare professionals from the

96

cardiac imaging committee of the council on clinical cardiology of the american heart association. Circulation. 2002;105:539–42.

186. Ubachs JFA, Engblom H, Koul S, et al. Myocardium at risk can be determined by ex vivo T2-weighted magnetic resonance imaging even in the presence of gadolinium: Comparison to myocardial perfusion single photon emission computed tomography. Eur Heart J Cardiovasc Imaging. 2013;14:261–8.

187. Srinivasan M, Rihal C, Holmes DR, Prasad A. Adjunctive thrombectomy and distal protection in primary percutaneous coronary intervention impact on microvascular perfusion and outcomes. Circulation. 2009;119:1311–9.

188. Porto I, Selvanayagam JB, Van Gaal WJ, et al. Plaque volume and occurrence and location of periprocedural myocardial necrosis after percutaneous coronary intervention: Insights from delayed-enhancement magnetic resonance imaging, thrombolysis in myocardial infarction myocardial perfusion grade analys. Circulation. 2006;114:662–9.

189. Carlsson M, Martin AJ, Ursell PC, Saloner D, Saeed M. Magnetic resonance imaging quantification of left ventricular dysfunction following coronary microembolization. Magn Reson Med. 2009;61:595–602.

190. Saeed M, Lee RJ, Weber O, et al. Scarred myocardium imposes additional burden on remote viable myocardium despite a reduction in the extent of area with late contrast MR enhancement. Eur Radiol. 2006;16:827–36.

191. Ikeda Y, Yutani C, Huang Y, et al. Histological remodeling in an ovine heart failure model resembles human ischemic cardiomyopathy. Cardiovasc Pathol. 2001;10:19–27.

192. Breuckmann F, Nassenstein K, Bucher C, et al. Systematic analysis of functional and structural changes after coronary microembolization: A cardiac magnetic resonance imaging study. J Am Coll Cardiol Img 2009;2:121–30.

193. Achilli F, Malafronte C, Lenatti L, et al. Granulocyte colony-stimulating factor attenuates left ventricular remodelling after acute anterior STEMI: Results of the single-blind, randomized, placebo-controlled multicentre Stem cell mobilization in acute myocardial infarction (STEM-AMI) Trial. Eur J Heart Fail. 2010;12:1111–21.

194. Goetti R, Kozerke S, Donati O, et al. Acute, subacute, and chronic myocardial infarction : quantitative comparison of 2D and 3D late gadolinium enhancement. Radiology. 2011;259:704–11.

195. Peukert D, Laule M, Taupitz M, Kaufels N, Hamm B, Dewey M. 3D and 2D Delayed-enhancement magnetic resonance imaging for detection of myocardial infarction: preclinical and clinical results. Acad Radiol. 2007;14:788–94.

196. Dewey M, Laule M, Taupitz M, Kaufels N. Myocardial Viability : Assessment with three-dimensional MR imaging in pigs and patients. Radiology. 2006;239:703–9.

197. Kühl HP, Papavasiliu TS, Beek AM, Hofman MBM, Heusen NS, van Rossum AC. Myocardial viability: rapid assessment with delayed contrast-enhanced MR imaging with three-dimensional inversion-recovery prepared pulse sequence. Radiology. 2004;230:576–82.

198. Judd R, Lugo-Olivieri C, Arai M, et al. Physiological basis of myocardial contrast enhancement in fast magnetic resonance images of 2-day-old reperfused canine infarcts. Circulation. 1995;92:1902–10.

199. Ugander M, Bagi PS, Oki AJ, et al. Myocardial edema as detected by pre-contrast T1 and T2 CMR delineates area at risk associated with acute myocardial infarction. J Am Coll Cardiol Img. 2012;5:596–603.

200. Choudhury L, Mahrholdt H, Wagner A, et al. Myocardial scarring in asymptomatic or mildly symptomatic patients with hypertrophic cardiomyopathy. J Am Coll Cardiol. 2002;40:2156–64.

201. Soler R, Rodriguez E, Monserrat L, Mendez C, Martinez C. Magnetic resonance imaging of delayed enhancement in hypertrophic cardiomyopathy: relationship with left ventricular perfusion and contractile function. J Comput Assist Tomogr. 2006;30:412–20.

202. Gao P, Yee R, Gula L, Krahn AD, et al. Prediction of arrhythmic events in ischemic and dilated cardiomyopathy patients referred for implantable cardiac defibrillator evaluation of multiple scar quantification measures for late gadolinium enhancement magnetic resonance imaging. Circ Cardiovasc Imaging. 2012;5:448–56.

203. Wu KC, Gerstenblith G, Guallar E, et al. Combined cardiac magnetic resonance imaging and C-reactive protein levels identify a cohort at low risk for defibrillator firings and death. Circ Cardiovasc Imaging. 2012;5:178–86.

204. Rayatzadeh H, Tan A, Chan RH, et al. Scar heterogeneity on cardiovascular magnetic resonance as a predictor of appropriate implantable cardioverter defibrillator therapy. 2013;15:31.

205. De Haan S, Meijers TA, Knaapen P, Beek AM, van Rossum AC, Allaart CP. Scar size and characteristics assessed by CMR predict ventricular arrhythmias in ischaemic cardiomyopathy: comparison of previously validated models. Heart. 2011;97:1951–6.